Numerical modelling and experimental validation of the microclimatic impacts of water mist cooling in urban areas

Energy & Buildings

Numerical modelling and experimental validation of the microclimatic impacts of water mist cooling in urban areas

--Manuscript Draft--

Manuscript Number:	ENB_2020_2350R2
Article Type:	VSI:Resilient city&building
Section/Category:	Outdoor Microclimate and Environmental Quality
Keywords:	Evaporative Cooling; outdoor comfort; heat mitigation; ENVI-met; Water mist spray; urban climate
Corresponding Author:	Giulia Ulpiani The University of Sydney Sydney, New South Wales Australia
First Author:	Elisa Di Giuseppe
Order of Authors:	Elisa Di Giuseppe
	Giulia Ulpiani
	Claudia Cancellieri
	Costanzo Di Perna
	marco d'orazio
	Michele Zinzi
Abstract:	Among water-based mitigation strategies against urban overheating, dry mist systems are especially promising, given their local impact, cost-effectiveness and controllability. Intense cooling capacity has been reported under a variety of climates, however, there is a growing need to define specific design guidelines towards an informed and optimized use of the technology. Parametric analysis on validated models would assist in determining type and degree of correlation between key parameters, as well as magnitude and predictability of the cooling capacity. In this paper, for the first time, a 3D microclimatic model in ENVI-met is used to simulate a misting system installed in Rome, Italy, with high prediction accuracy for the air temperature ($R2 \approx 0.87$, $RMSE \approx 0.84$ °C). The calibrated ENVI-met model is used then to perform parameterizations on the water mist system, focused on the role of three key design variables: i) water flow rate, ii) injection height and iii) local wind speed. Results show that the most significant thermal drops tend to occur close but out of the misted perimeter following the wind direction, with cooling effects further stretched for tens of meters. The cooling capacity increases with the total water flow rate (+0.2 °C per 10 l/h increment) and in presence of calm air (+35-40 % per 0.8 m/s deceleration). Lower injections intensify the cooling a pedestrian height, which could be especially beneficial under windy conditions. Further research would target climate dependencies to extend the applicability of the above results and build up cohesive guidelines at the hands of urban planners and practitioners
Suggested Reviewers:	Dionysia Kolokotsa dkolokotsa@enveng.tuc.gr Denia (Dionysia) Kolokotsa is Associate Professor at the School of Environmental Engineering of the Technical University of Crete, Greece. Her research interests include energy management for the built environment, energy efficiency and renewables, integration of advanced energy technologies, indoor and outdoor environmental quality and energy efficiency in buildings
	Kevin Lanza kevin.l.lanza@uth.tmc.edu Dr. Lanza research activity focuses on sustainable urban development; ecological gentrification; temperature, thermal comfort, and health; urban heat island adaptation. His postdoc focuses on green and blue spaces against urban heat island. He was member of the Urban Climate Lab at the Georgia Institute of Technology

	Shamilla Haddad s.haddad@unsw.edu.au Her research is devoted to microclimatic analysis, urban heat island mitigation, thermal comfort (indoor and outdoor) and on environmental & occupational health. In her papers she has made extensive use of the software ENVI-met which was used in the submitted paper as well.
	Craig Farnham farnham@life.osaka-cu.ac.jp Prof. Farnham is expert in developing and optimizing evaporation spray cooling systems to reduce thermal stress on humans and reduce energy consumption for air conditioning, by experiment, CFD simulation, and fundamental research.
Opposed Reviewers:	
Response to Reviewers:	

THE UNIVERSITY OF SYDNEY

Giulia Ulpiani
Postdoctoral Research Associate
School of Civil Engineering
The University of Sydney
giulia.ulpiani@sydney.edu.au
+61481600997

31 July 2020

To:
Professor Veronica Soebarto and Professor Evyatar Erell
Guest Editors
Special Issue on Advances in Research for Resilient Cities and Building Energy Use Minimisation
Energy and Buildings

Dear Guest Editors,

I am pleased to submit to your attention our latest manuscript “Numerical modelling and experimental validation of the microclimatic impacts of water mist cooling in urban areas” by Elisa Di Giuseppe, Giulia Ulpiani, Claudia Cancellieri, Costanzo Di Perna, Marco D'Orazio and Michele Zinzi.

Dry mist systems may play a crucial role in combating the phenomenon of urban overheating at local scale. Compared to alternative evaporative technologies, the water consumption is very modest and the risk of wettedness very marginal, especially when the cooling action is smartly controlled. Their beneficial action on the outdoors is reflected in terms of air conditioning energy use minimization, which comes on top of other positive impacts such as solar radiation attenuation and pollution removal. These systems could be deployed throughout the cityscape in strategic hot or vulnerable spots, yet much is still to be disclosed in terms of design optimization and cooling efficiency dependence on contextual environmental conditions.
This study aimed at investigating how misting systems perturb the local urban climate by validating a 3D microclimatic model in ENVI-met on experimental evidence and then testing different design and environmental scenarios. It was proved that ENVI-met is able to track the temperature evolution both under undisturbed and misted conditions as quantified by Pearson’s coefficient of determination, Root Mean Square Error and Wilmott’s index of agreement. With a horizontal discretization of 2 m x 2 m and a vertical discretization of 0.5 m, the temperature distribution was well replicated both horizontally and vertically. The simulations tracked the cooling action in and out of the misted perimeter, allowing to quantify the spatial extension of the influence area. The sensitivity analysis further delved into the role played by water flow rate, injection height and wind speed. Results show that the most significant thermal drops tend to occur close but out of the misted perimeter

following the wind direction, with cooling effects further stretched for tens of meters. The cooling capacity increases with the total water flow rate (+0.2 °C per 10 l/h increment) and in presence of calm air (+35-40 % per 0.8 m/s deceleration). Lower injections intensify the cooling a pedestrian height, which could be especially beneficial under windy conditions. Overall, this study contributes to the current body of knowledge on water mist systems as urban overheating countermeasures i) by simulating the impacts at neighbourhood scale by means of a well-established urban climate modelling platform, capable of considering the competing effects of greenery and urban forcing, ii) by quantifying the spatial extension of the cooled area under different environmental conditions, to complement the experimental results and iii) by suggesting design criteria to be applied at both manufacturing and urban planning level via parametric analysis on the experimentally validated model. Further research would target climate dependencies to extend the applicability of the above results.

The authors affirm that the submission represents original work, that the manuscript has not been submitted to another journal and that we have the permission to reproduce the published materials in our manuscript.

Please address all correspondence to:

Giulia Ulpiani
e-mail: giulia.ulpiani@sydney.edu.au
mobile: +61 481600997
School of Civil Engineering, Building J05, The University of Sydney, NSW 2006, Australia

Looking forward to hearing from you and thanking you for your time and consideration.

Sincerely yours,
Giulia Ulpiani
Corresponding Author
On behalf of the Authors

School of Civil Engineering
Building J05
The University of Sydney
NSW 2006 Australia

T +61 481 600 997
E giulia.ulpiani@sydney.edu.au
sydney.edu.au

Dear Reviewers,

Thanks again for evaluating our work carefully. The raised points led us to further improve the manuscript and disclose many critical points. Please consider our replies below.

-Reviewer 1

The authors have implemented most of the comments. However, two of my main questions have remained unanswered. As I mentioned in my previous review, I am concerned about the accuracy and reliability of the simulations, and this should certainly be revised:

- The first comment is about the droplet size distribution. It is mentioned that the droplet size distribution is measured in a test room, and it is known that the mean Sauter diameter is about 10 μm, and the diameter of the smallest and largest droplets is about 7 μm and 27 μm, respectively. The authors should better clarify why the measured data is not used to model the droplet size distribution. For example, semi-empirical methods such as the Rosin-Rammler model could be implemented. As the authors are very well aware, the geometric properties of droplets in a spray system are of the most critical factors that affect the dynamic behavior of the droplets, but also the heat and mass transfer rates between the continuous and discrete phase. It is stated that "by setting a particle diameter of 5 μm, the best matching with the measured data was achieved". I am afraid this is not convincing enough for a scientific journal paper. I understand that due the complex wind-droplets interactions, it would be complicated to translate the measured data into the boundary conditions for the CFD simulations. Still, the authors should note that validation is to assess how accurately the computational results compare with the experimental data, with quantified error and uncertainty estimates for both. Therefore, the author should better clarify this and at least perform a sensitivity analysis for different mean droplet diameters to show how the droplet size distribution affects the results.

We thank the Reviewer for this observation as indeed it catches one of the limitations that come with ENVI-met in the simulation of water spray, compared to other CFD platforms like Fluent. ENVI-met's water spray module does not require in input the diameter distribution, but only the mean diameter. We are well aware that the geometric properties of droplets affect profoundly the heat and mass transfer rates between the continuous and discrete phase. We used Fluent in the past, applied the Rosin-Rammler model and could get a feeling of such a role. However, the intent of the paper is to check if ENVI-met can reasonably capture the spatial and temporal trends of mist cooling despite a simplified approach, and thus be used for overheating mitigation scenario analysis in urban context.

We first used the measured mean Sauter diameter (10 μm) and obtained a good agreement with the experimental data. However, being aware that in reality the mist is a mix of smaller and larger droplets (the former having a fundamental role in the cooling intensity) and also considering the differences between the test room and the outdoors we decided to run a sensitivity analysis on the droplets' size. For the sake of brevity, we didn't report it in the paper, but in light of the raised concerns, we decided to incorporate it in the revised manuscript. The following paragraph has been added to Section 2.2.2:

"As stated above, ENVI-met represents the whole cloud of droplets by a single mean diameter, rather than a statistical distribution (e.g. Rosin Rammler, commonly adopted in other CFD software [49]). This simplification may underestimate both the cooling potential (since smaller droplets are not concerned) and the humidification (since larger droplets are not concerned). To verify which mean diameter best captured the experimental temperatures, we carried out a sensitivity analysis. Fig. 4 shows that smaller diameters performed better than that experimentally measured (10 μm). This was likely ascribable to the differences between the test room and the actual urban setting where solar radiation, wind and other factors enhanced the evaporation rate and the break-up into child particles. Diameters as low as 3 μm were statistically compared by quantifying the difference from the hourly averaged experimental temperature. By setting a particle diameter of 5 μm, the best RMSE, Pearson coefficient (r) and R^2 were attained (see Fig. 4). This setting was maintained in all subsequent simulations."

Further, we highlight this limitation in the Discussion. We added the following lines:

"Compared to other CFD platforms, ENVI-met's approach to water spray tracking relies on two simplifying assumptions: i) all droplets have the same diameter (no statistical distribution) and ii) the amount of droplets in a given air volume changes due to evaporation, but not their size. By not considering any statistical distribution, ENVI-met's water spray model might be prone to inaccuracies both in terms of cooling and humidification, since the droplet size governs the heat and mass transfer rates between the continuous (air) and discrete (water) phase. To overcome this issue, a preliminary tuning procedure on the mean droplet diameter was proposed."

- The information provided about the turbulence model used is not sufficient. The authors should explicitly mention which turbulence model is used (e.g., k-epsilon, k-omega, SSTk-omega, etc.?). As the sensitivity of the results to the turbulence model is not investigated in this study, the authors can study and refer to those studies in the literature in which a sensitivity analysis is performed to assess the impact of the turbulence model on the simulation results.

In section 2.2.3, we state that the turbulence model is a k-epsilon one. We also included the reference to the work by Montazeri et al. which demonstrates how changing the turbulent model has negligible impact on water spray simulation as none was found to be superior over the others.

H. Montazeri, B. Blocken, J.L.M. Hensen, Evaporative cooling by water spray systems: CFD simulation, experimental validation and sensitivity analysis, Build. Environ. (2014), http://dx.doi.org/10.1016/j.buildenv.2014.03.022.

- It is not yet clear how the evaporation is modeled in ENVI-met. It is stated that the authors are not aware of this as "no technical information is provided on this model by the ENVI-met staff yet". This is not acceptable for a scientific journal paper. This would also be weird for the readers to see that a good agreement between simulation and measurement is achieved. However, it is not clear how the simulations are performed. This should certainly be clarified before this paper can be accepted for publication.

We understand the raised point, as it has been already raised repeatedly in ENVI-met's forum by other users willing to better understand the physics behind the water spray module. We further

investigated into this and managed to get the very first official document directly from Michael Bruse (ENVI-met's developer). This is now included in the paper (section 2.2.2) and goes as follows:

"According to the technical documentation provided by M. Bruse (personal communication, September 29, 2020), ENVI-met computes the energy required to evaporate the water and the corresponding local decrease in air temperature. Unevaporated droplets are entrained in the wind flow and are subject to sedimentation processes with a downward settling velocity depending on their size. The main simplification relies on the particle tracing. Two main approaches are commonly used in CFD analysis, both considering that the droplet diameter would decrease along with evaporation until the droplet has vanished. The first one is the discrete approach, according to which different droplets sizes in the air volume are grouped into n bins and evaporation at their surface is numerically translated into a shift of the number of droplets towards smaller bins [45]. The second is the Lagrangian approach, in which the state and size of each droplet is monitored and calculated individually. Both ways are not realistic for a relativity small sub model of ENVI-met, in terms of required computing resources and calculation time. To simplify the process of droplet evaporation, the droplets do not change their size (nor their mass) in ENVI-met, but their quantity. The prognostic variable is the amount of liquid droplets within a given air volume, w_D (g/m^3) which is related to the number of droplets N_D and the mean droplet radius r_D (μm) as follows:

$$N_D = \frac{w_D}{0.001 \cdot \rho_w \cdot \frac{4}{3}\pi \cdot r_D^3} \quad (1)$$

Beyond evaporation, ENVI-met considers a number of drivers for the spatial and temporal distribution of water spray, namely advection, diffusion, transport, local production (sources of spray) and sedimentation (sinks of spray). Transport is assumed to be instantaneous as very small droplets tend to behave like gases. As such, the droplets follow the air flow stream lines without inertial delays and the only extra velocity component is the settlement velocity due to gravitational forces. All other parameters (e.g. turbulent diffusion) are assumed to be equal to each other inert mass component. Overall, the partial differential equation that describes the atmospheric balance over time is of the same form of the advection-diffusion equation, used for the dispersion of gases and particulate matter:

$$\frac{\partial w_D}{\partial t} + u_i \frac{\partial w_D}{\partial x_i} = \frac{\partial}{\partial x_i}\left(K_q \frac{\partial w_D}{\partial x_i}\right) + Q_{w_D}(x,y,z) + S_{w_D}(x,y,z) \quad (2)$$

where u_i={u,v,w} is the wind velocity vector corresponding to the Cartesian coordinates x_i={x,y,z}, K_q is the water vapor diffusion coefficient while Q_{w_D} and S_{w_D} are the source and sink terms, respectively. In Eq. 2, w_D is expressed in μg/kg. The rate of evaporation is strongly dependent on the droplet's temperature, which is estimated through the energy conservation equation:

$$L(T_D)\frac{\partial m_D}{\partial t} = A_D \cdot K \cdot (T_D - T_a) + Q_{kw} + A_D \cdot \sigma_B \varepsilon (T_D^4 - T_{env}^4) \quad (3)$$

where L is the latent heat, A_D is the droplet surface area ($4\pi r_D^2$), K is the sensible heat transfer coefficient between droplet and air (inclusive of molecular and turbulent processes), Q_{kw} is the shortwave radiation, σ_B is the Stefan-Boltzmann constant, ε the emissivity and T_{env} is the radiant

temperature of the surroundings (representative of the longwave radiative fluxes from the environment). Based on the transient resolution of Pruppacher and Klett's heat transfer equation, Edson [46] and Andreas [47] observed that sprayed droplets tend to quickly approach the wet bulb temperature T_{wb}, regardless of the initial conditions. As such, the estimation of T_D can be directly replaced by the estimation of T_{wb}. This simplified procedure is adopted in ENVI-met.

The change of mass of a single droplet depends on the vapor pressure difference Δe between air and droplet according to the following equation:

$$\frac{\partial m_D}{\partial t} = -4\pi r_D \cdot f_v \cdot D_v \cdot \frac{\Delta e}{\left(1 - \frac{\bar{e}}{p}\right) R_v \bar{T}} \tag{4}$$

where $\bar{T}$ and $\bar{e}$ are the arithmetic means of the droplet and air temperatures and of the saturation (e_{sat}) and vapour partial (e_a) pressures, respectively, Δe is the difference between $e_{sat}(T_D)$ and e_a, p is the total pressure, R_v is the water vapor gas constant (taken at 461.5 J/kgK), whereas D_v and f_v are the vapor mass diffusivity and the ventilation factor, calculated according to Bird et al. [48] and Rouault et al. [45] respectively:

$$D_v = 2.4995 \cdot 10^{-5} \left(\frac{T_a}{292.88}\right)^{2.334} \tag{5}$$

$$f_v = \begin{cases} 0.78 + 0.308\, N_v, & for\ N_v \leq 1.4 \\ 1.0 + 0.108\, N_v^2 & elsewhere \end{cases} \tag{6}$$

The ventilation factor takes into account the motion of air around the droplet due to wind flow and settling of the droplet, based on N_v, which is a function of the Schmidt and Reynolds numbers."

We hope this will be a useful reference for all ENVI-met users and thank the Reviewer for the suggestion.

-Reviewer 2

- Thank you for the corrections.

1- Going through your responses to the feedback, now there is a visible advocacy for ENVImet which is not suitable for a scientific paper.

Phrases such as "This study proved that ENVI-met is able to track the temperature evolution both under undisturbed and misted conditions as ... " at the beginning of section 4.discussion are very strong, especially when we do not know the basic code behind the misting calculation in ENVImet.

Do we really need to use "prove" here?

If I want to rephrase it, the study made a model in ENVImet that matches a real experimental data. So ENVimet can mimic a reality but tracking and predicting future scenarios are different matters.

The model is validated against the experimental data and it is enough to trust the model in this case. It would be more appropriate if the model was used to predict a future scenario and then a further experiment provided the margins of error but I think this is not what the authors wanted to do so I suggest removing all such strong claims from the results, discussion and conclusion.

We removed all strong claims as suggested. Further, we highlighted the limitations of the software throughout the discussion (see red-marked paragraphs) and added a dedicated paragraph in 2.2.2 to emphasize the simplifications adopted in the tracking of the particles. Thanks for your comment.

2- I am not sure if the journal is responsible for proof reading of technical terms.

Technical terms have been reviewed.

Numerical modelling and experimental validation of the microclimatic impacts of water mist cooling in urban areas

Elisa Di Giuseppe[a], Giulia Ulpiani[b]*, Claudia Cancellieri[a], Costanzo Di Perna[b], Marco D'Orazio[a], Michele Zinzi[c]

[a] Department of Civil and Building Engineering and Architecture (DICEA), Università Politecnica delle Marche, Via Brecce Bianche 12, 60131 Ancona, Italy
e.digiuseppe@univpm.it (E. Di Giuseppe)
claudia@cancellieri.eu (C. Cancellieri)
m.dorazio@univpm.it (M. D'Orazio)
[b] Department of Industrial Engineering and Mathematical Sciences (DIISM), Università Politecnica delle Marche, Via Brecce Bianche 12, 60131 Ancona, Italy
giuliaulpiani@gmail.com (G. Ulpiani)
c.diperna@univpm.it (C. Di Perna)
[c] ENEA, Via Anguillarese 301, 00123 Rome, Italy
michele.zinzi@enea.it (M. Zinzi)

* Corresponding author.

Abstract

Among water-based mitigation strategies against urban overheating, dry mist systems are especially promising, given their local impact, cost-effectiveness and controllability. Intense cooling capacity has been reported under a variety of climates, however, there is a growing need to define specific design guidelines towards an informed and optimized use of the technology. Parametric analysis on validated models would assist in determining type and degree of correlation between key parameters, as well as magnitude and predictability of the cooling capacity. In this paper, for the first time, a 3D microclimatic model in ENVI-met is used to simulate a misting system installed in Rome, Italy, with high prediction accuracy for the air temperature ($R^2 \simeq 0.87$, RMSE$\simeq$0.84 °C). The calibrated ENVI-met model is used then to perform parameterizations on the water mist system, focused on the role of three key design variables: i) water flow rate, ii) injection height and iii) local wind speed. Results show that the most significant thermal drops tend to occur close but out of the misted perimeter following the wind direction, with cooling effects further stretched for tens of meters. The cooling capacity increases with the total water flow rate (+0.2 °C per 10 l/h increment) and in presence of calm air (+35-40 % per 0.8 m/s deceleration). Lower injections intensify the cooling a pedestrian height, which could be especially beneficial under windy conditions. Further research would target climate dependencies to extend the applicability of the above results and build up cohesive guidelines at the hands of urban planners and practitioners.

Keywords

Water mist spray; Evaporative cooling; Urban climate; Outdoor comfort; Heat mitigation; ENVI-met

Nomenclature and units

A_D	droplet area	m^2
b	Clapp&Hornberger's constant	-
C	Centre	-
CP	volumetric heat capacity	$10^6 J/m^3K$
Cs	specific heat	J/kg·K
d	Wilmott's index of agreement	-
D_v	vapor mass diffusivity	m^2/s
E	East	-
$\bar{e}$	mean air-droplet vapor pressure	Pa
e_a	vapor partial pressure	Pa
e_{sat}	saturation pressure	Pa
f_v	ventilation factor	-
GSR	global solar radiation	W/m^2
hydr	hydraulic conductivity	$10^{-6}m/s$
K	sensible heat transfer coefficient	$W/m^2·K$
K_q	water vapor diffusion coefficient	m^2/s
L	latent heat of evaporation	W
MatPot	mean Matrix Potential at water saturation	m
MC	misted condition	-
m_D	droplet mass	kg
m_f	mass flow	l/m
N	North	-
N_D	number of droplets	-
n_s	water content at saturation	m^3/m^3
N_v	ventilation number	-
p	total pressure	Pa
Q_{kw}	shortwave radiation	W
Q_{wD}	sources of spray	µg/kg·s
r	Pearson coefficient	-
R^2	Pearson's coefficient of determination	-
r_D	mean droplet radius	µm
RH	relative humidity	%
RMSE	root-mean-square error	°C
R_v	water vapor gas constant	J/kg·K
S	South	-
S_{wD}	sinks of spray	µg/kg·s
$\bar{T}$	mean air-droplet temperature	°C
Ta	ambient temperature	°C
T_D	droplet temperature	°C
T_{env}	radiant temperature of the surroundings	°C
th	thickness	m
T_{wb}	wet-bulb temperature	°C
UC	undisturbed condition	-
u_i	velocity vector	m/s
V	index of permeability of the soil	-
W	West	-
wd	wind direction	°

w_D	amount of liquid droplets within a given air volume	g/m^3 or $\mu g/kg$
ws	wind speed	m/s
x_i	Cartesian coordinates vector	m
α	solar absorptance	-
Δe	vapor pressure difference	Pa
ΔTa	ambient temperature difference between undisturbed and misted conditions	°C
ε	thermal emissivity	-
λ	thermal conductivity	$W/m \cdot K$
ρ	solar reflectance (or albedo)	-
ρ_{mat}	density of materials	kg/m^3
ρ_W	water density	kg/m^3
σ_B	Stefan-Boltzmann constant	$W/m^2 \cdot K^4$
τ	solar transmittance	-
ϕ_D	mean droplet diameter	μm
n_{fc}	water content at field capacity	m^3/m^3
n_{wilt}	water content at wilting point	m^3/m^3

1. Introduction

Urban overheating is a well-known environmental hazard at both global and local scale, as documented by several scientific studies and observations of air temperature trends. Main consequences are the thermal deterioration of both indoor and outdoor thermal environments, serious thermal comfort concerns for human beings, and enhanced cooling energy uses in buildings [1,2]. Measured temperatures' rise and evolution scenarios are the object of many studies. The most significant are those produced under the UN framework by the Intergovernmental Panel on Climate Change [3], dedicated to global strategies and countermeasures to limit the temperature rise to 1.5 °C. Beyond global warming, the "Urban Heat Island" (UHI) phenomenon is a major cause of overheating in the urban built environment, investigated for decades. Its intensity depends on several factors as: climate, size of the city, urban texture, etc. Peak values up to 12 °C are reported in literature, whereas the average maximum orbits around 2 °C [4]. Moreover, UHI intensity is typically higher in cooling dominated climates [5].

Urban overheating has a strong impact on the energy use in buildings especially for cooling, as documented worldwide in [4]. It further enhances the risks related to energy poverty for an impressive share of the global population: 1 billion people living in poorer countries [7] and more than 60 million living in Europe [8]. The risk of skyrocketing energy uses for cooling and the unfeasibility of ensuring decent outdoor thermal conditions for many citizens call for diversified and effective thermal mitigation/adaptation plans and architectural rehabilitation of urban spaces, in the attempt of improving health, comfort and liveability in the outdoor realm [6,7]. Many studies have been carried out to size the impact of different UHI mitigation technologies and strategies: green infrastructures, innovative cool materials, blue technologies, as reviewed in [5,8,9].

Main findings prove that passive solutions offer moderate mitigation potentials (generally below 2 °C) and are effective if applied at large scale in the city. Urban overheating can be combated, at

local scale, through the inclusion of blue features, as evaporative processes largely influence both the natural hydrological balance and the human thermoregulation, thus strongly impacting on comfort and liveability [10]. Especially on hot and dry days or during heat waves, evaporation is a fairly effective way to draw the excessive heat from the air through a thermodynamically spontaneous phase change process, that naturally magnifies as temperature rises (at equal specific humidity) [11] and that is way more intense than a purely sensible heat transfer between air and water [12].

Beyond natural water bodies, a whole spectrum of artificial installations can be considered (ranging from fountains, to sprinklers, to evaporative towers, to ponds). Among them, an especially promising blue mitigator is represented by dry mist systems, namely high-pressure water injectors able to pulverize the water into fine droplets of few tens of microns. The high surface-to-volume ratio promotes flash evaporation, hence i) the water consumption can be minimized compared to alternative technologies and ii) the risk of wettedness, even close to the nozzles, can be neutralized as long as a proper layout is configured [11]. Further, it was experimentally demonstrated that dry misters are beneficial in terms of building energy use minimization: Ishii et al. [13] projected a 10 % air conditioning energy reduction at the expense of 5 % humidity gain per degree of air cooling, whereas Narumi et al. monitored three misting techniques (rooftop spraying, veranda spraying, and outdoor air-conditioning spraying) in an apartment house in Osaka and reported on cooling consumptions decremented by more than 80 % [14]. Other secondary benefits are related to air quality and erythema reduction since finely pulverized droplets help at scavenging dust, removing pollutants [15] and attenuating solar attenuation [16].

These systems could be deployed throughout the cityscape in strategic hot or vulnerable spots to alleviate the risk of heat-related mortality and morbidity with expected higher impact than single massive water bodies [17]. Furthermore, compared to water bodies, these systems can be controlled in capacity and can be triggered by specific events (temperature, humidity, wind speed exceedances or rain occurrences) not to provide evaporative cooling when unneeded or potentially counterproductive [18]. This is especially attractive for heating-dominated countries, where overheating concerns are sporadic yet extreme events.

On the other side, the efficacy of a misting system is largely a function of the environmental conditions. In a recent review by Ulpiani dedicated to mist cooling [11], the author collected data from 12 countries and 7 climatic zones. Air temperature and relative humidity were identified as driving factors, as they dictate the wet bulb depression (difference between dry-bulb and wet-bulb temperature) which represents the theoretical limit for evaporative cooling [19]. Additionally, wind speed (and gusts) proved to be pivotal as directly related to the level of particle dilution [20]. Demonstration of the governing role of local wet bulb depression as both instantaneous and short-term trend is reported in [21], where the cooling capacity of an overhead dry mist system was found to be negatively and positively correlated with solar irradiation and wind speed, respectively. This implies that not just the microclimate of the installation site deeply affects the results, but also the very local urbanscape (e.g. space enclosure, canyon effect, greenery and other competing evaporative sources, wind-breaking features and provisions, etc.). In such a complex scenario, modelling and parameterization, based on adequate experimental validation, are especially useful to determine type and degree of correlation between key parameters, as well as magnitude and predictability of the cooling capacity. This is pre-condition to define substantiated design guidelines towards an informed and optimized use of the technology [11].

Almost all numerical models of mist cooling are platformed in ANSYS Fluent [11]. In 2008, Yamada et al. reproduced a 50 m x 15 m x 4 m semi-enclosed outdoor space in Tokyo (Japan, Cfa climate)

fitted with an overhead misting system, using a mesh grid of 11,200 cells [22]. On a typical summer day (Ta of 33.4 °C, RH of 58 %, ws of 0.1 m/s), the cooling reached -1.5 °C at the spray location and -0.5 °C about 2.5 m away, at the expense of a +0.8 and + 0.3 g/kg gain in absolute humidity, respectively. In 2010, Wang et al. [23] investigated the role of airflow rate and site of installation (open outdoors, semi-enclosed area) when a misting fan was introduced in a 15 m x 10 m x 4 m domain represented by 570,000 hexahedral cells, under initial Ta of 35 °C, RH of 60 % and solar radiation of 600 W/m^2. The change in airflow simply moved the region of higher cooling closer or farther from the injection. On the other hand, the maximum temperature drop more than doubled (from 2 °C to 5 °C) when shifting from the open to the semi-enclosed scenario, bringing out the role of wind. The humidity gain was found to be negligible (1- 6 %) in any case. In 2015, Farnham et al. [12] ran an experimental and numerical study in Osaka (Japan, Cfa climate). They used Fluent to investigate the role of i) water temperature in almost the whole liquid range (8 - 92 °C), ii) the distance from the injection and iii) the initial T, RH conditions (7 cases) by looking at a single injection with mean droplet diameter of 23.4 – 25.5 μm. A 400 cm x 45 cm x 45 cm air volume was discretized into 1-cm tetrahedral mesh near the nozzle, ranging up to 4-cm mesh at the air inlet and outlet, for a total of 1.2 million elements. The cooling ranged between 0.5 and 2.5 °C, with negligible loss due to the different water temperature (0.26 °C when water was heated up from 20 °C to 60 °C). In the same year, Montazeri et al. systematized the CFD analysis of the impact of physical parameters on evaporative cooling by a mist spray system [24]. The authors modelled a 0.585 m x 0.585 m x 1.9 m wind tunnel, meshed into 1,018,725 hexahedral cells, to parameterize i) the inlet air temperature, ii) the inlet air humidity ratio, iii) the inlet airflow rate, iv) the inlet water temperature, v) the inlet droplet mean diameter and vi) the droplet spread. Five different cases were considered for each parameterization. It was found that the maximum temperature drop incremented from 3.3 to 9.3 °C by increasing the air temperature, from 3 to 9 °C by decreasing the humidity ratio, from 0.8 to 7 °C by reducing the relative velocity, from 2 to 9 °C by cooling down the water (in contrast with [12]), from 4 to 10 °C by reducing the mean droplet size and remained fairly unchanged at 5.8 °C when tweaking the spread. The same authors, in [25], extended the simulation to an outdoor location, by modelling a courtyard in the Bergpolder Zuid region of Rotterdam (The Netherlands, Cfb climate), equipped with 15 nozzles featuring mean droplet diameter of 20 μm. A circular inner subdomain of diameter equal to 1,200 m was populated with explicitly modeled buildings, while the surrounding outer hexagonal subdomain (side 1,200 m) was implicitly modeled in terms of roughness, for a total of 6,610,456 hexahedral and prismatic cells. Three different values for i) total mass flow (2 - 9 l/min) and ii) height above the ground (3 - 5 m) were considered. The maximum temperature drop (underneath the injection in the middle of the spray line, at a pedestrian height of 1.75 m) increased from 1 to 7 °C as higher flow rates were processed. Spatially, a 2 °C maximum drop was reported to stretch up to a distance of 8 m from the spray line. By decreasing the height of the injections, the cooling capacity incremented from 5 to 7 °C. Results are to be trusted for relatively low pedestrian ws (0.5 - 1.5 m/s).

Other than Fluent, Q-basic was used at first [26], then also Fire Dynamics Simulator [27] and Simplified Analysis System for Housing Air Conditioning Energy [14]. In some instances [28–30] the software was left unspecified. These models typically apply an Eulerian-Lagrangian approach to follow the discrete phase (water) in its kinetics and thermodynamics inside the continuous medium (air) and thus provide a punctual representation of the two-phase interaction. Yet, as mist cooling gains ground into the world of urban heat island mitigation, there is a need to incorporate and validate its effects in urban-scale simulations, contemplating the complex interplays with other microclimatic

phenomena, distinctive of the urban environment (e.g. canyon effects, evapotranspiration, reduced soil permeability, anthropogenic heat).
ENVI-met is a three-dimensional microclimate modelling system designed to simulate the surface-plant-air interactions in urban environment, based on the fundamental laws of fluid- and thermodynamics. Recently, it has been widely adopted to estimate the thermal benefits of urban heat mitigation strategies [31–36]. This software includes a water droplet dispersion and evaporation model to simulate the cooling effect of water spray. However, to the best of our knowledge, no study reports on experimentally-validated water mist models corroborated by multi-point in-situ measurements using ENVI-met. This study contributes to the current body of knowledge on urban overheating countermeasures based on evaporative cooling in two ways: i) by assessing the effectiveness of the software ENVI-met in predicting the microclimate perturbation in the misted area and ii) by determining substantiated design criteria to be applied at both manufacturing and urban planning level. The calibration of the ENVI-met model for water misting poses some challenges, essentially due to the non-trivial interlacement between droplets' behaviour and the other climate-impinging urban elements: a suite of solutions is proposed and discussed, leading to accurate simulations that capture real trends and evolutions. Recommended settings are presented to be used in future scenario analysis for UHI mitigation.

2. Materials and method

In this paper, ENVI-met version 4.4.3 is used to model a grid of overhead dry misters installed in a green playground in Rome (Italy, Csa climate). The simulation results for both the "misted condition" (MC) and the "undisturbed condition" (UC) of the site are validated on the basis of the thermal and hygrometric mapping obtained through a bespoke sensor network. The calibrated ENVI-met model is then used to perform parameterizations on the water mist system, focused on the role of three key design variables: i) wind speed, ii) water flow rate and iii) height of nozzles above the ground. Next section 2.1 provides information on the experimental rig, while the model is described in section 2.2. Results from the model validation and subsequent parameterizations are reported in section 3 and conclusively discussed in section 4.

2.1 Experimental rig

The dry mist system was erected in a green area of about 50 m x 16 m, stretched along the north-south axis, in the East of Rome city (Italy, 41°52'34.7"N 12°33'59.6"E, 44.5 m a.s.l.) during summer 2018. Low-rise residential blocks, originally for military officials, dominate the local landscape. The perimeter is framed with ornamental bush specimens, about 1 m high and dense in foliage. A line of five linden trees runs approximately 11 m away from the eastern boundary. The trees are 9.6 m inter-spaced, with a mean girth of 0.25 m. At 3 m above the ground, the crown expands within a 3.5 m radius from the trunk, on average. Consequently, solar shading is provided from 4:30 pm on.
The green area is enclosed by a church, the elders' bowls club and the local polyclinic along the east-west axis, a small playground due north and a lower-floor street running along the southern border. Strewn with toys, it is destined to families, notably those with children under 4 years old. The quite concealed position and designated use make it the perfect test rig for the misting system: low dominant wind speeds, proximity to vulnerable population (children, youngsters, mothers and elders) and proximity to gathering points (church and its square, playground, sports clubs, healthcare facilities) (Figure 1).

The injections, consisting of 24 hollow-cone nozzles, were suspended through a system of pulleys and tensioned cables at an average height of 2.8 m, in line with customary setups [11] and distributed in 4 parallel strings of 6 nozzles each. The interspace was 1 m along the string and 1.25 m in-between the strings. A self-compensating 70 bar water pump, absorbing about 990 W_e, was utilized to pressurize the water supplied from a local fountain, with a flow rate of 1.5 l/min. In order to quantify the droplet diameter distribution, the nozzles were previously tested under a pressure of 1000 psi (68.9 bar) using water at 21.1 °C in a test room whose humidity was maintained at 40-50 %. Patternation measurements were conducted using the SETscan OP600. The cloud of dispersed droplets featured mean Sauter diameter around 10 µm, with the smallest droplets under 7 µm in diameter and the biggest over 27 µm.

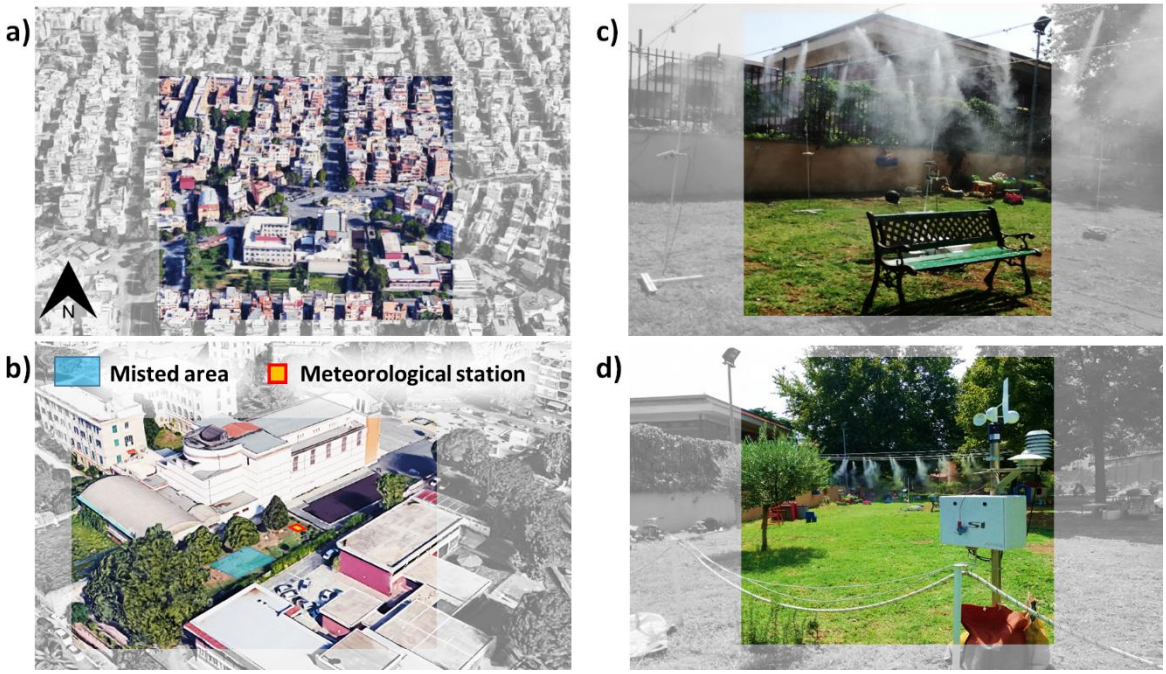

Figure 1 Aerial view of the urban district of Centocelle, Rome (a), close-up on the installation site (b), detail of the misting system (c), detail of the meteorological station and relative position to the misted area (d)

The microclimatic conditions in July-August in Rome reflect typical hot-summer Mediterranean characteristics (Csa Köppen-Geiger class) with temperatures about 8.7 °C above the annual mean and protracted dry conditions (around 17 mm of rain compared to a monthly average of 114 mm) [18].
The dry mist system was tested under diverse weather conditions on different days [10]. However, ENVI-met was calibrated on one day (see section 2.2.3), when the misting operated continuously from 11 am to 7 pm (CET/UTC+2). A suite of sensors recorded the perturbation induced by the mist. Notably:

- a weather station was installed about 16 m away from the ground-projected perimeter of the misting matrix, to characterize the undisturbed condition for comparative analysis. The station measured Ta (accuracy 0.2 °C), RH (accuracy 1.5 %), GSR (accuracy 5 %), ws and wd (accuracy 1.5 % and 1 °) with a time step of 1 minute.
- A grid of 5 thermohygrometers (accuracy ± 0.2 °C and ±2 %) was placed at 1.1 m above the ground, in compliance with ISO 7726 in case of standing subjects [37]. One sensor was placed in the middle of the misted area, while the remaining four were distributed underneath the outermost lines of nozzles along the cardinal directions. This sensing network mapped the spatial heterogeneity and the temporal variability of cooling and humidification. Accordingly,

it featured high responsiveness (10 s response time), low risk of saturation (by means of anti-wetting HDPE covers) and sun-protection (white screens).

The meteorological station was aligned with the central, northern and southern thermohygrometers to be exposed to equal solar radiation in view of the local shading elements. Water temperature was also monitored by performing time-discretized measurements with a PT100 during the day: it ranged within 19±1 °C.

The schematics of the sensor distribution in the misted area is showed in Figure 2, in overlap with the nodes of ENVI-met's grid and receptors, that will be described in section 2.2.1.

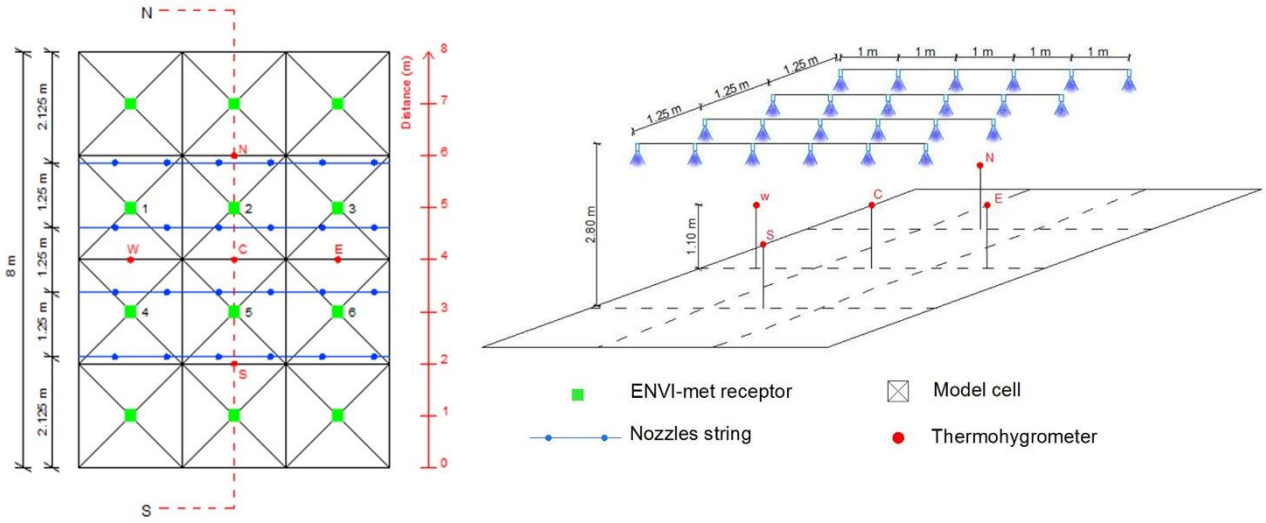

Figure 2 Schematics of the misted area with the nozzles' distribution overlapped to the ENVI-met model cells. Thermohygrometers and ENVI-met receptors are also indicated. Thermohygrometers are identified with letters according to their position: N (north), C (centre), S (south), W (west), E (east). The North (N) - South (S) section of the area is identified for subsequent analyses.

2.2. Numerical model

ENVI-met is a software based on a three-dimensional model for the simulation of surface-plant-air interactions, often used to simulate urban environments [36]. It includes a full 3D Computational Fluid Dynamics model which solves the Reynolds-averaged non-hydrostatic Navier-Stokes equations for each grid in space and for each time step [38]. The software also includes models for: shortwave and longwave radiation fluxes with respect to shading, reflection and re-radiation from buildings, soils and vegetation; evapo-transpiration and sensible heat flux from the vegetation [39]; water balance and water uptake of vegetation; dynamic heat balance in the buildings envelope; water- and heat exchange inside the soil; dispersion of gases and particles and their deposition on pervious and impervious surfaces [38]. ENVI-met also includes the possibility to model water sprayed into the local atmosphere as a specific "particle dispersing source". The main input parameters required to perform ENVI-met simulations include meteorological data, features and properties of ground surfaces, vegetation and buildings, initial soil wetness and temperature profiles [40]. The following sub-sections provides details on the ENVI-met model developed within this study.

2.2.1. Model Area and characteristics of buildings and surfaces

Stretched over 800 m², the park was discretized with 50x50x30 grid cells (XxYxZ) in the ENVI-met area input file. The horizontal resolution was 2 m, whereas the vertical resolution was 0.5 m from ground-level to 3 m height, then followed a 20 % telescoping increment to the top of the domain (about 180 m). Six "nesting grids" surrounding the core of the 3D model were included at the borders,

to take into account the local roughness and thermal contribution given by the surrounding buildings and the asphaltic/green surfaces around (Figure 3).

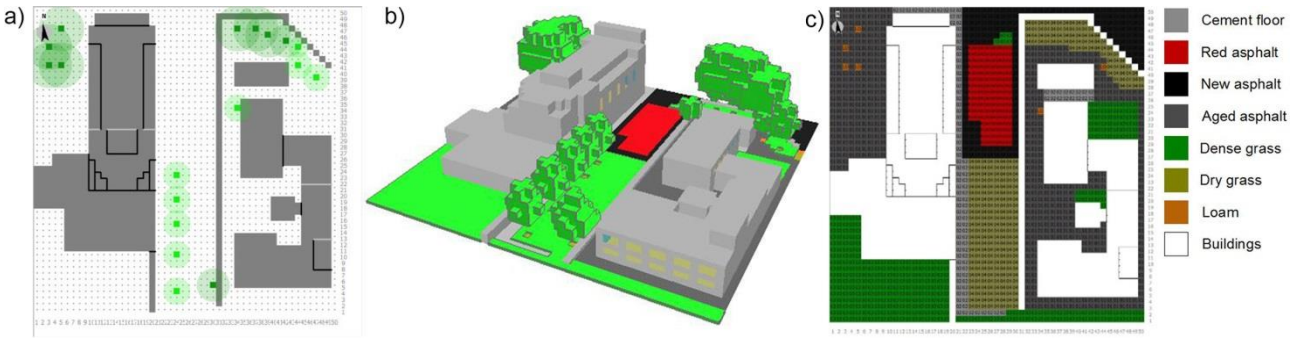

Figure 3 Plan view (a), 3D view (b), plan view with soil features (c) of the geometric model

The two buildings included in the core domain were characterized in terms of envelope's thermo-physical properties, based on standard values tabulated in ISO 10456 [41] and UNI 10351 [42]. Erected in the early 30s, the church is built in reinforced concrete, with brick roofing tiles, plastered on all facades, but the northern one, which is covered with red bricks. The polyclinic dates back to the 60s, hence the structure is in reinforced concrete, plastered infill wall and flat waterproofed roof. Given the specific dating, we assumed no thermal insulation.

The local arboreal species (linden, pine, sycamore and robinia) were included in the dedicated ENVI-met module to rely on appropriate proportion, while the grassy mantle was specified through the "Plants" database, within the sub-categories dense and dry grass.

The other types of soil surfaces present in the study area were therefore defined in the software database "soil" (Figure 3(c)). The soil parameters were obtained through the Clapp & Hornberger hydraulic scheme which allows to describe the thermal conductivity of the soil according to its water content [43]. The stratigraphic profile of the soil for a thickness of 4.5 m was defined on the basis of documentation available on the site of the Department for the Geological Service of Italy [44]. Appendix A reports the summary tables on: the thermo-opto-physical properties of the materials used for the modelled built elements and the main characteristics of trees and soils.

Finally, within the study area, the "receptors" have been defined, i.e. the projections of the vectors in the vertical direction used to probe the simulation results (atmospheric data, exchanged radiative flows and soil characteristics). As displayed in Figure 2, 12 receptors were located in the misted area, while another receptor was placed at the weather station location.

2.2.2. Water mist cooling properties

The water nozzles can be inserted in ENVI-met as punctual "water sources" at the center of the grid cells. Having cells of 2 m x 2 m, 6 water sources (each corresponding to 4 nozzles) were placed in the misted area in correspondence with the receptors, but at the specific height of 2.8 m, providing a total water flow of 90 l/h (15 l/h per water source), which is equivalent to the experimental supply (Figure 2). Their features were managed in the section "pollutant conditions" of the project advanced settings in ENVI-met.

According to the technical documentation provided by M. Bruse (personal communication, September 29, 2020), ENVI-met computes the energy required to evaporate the water and the corresponding local decrease in air temperature. Unevaporated droplets are entrained in the wind flow and are subject to sedimentation processes with a downward settling velocity depending on their size.

The main simplification relies on the particle tracing. Two main approaches are commonly used in CFD analysis, both considering that the droplet diameter would decrease along with evaporation until the droplet has vanished. The first one is the discrete approach, according to which different droplets sizes in the air volume are grouped into n bins and evaporation at their surface is numerically translated into a shift of the number of droplets towards smaller bins [45]. The second is the Lagrangian approach, in which the state and size of each droplet is monitored and calculated individually. Both ways are not realistic for a relativity small sub model of ENVI-met, in terms of required computing resources and calculation time. To simplify the process of droplet evaporation, the droplets do not change their size (nor their mass) in ENVI-met, but their quantity. The prognostic variable is the amount of liquid droplets within a given air volume, w_D (g/m^3) which is related to the number of droplets N_D and the mean droplet radius r_D (μm) as follows:

$$N_D = \frac{w_D}{0.001 \cdot \rho_w \cdot \frac{4}{3}\pi \cdot r_D^3} \quad (1)$$

Beyond evaporation, ENVI-met considers a number of drivers for the spatial and temporal distribution of water spray, namely advection, diffusion, transport, local production (sources of spray) and sedimentation (sinks of spray). Transport is assumed to be instantaneous as very small droplets tend to behave like gases. As such, the droplets follow the air flow stream lines without inertial delays and the only extra velocity component is the settlement velocity due to gravitational forces. All other parameters (e.g. turbulent diffusion) are assumed to be equal to each other inert mass component. Overall, the partial differential equation that describes the atmospheric balance over time is of the same form of the advection-diffusion equation, used for the dispersion of gases and particulate matter:

$$\frac{\partial w_D}{\partial t} + u_i \frac{\partial w_D}{\partial x_i} = \frac{\partial}{\partial x_i}\left(K_q \frac{\partial w_D}{\partial x_i}\right) + Q_{w_D}(x,y,z) + S_{w_D}(x,y,z) \quad (2)$$

where u_i={u,v,w} is the wind velocity vector corresponding to the Cartesian coordinates x_i={x,y,z}, K_q is the water vapor diffusion coefficient while Q_{w_D} and S_{w_D} are the source and sink terms, respectively. In Eq. 2, w_D is expressed in μg/kg. The rate of evaporation is strongly dependent on the droplet's temperature, which is estimated through the energy conservation equation:

$$L(T_D)\frac{\partial m_D}{\partial t} = A_D \cdot K \cdot (T_D - T_a) + Q_{kw} + A_D \cdot \sigma_B \varepsilon (T_D^4 - T_{env}^4) \quad (3)$$

where L is the latent heat, A_D is the droplet surface area ($4\pi r_D^2$), K is the sensible heat transfer coefficient between droplet and air (inclusive of molecular and turbulent processes), Q_{kw} is the shortwave radiation, σ_B is the Stefan-Boltzmann constant, ε the emissivity and T_{env} is the radiant temperature of the surroundings (representative of the longwave radiative fluxes from the environment). Based on the transient resolution of Pruppacher and Klett's heat transfer equation, Edson [46] and Andreas [47] observed that sprayed droplets tend to quickly approach the wet bulb temperature T_{wb}, regardless of the initial conditions. As such, the estimation of T_D can be directly replaced by the estimation of T_{wb}. This simplified procedure is adopted in ENVI-met.

The change of mass of a single droplet depends on the vapor pressure difference Δe between air and droplet according to the following equation:

$$\frac{\partial m_D}{\partial t} = -4\pi r_D \cdot f_v \cdot D_v \cdot \frac{\Delta e}{\left(1 - \frac{\bar{e}}{p}\right) R_v \bar{T}} \quad (4)$$

where $\bar{T}$ and $\bar{e}$ are the arithmetic means of the droplet and air temperatures and of the saturation (e_{sat}) and vapour partial (e_a) pressures, respectively, Δe is the difference between $e_{sat}(T_D)$ and e_a, p is the

total pressure, R_v is the water vapor gas constant (taken at 461.5 J/kgK), whereas D_v and f_v are the vapor mass diffusivity and the ventilation factor, calculated according to Bird et al. [48] and Rouault et al. [45] respectively:

$$D_v = 2.4995 \cdot 10^{-5} \left(\frac{T_a}{292.88}\right)^{2.334} \quad (5)$$

$$f_v = \begin{cases} 0.78 + 0.308\, N_v, & for\ N_v \leq 1.4 \\ 1.0 + 0.108\, N_v^2 & elsewhere \end{cases} \quad (6)$$

The ventilation factor takes into account the motion of air around the droplet due to wind flow and settling of the droplet, based on N_v, which is a function of the Schmidt and Reynolds numbers.
In the simulations, the water density was set to 1 g/cm^3 to suit the measured temperature range (19±1 °C), while the droplet's mean diameter was set to reflect that measured by patternation (see Section 2.1). As stated above, ENVI-met represents the whole cloud of droplets by a single mean diameter, rather than a statistical distribution (e.g. Rosin Rammler, commonly adopted in other CFD software [49]). This simplification may underestimate both the cooling potential (since smaller droplets are not concerned) and the humidification (since larger droplets are not concerned). To verify which mean diameter best captured the experimental temperatures, we carried out a sensitivity analysis. Fig. 4 shows that smaller diameters performed better than that experimentally measured (10 µm). This was likely ascribable to the differences between the test room and the actual urban setting where solar radiation, wind and other factors enhanced the evaporation rate and the break-up into child particles. Diameters as low as 3 µm were statistically compared by quantifying the difference from the hourly averaged experimental temperature. By setting a particle diameter of 5 µm, the best RMSE, Pearson coefficient (r) and R^2 were attained (see Fig. 4). This setting was maintained in all subsequent simulations. The water sources were activated in the model from 11 a.m. to 7.00 p.m. as in the experimental conditions.

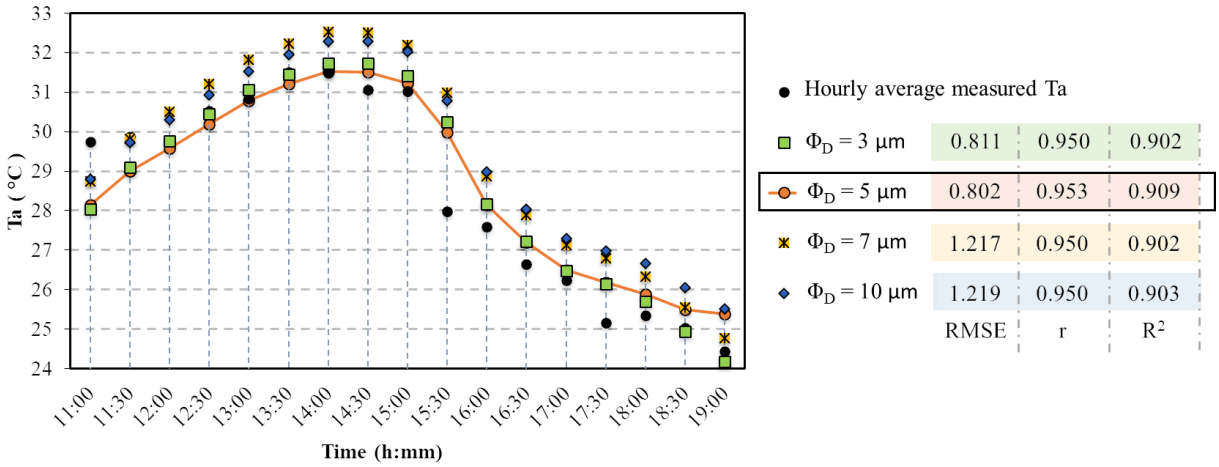

Figure 4 Sensitivity analysis to tune the mean droplet diameter. Tabulated results refer to the difference between the hourly average of the measured air temperature and the corresponding simulated value for different diameters at the central receptor.

2.2.3. Boundary and operational conditions

In the time window of the monitoring campaign, the 25th of August provided an optimal frame to simulate the mist cooling: high air temperature (average above 33 °C during the central hours of the day), cloudlessness and uninterrupted activation of the pump.

The start time was set at 5:00 a.m. of the 24th of August and the total simulation time at 48 hours [50]. Hence, a spin-up time of 19 hours was adopted. Using the metereological measurements and ENVI-met's "simple forcing" option, we set Ta and RH boundary conditions in the 11 a.m.-7 p.m. time slot. Data from a nearby weather station were used to cover the remaining hours of the day [51]. The temperature and relative humidity profiles are shown in Figure 5. The solar irradiation adjustment was set at 0.87 to fit the measurements.

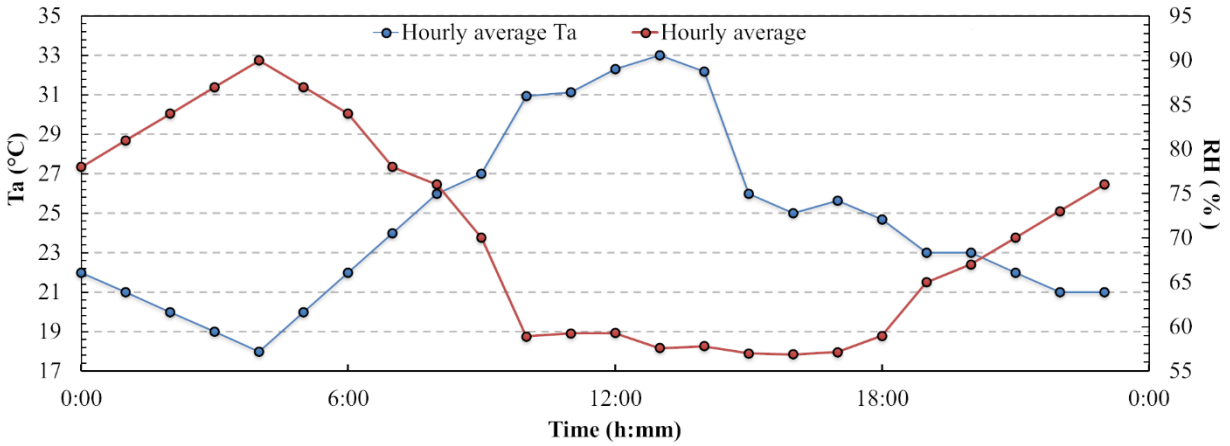

Figure 5 Ta and RH profiles on the simulated day.

The initial meteorogical conditions and the main advanced project settings are reported in Table 1. The roughness length at the measurement site was set at 0.3 m considering data reported in [52,53] for a suburban area. Wind speed at 10 m height was imposed at 2.4 m/s, considering the average speed value recorded on the ground by the climatic station (1.2 m/s) and the formula by Camacho et al. [54]. To estimate the wind direction, a frequency distribution analysis was performed, revealing a dominant south-westerly component (225 °). The imposed wind speed and direction values were confirmed by the data available online collected from a nearby climatic station [51]. The initial soil temperature conditions were set according to [55], while for the RH the default values were retained. The standard K-epsilon model was used to account for turbulence and gusts by describing the distribution and evolution of the kinetic energy in the air based on production, advection, diffusion and destruction, as well as its dissipation rate [56]. However, it was found in the literature that changing the turbulent model has negligible impact on water spray simulation [57].
The simulation time step was dynamically adjusted by ENVI-met considering the different solar angles during the days, which were mantained at the default values of 40 deg and 50 deg. The timestep was set at 2 s under the threshold of 50 deg and at 1 second over this value. The update timing was left at the default value. The output timing was set at 30 minutes for buildings and receptors and 60 minutes for the other files.

Parameters		***Value***
Wind	ws measured at 10 m height (m/s)	2.4
	wd (°)	225
	roughness length at measurement site	0.3
Ta	min. (°C)	18.0
	max. (°C)	33.0
RH	min. at 2 m height (%)	56.9
	max. at 2 m height (%)	90.0

T_i	initial building indoor temperature (°C)	26.0
Cloud cover	low clouds	0.0
	medium clouds	0.0
	high clouds	0.0
Initial soil conditions		
Soil layer	*Soil humidity (%)*	*Initial temperature (°C)*
Upper layer (0-20 cm)	70.0	25.8
Middle layer (20-50 cm)	75.0	24.8
Deep layer (50-200 cm)	75.0	19.8
Bedrock layer (below 200 cm)	75.0	17.8

Table 1 Initial meteorogical conditions and main advanced project settings

2.2.4.Simulations and sensitivity analysis on wind speed, nozzle height and density

The simulations were conducted for both the UC and for the MC scenarios. The simulated Ta and RH at receptors' level were compared to the experimental trends. Once validated (results in section 3.1), the model was used to assess the impact of the water mist cooling system on the microclimatic conditions (section 3.2). Further, to unveil the mitigation potential of the misting system and identify the room for design optimization, a sensitivity analysis was carried out in terms of: i) water flow rate, ii) injection height and iii) local wind speed (section 3.3). The following design variants were modelled and compared:

- three water flows, by doubling and halving the base-case number of injections per equal perimeter area (i.e.180 l/h, 90 l/h and 45 l/h);
- three injection heights, by moving 0.5 m above and below the base-case (i.e. 2.3 m and 3.3 m).

For each design option, the influence of wind speed was estimated by varying the 2 m value from 1 m/s to 3 m/s with a 1 m/s step, to be compared with the base-case value of 1.2 m/s. The combination of design and environmental parameterizations resulted in a total of 36 model variants.

3. Results

3.1. ENVI-met model validation

The accuracy of ENVI-met simulations at different heights and locations, under the misted and undisturbed conditions was examined with reference to the observed data. Concerning the UC, Figure 6 shows the comparison between the values measured by the climatic station and those simulated (Ta, RH, GSR). Owing to the vertical grid resolution, values are averaged between the cells centres at 0.5 m and 1.5 m, to be closest to the weather station. It can be observed how the simulated values of Ta and GSR represent a good estimate of the real trends, especially in the central and hottest hours of the day. On the other hand, the average relative humidity was systematically underestimated by the model. This has been widely reported in previous research, mostly due to the fact that the ENVI-Met model for relative humidity calculations has a limitation in the estimation of emissions and other anthropogenic sources as well as of the nocturnal plant transpiration [58,59].

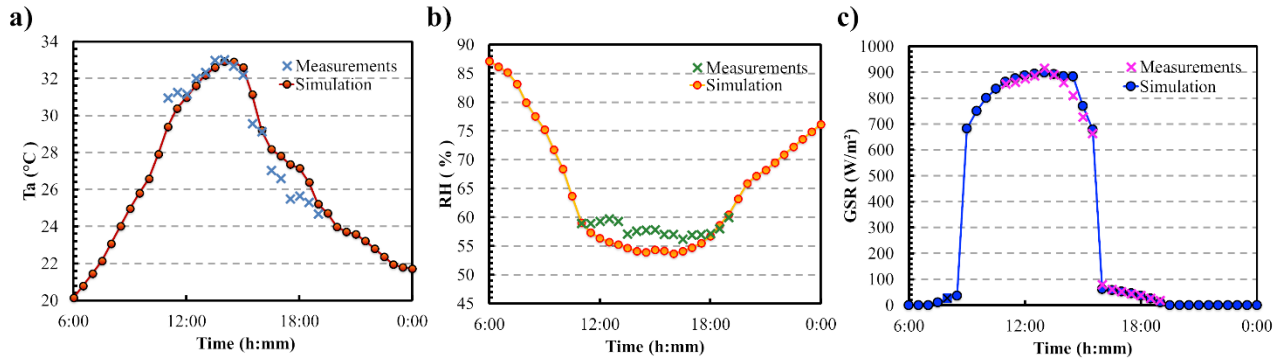

Figure 6 Comparison between the average hourly quantities measured and simulated every half an hour in the period 11 a.m-7 p.m.: Ta (a), RH (b) and GSR (c)

Table 2 shows the main statistics on the model accuracy: Pearson's coefficient of determination (R^2), Root Mean Square Error (RMSE) and Wilmott's index of agreement (d) [40,60]. The reliability increases for $R^2 \rightarrow 1$, RMSE$\rightarrow$0 and d$\rightarrow$1. Air temperature is well estimated (R^2=0.93, d=0.97) in line with the studies by Yang e al. [40] (R^2=0.94, RMSE=1.01 K), Ketterer e al. [61] (R^2=0.88, RMSE=0.28 K), Acero e al. [62] (R^2=0.92). The RMSE for RH lies within the range commonly reported in literature (2.04 %-10.20 %) [63]. Based on these results, we concluded that the ENVI-met model could provide reasonable predictions of Ta under UC.

	R^2	**RMSE**	**d**
Mean hourly Ta	0.93	0.98	0.97
Mean Hourly RH	0.29	2.7	0.38

Table 2 Performance indicators for the ENVI-met model under UC, based on measured and simulated Ta and RH (sample size for each receptor:17)

Concerning the MC, the simulated and measured values of Ta were examined between 11 a.m. and 19 p.m at each thermohygrometers' location. The validation was thus based on 85 pairs of values (17 for each point) (Figure 7, Table 3). The R^2 and d values indicate a strong agreement between simulated and measured Ta. The R^2 ranges from 0.81 to 0.93 depending on the site, with an average of 0.87, whereas d ranges from 0.93 to 0.98, being 0.96 on average. The RMSE never exceeds 0.99 °C and is 0.84 °C on average.

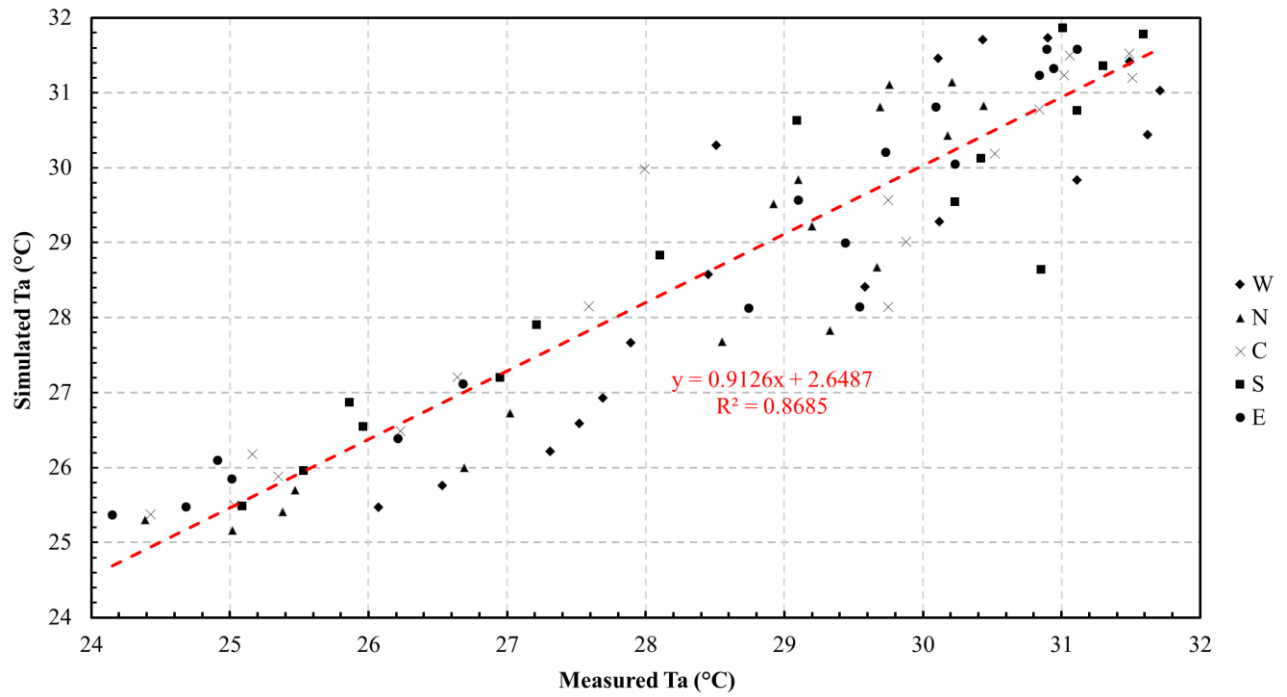

Figure 7 Comparison between simulated and measured values of Ta every half an hour in the period 11 a.m-7 p.m. at the thermohygrometers' locations

	R^2	RMSE (°C)	d
Ta (N)	0.87	0.79	0.96
Ta (S)	0.88	0.87	0.96
Ta (W)	0.81	0.99	0.93
Ta (C)	0.91	0.80	0.97
Ta (E)	0.93	0.73	0.98
Ta (all points)	0.87	0.84	0.96

Table 3 Performance indicators for the ENVI-met model under MC, based on measured and simulated Ta at the thermohygrometers' locations

By way of example, Figure 8 reports the trend of Ta at the centre of the misted area by comparing the output of the thermohygrometer C with the average between the two surrounding central receptors. Over peak hours (12 p.m to 3 p.m.) the absolute difference in average temperature is always less than 0.5 ° C. At 3.30 p.m. the measured Ta suddenly drops, due to the partial shading of the tree canopy. The simulation fails at capturing this transient phenomenon. Alignment is re-established within one hour.

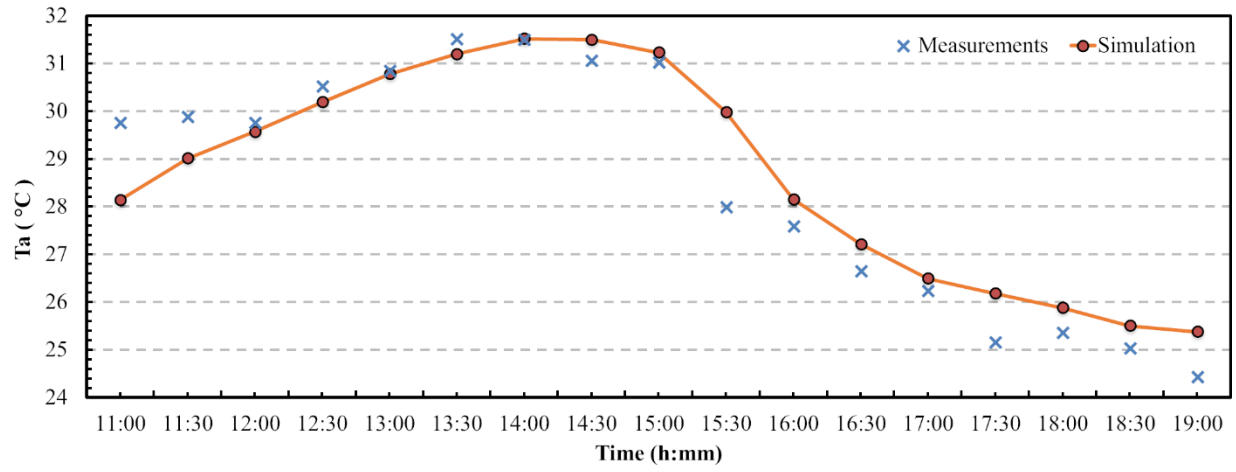

Figure 8 Comparison between average hourly measured and simulated Ta every half an hour in the period 11 a.m-7 p.m., collected at the centre of the misted area.

Figure 9 displays the box-plots of the measured and simulated Ta along the North-South section of the misted area (section line indicated in Figure 2), so as to compare trends in space. From the analysis of the experimental values (blue box-plots) recorded by the thermohygrometers at points S (south), C (centre), N (north), it can be observed that Ta decreases following the wind direction from south to north, owing to the transport of the misted droplets. The phenomenon is also correctly captured in the simulation (red box-plots). The offset between the medians at locations S and N (4 m apart) is approximately 0.8 °C, while that between the southernmost and northernmost receptors (6 m apart) reaches 1.35 °C.

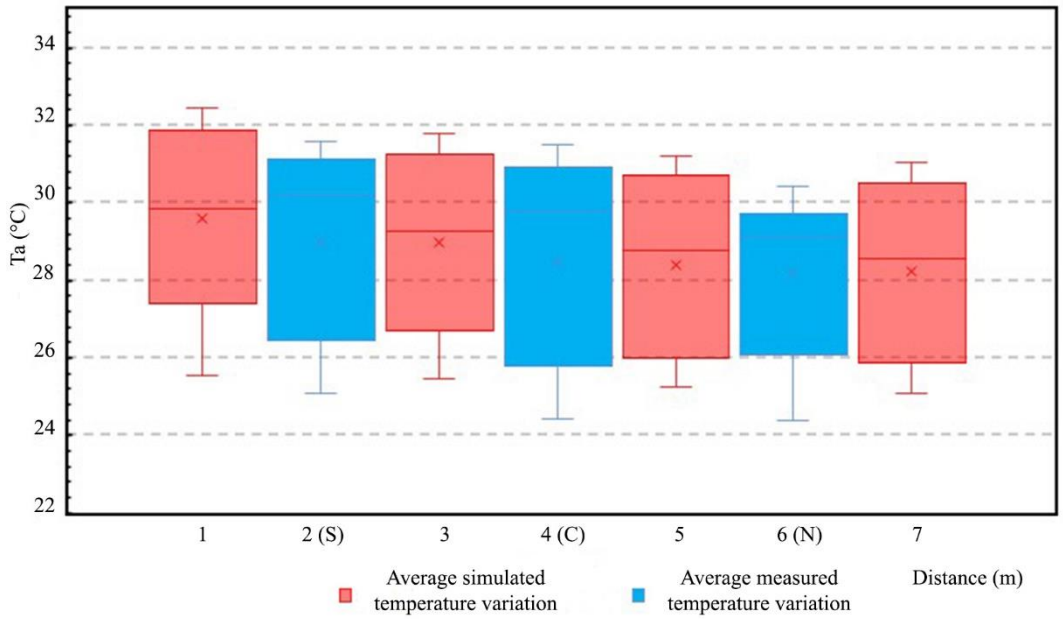

Figure 9 Box-plots of the measured (blue) and simulated (red) Ta along the N-S section of the misted area, collected every half an hour in the period 11 a.m-7 p.m.

3.2. Assessment of the impact of water mist cooling on the microclimatic conditions

With the ENVI-met model validated under both UC and MC conditions, we proceeded with the quantification of the thermal distribution induced by the mist system in the test area, to then verify the effect on the microclimate of the wider neighbourhood context.

Figure 10 shows the spatial distribution of ΔTa (difference between MC and UC) in the whole simulation domain, at 1.25 m (cell centre closest to the thermohygrometers' height) and 1.75 m (reference height of a standing person). The thermal maps refer to the peak hour (2 p.m.). The temperature ranges from about 31°C to about 34°C, consistent with the recordings of the weather station. The highest values are found over the asphalted area south-east of the domain, while the lowest ones correspond to the green area to the north-east. Significant thermal differences occur in the area right beneath the nozzles, whose effects spread further downwind, towards the north-east quadrant. At a height of 1.25 m, ΔTa peaks at 1.98 °C at 2 m distance from receptor #3 (refer to Figure 2) due north, while the minimum temperature difference (< 0.3°C) is recorded at the same distance, but due south. The evaporative cooling propagates in the north-east direction, following the wind, with reductions in the order of 0.3-0.5°C up to about 24 m away from the misted perimeter. At

a height of 1.75 m, the average thermal deviations are greater as they are detected closer to the nozzles, yet the maximum is only slightly higher (2 °C) and is recorded at the same location.

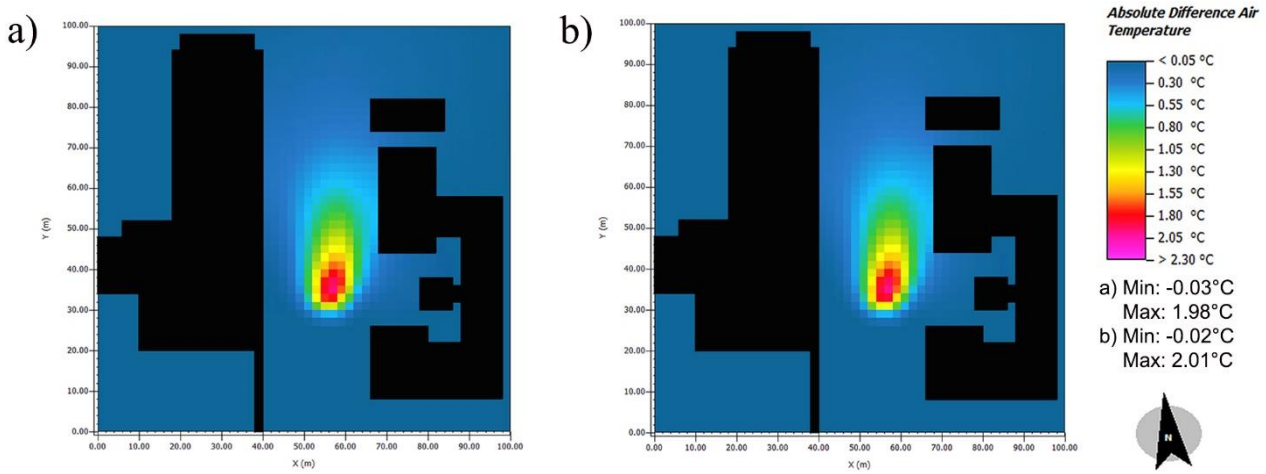

Figure 10 Simulated temperature drop in the test area at a height of 1.25 m (a) and of 1.75 m (b) at 2 p.m.

Figure 11 shows the daily ΔTa trend in the test area at 1.25 m and at 1.75m above the ground, computed as the average at the nearest receptors to N, S, W, C and E locations (see Figure 2 for reference).

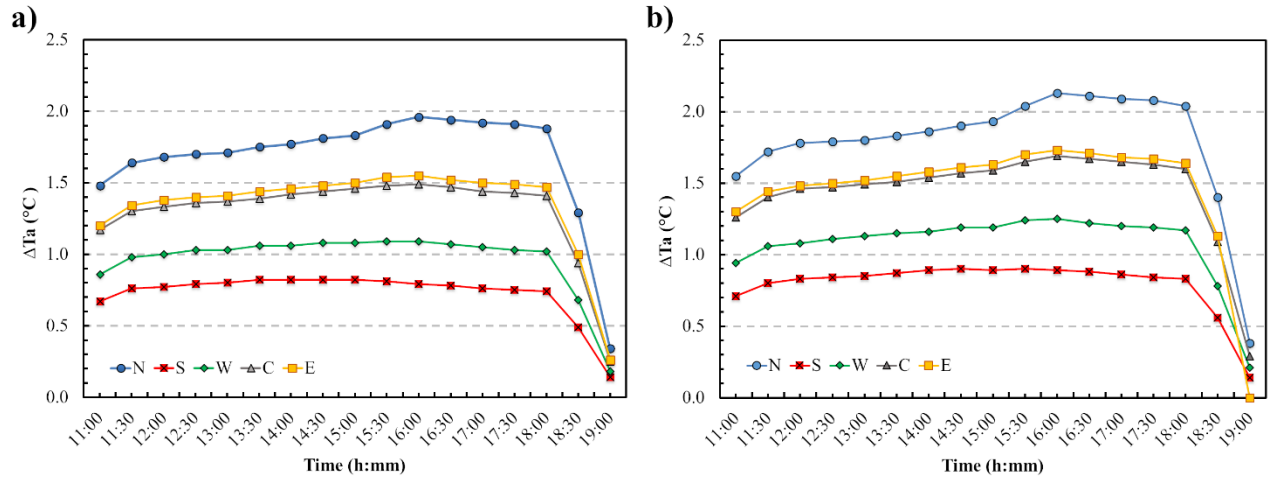

Figure 11 Simulated ΔTa in the test area (points N, S, W, C, E) at a height of 1.25 m (a) and 1.75 m (b).

The ΔTa distribution follows a similar trend at all points: generally, the most significant mean difference occurs during the hottest hours of the day, notably between 3.30 p.m. and 4 p.m. In fact, when the air temperature rises, evaporation accentuates [11,18]. The difference decreases considerably from 6 p.m. and completely vanishes half an hour after injection cessation (7.30 p.m.). At 1.25 m (Figure 11a), the maximum ΔTa is observed at point N, where it peaks just below 2 °C. Second in line are points E and C, where the thermal differences exceed 1.50 °C during the central hours of the day with a rather overlapped trend, followed by point W, whose ΔTa touches 1 °C. At point S, the smallest deviations are observed (less than 1 °C) and are maintained throughout the time of injection. At 1.75 m the thermal differences induced by the misting system are slightly higher, but with a similar spatial heterogeneity (Figure 11b).

These results confirm what has already been noted on the influence of the wind direction (Figure 9): as the microparticles of liquid water are entrained in the airflow towards the north-east, a greater local cooling effect is observed downwind. The box-plots of ΔTa along the N-S section of the site (Figure 12) highlight both the greater cooling effect and the greater dispersion of data, proceeding from south to north in the misted area.

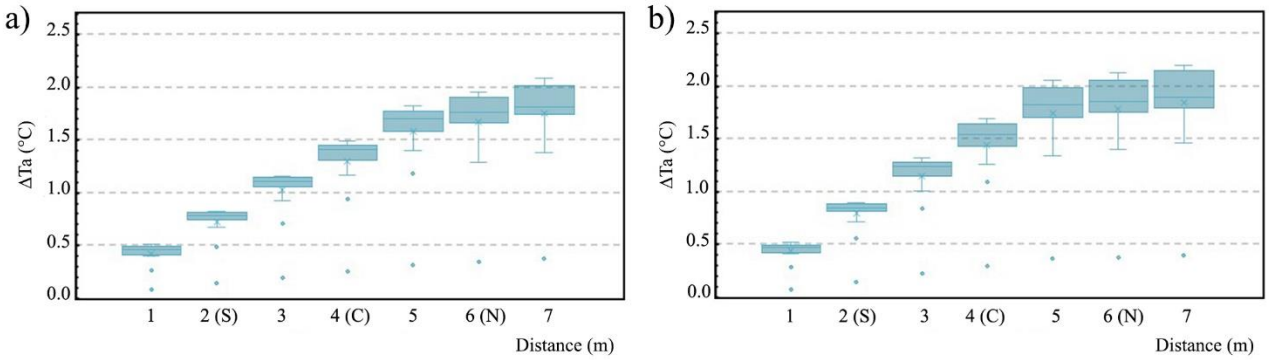

Figure 12 Box-plots of ΔTa in the test area along the N-S section at a height of 1.25 m (a) and 1.75 m (b).

3.3. Sensitivity Analysis

In this section, the mitigation potential of the mist system is analysed for the design variants described in 2.2.4, related to water flow rate, injection height and local wind speed. The graphs in Figure 13 summarize the results in terms of maximum ΔTa (recorded at 2 p.m.) at the point of maximum temperature variation (north-east of the misted area) and at a height of 1.25 m, depending on the water flow rate and for the different wind speeds considered. The three figures refer to the different injection heights, namely 2.3 m, 2.8 m (base case) and 3.3 m, in the order.

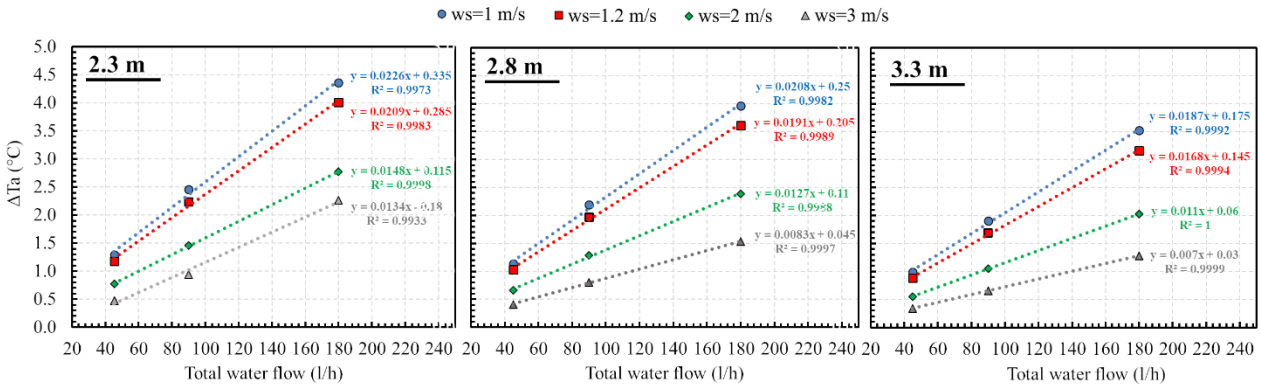

Figure 13 Maximum ΔTa recorded at 2 pm in the north-east side of the misted area and at a height of 1.25 m, as a function of water flow rate and wind speed, for injection heights of 2.3 m, 2.8 m and 3.3 m.

As expected, ΔTa increases with the water flow rate, i.e. the number of nozzles in the misted area, and decreases with higher nozzles heights. Looking at the figures, it is also clear that the mitigation potential of the water mist coolers is decreasing with an increasing wind speed. In particular, when wind speed is increasing to 2 m/s, the average decrease of the cooling potential is about 35-40 % regardless of the water flow rate. When the injection is set at 2.8 m and for ambient temperatures around 33°C, an increase in water flow rate of 10 l/h determines a magnification of the maximum

temperature delta of nearly 0.2 °C for low wind speeds (around 1-1.2 m/s), 0.1 °C at 2 m/s and <0.1 °C for higher speeds. This is also visible in the thermal maps in Figure 14 compared to those of Figure 10: here we plot the temperature drop of the model with a doubled water flow rate compared to the base case, and wind speed of 1 m/s (Figure 14 a and b) and 3 m/s (Figure 14 c and d). In presence of higher flow rate and lower wind speed, the cooling effect is significantly enhanced. On another note, higher wind speeds extend the area of influence of the system, thus providing cooling to a potentially wider number of users, although in a milder fashion. The vertical profile of the temperature drop appears fairly constant when we compare the maps at 1.25 m and 1.75 m.

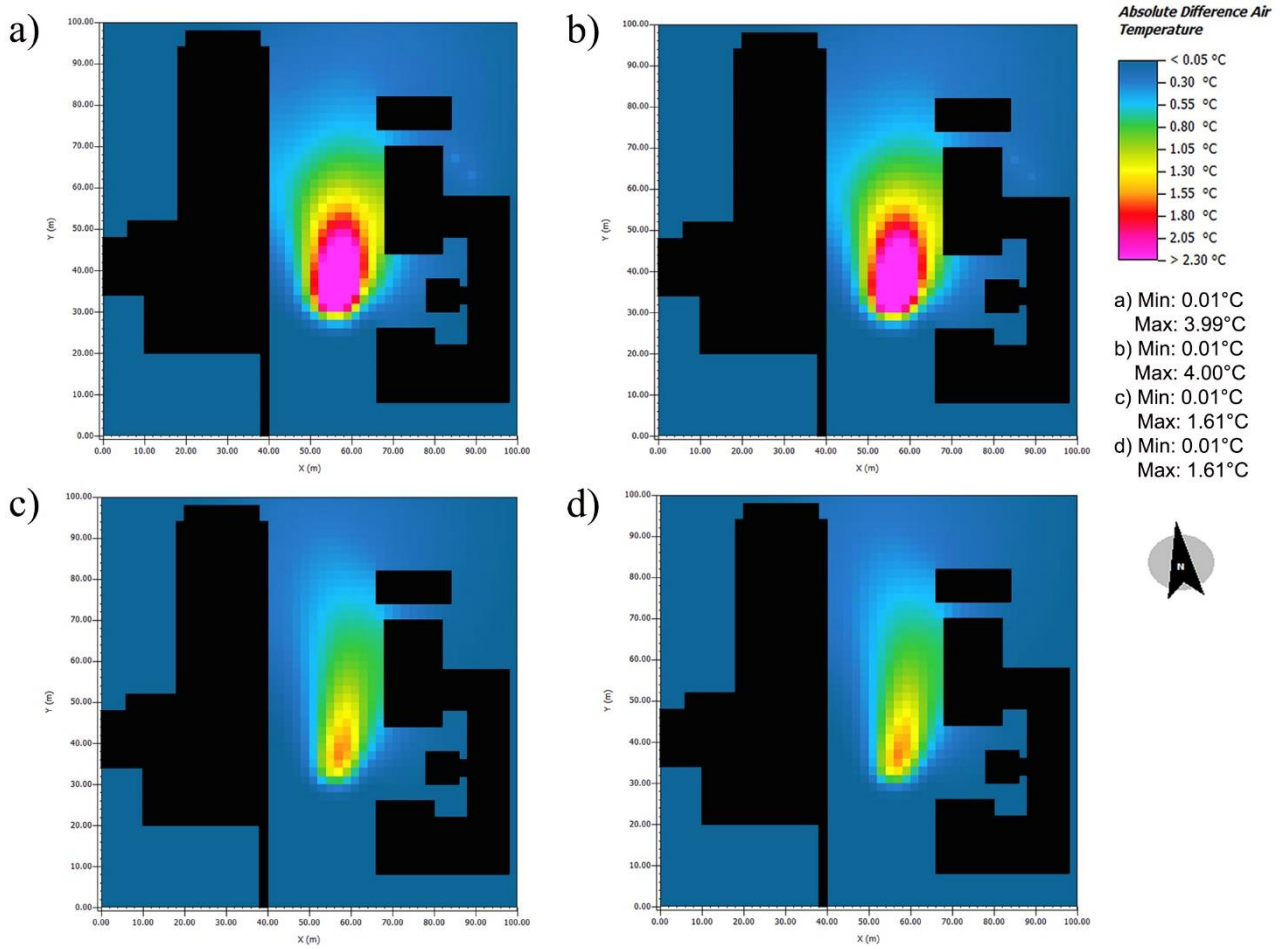

Figure 14 Simulated temperature drop in the misted area at 2 p.m with the following settings: nozzles height of 2.80 m, doubled water flow rate (180 l/h), wind speed 1 m/s at a height of 1.25 m (a) and of 1.75 m (b), wind speed 3 m/s at a height of 1.25 m (c) and of 1.75 m (d)

Looking at the leftmost and rightmost charts in Figure 13, the mitigation potential decreases by 0.1-0.5 °C when the nozzle height reaches 3.3 m and increases by 0.1-0.7 °C when the height is reduced to 2.3 m. The thermal maps in Figure 15 show that at 2.3 m and in presence of higher water flow rates, a significant cooling effect can be achieved even at relatively high wind speeds of 3 m/s (Figure 15 c and d) with the benefit of a wider cooled area.

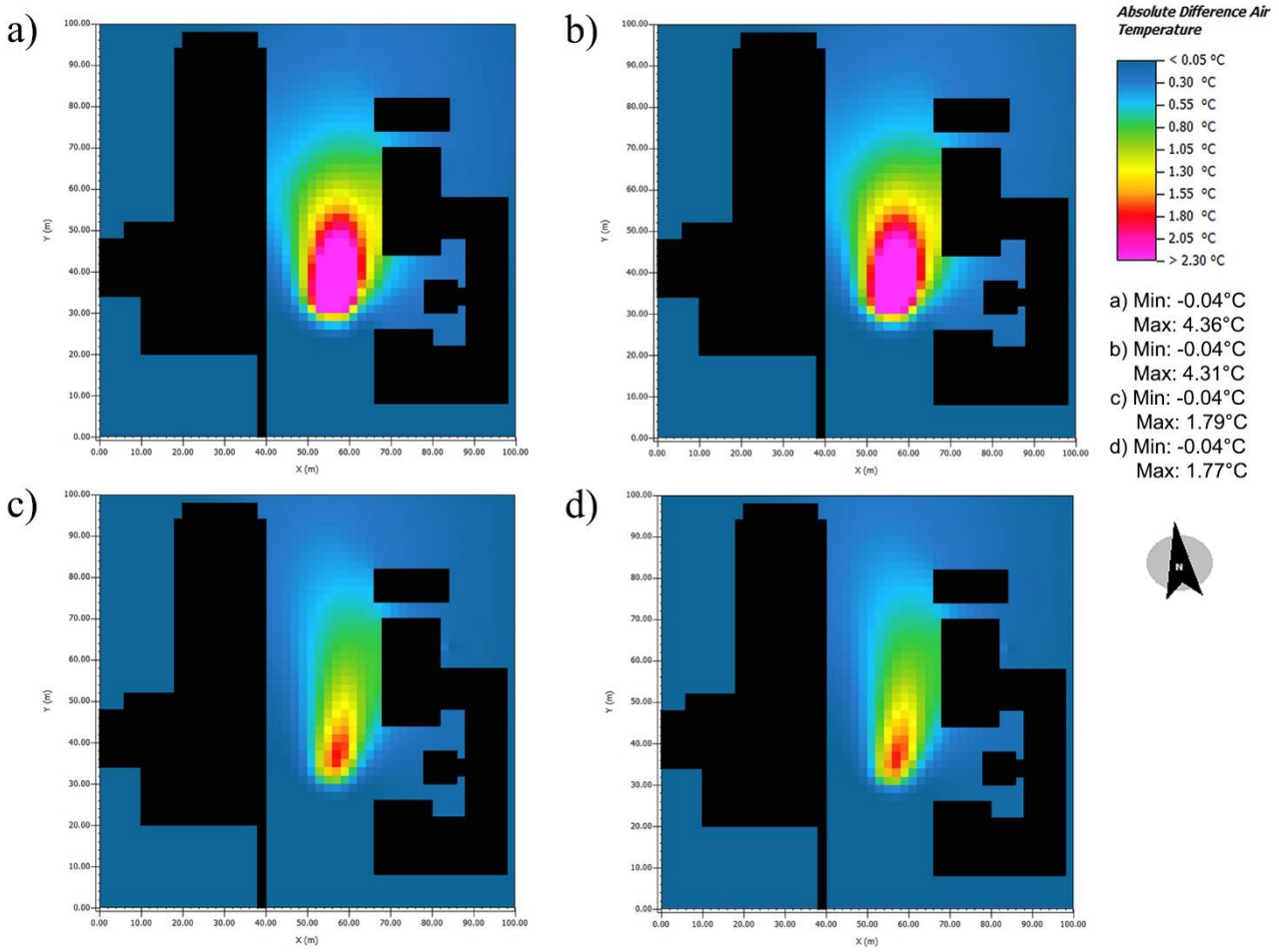

Figure 15 Simulated temperature drop in the misted area at 2 p.m with the following settings: nozzles height of 2.30 m, doubled water flow rate (180 l/h), wind speed 1 m/s at a height of 1.25 m (a) and of 1.75 m (b), wind speed 3 m/s at a height of 1.25 m (c) and of 1.75 m (d)

Finally, Figure 16 represents the vertical profiles of Ta and ΔTa recorded at 2 p.m. at the point of maximum temperature variation in the base case model compared to that of the models with different injection height. Once again, the greatest cooling effect is confirmed for a height of 2.3 m. In all cases, the maximum cooling effect is recorded in the model cell where the injectors are located, or immediately below, then it decays moving towards the soil. Interestingly, the cooling effect is also maintained at higher heights.

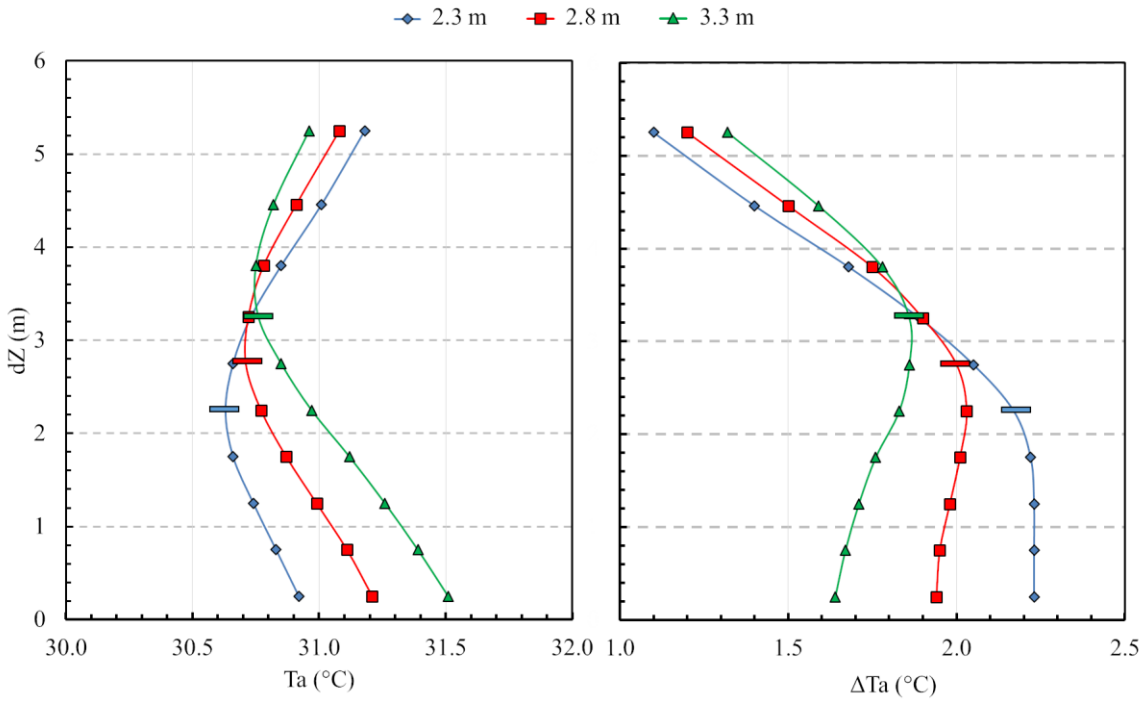

Figure 16 Vertical profiles of Ta (left side) and ΔTa (right side) recorded at 2 p.m. in the north-east side of the misted area in the base case model (red line) compared to that of the models with increased (green line) and decreased (blue line) nozzles height. The rectangular indicators represent the height of the nozzles along the vertical profile.

4. Discussion

In this study, a water spray model was developed in ENVI-met. Compared to other CFD platforms, ENVI-met's approach to water spray tracking relies on two simplifying assumptions: i) all droplets have the same diameter (no statistical distribution) and ii) the amount of droplets in a given air volume changes due to evaporation, but not their size. By not considering any statistical distribution, ENVI-met's water spray model might be prone to inaccuracies both in terms of cooling and humidification, since the droplet size governs the heat and mass transfer rates between the continuous (air) and discrete (water) phase. To overcome this issue, a preliminary tuning procedure on the mean droplet diameter was proposed. The results reasonably matched the experimental data from a real case in urban settings in terms of temperature evolution both under undisturbed and misted conditions as quantified by Pearson's coefficient of determination, Root Mean Square Error and Wilmott's index of agreement. With a horizontal discretization of 2 m x 2 m and a vertical discretization of 0.5 m, the temperature distribution was replicated with good accuracy both horizontally and vertically. Notably, the vertical profile of the temperature difference beneath the injections responded to a Lorentzian-like distribution, matching the experimental results by Ulpiani et al. [10]. Conversely, the model failed at predicting the relative humidity, as also reported elsewhere.

The simulations tracked the cooling action in and out of the misted perimeter, allowing to quantify the spatial extension of the influence area. Indeed, it was proved that the most significant thermal drops (1.95 °C at 1.25 m height) occurred close but out of the misted perimeter, following the wind direction. Temperature reductions (in the order of 0.3-0.5 °C) persisted downwind, up to about 24 m away from the misted perimeter. The mist cooling was most impactful, on average, during the hottest hours of the day, which is in line with well-established results in literature [11] and is a direct consequence of psychrometric conditions more conducive to evaporative cooling.

As displayed in Figures 6-9, there was a systematic offset between measured and simulated air temperature (amounting at 1 °C, on average), which was positive during morning hours (before midday) and negative during afternoon and evening hours (after 3.30 p.m.). Conversely, over peak hours, the absolute values were captured almost perfectly. It is straightforward to assume that the effect of solar shading from the tree leaves and the buildings all around was not fully reflected in the simulation and, as such, represented a major source of error. Also, the morning time mismatch suggests that the model may have not captured the decline in evaporative cooling potential that occurred due to the concurrent evaporation of condensed moisture and water stored in the green soil overnight. From Figure 7, it is also evident that the dispersion of values incremented at higher air temperatures (over 28-29 °C). The reason might be found in the increased local turbulence that is engendered close to ground level as a result of mightier upward moving thermals, which may have had an impact on the dilution and dispersion of droplet particles.

The sensitivity analysis further delved into the role played by water flow rate, injection height and wind speed. As expected, at 1.25 m above the ground, the temperature difference in the misted scenario compared to the undisturbed case increased with the density of nozzles and decreased with higher injection height. This is in contrast with the simulation results by Yamada et al., in which nor the number of nozzles (varied from 1 to 3, at 2.5 m intervals) nor the size (average diameter change in the order of 10 µm) significantly affected the cooling potential [22]. The cooling decreased by 0.1-0.5 °C when the nozzle height was lifted to 3.3 m and increased by 0.1-0.7 °C when the height was reduced to 2.3 m, compared to the baseline at 2.8 m. It was also clearly demonstrated that the cooling capacity of mist coolers diminished with increasing wind speed (average decrease of 35-40 % in response to 0.8 m/s acceleration). Notably, when the injection was set at 2.8 m above the ground, and for ambient temperatures around 33°C, an increase in water flow rate of 10 l/h determined a magnification of the maximum temperature drop of nearly 0.2 °C for low wind speeds (around 1-1.2 m/s), 0.1 °C for winds of 2 m/s and <0.1 °C for higher speeds. Hence, doubling the number of nozzles caused the maximum ΔTa to rise from 1.97 °C to 3.62 °C, with extra +0.3 °C under light breeze (1 m/s). Conversely, the drop decreased down to 1.53 °C when the wind blew at the maximum considered speed of 3 m/s.

This study offers itself as a guideline for other users in the setup of water spray modelling scenarios in ENVI-met, to be gradually refined as more data and documentation will be available. Indeed, the evaporative cooling provided by the present water spray system is not high in absolute values and thus non-optimal for the software validation. Further verification may be needed to substantiate our findings. On the other hand, the model captured with good accuracy the experimental magnitude and the trends both in space and in time. This entails that the underlying equations well reflected the effects of diffusion, dilution, directionality, dynamic variability and the interlacement with other phenomena pertaining to the local surroundings. Moreover, experimental and modelled results are in good agreement only for a droplet diameter distribution that is very close with that obtained by direct measurement and deviate for smaller or larger diameters. This demonstrates that the model responds with sufficient accuracy, despite the assumptions. Further research will be conducted to test different experimental setups and thus different evaporative cooling intensities under diverse climatic contexts and possibly with due attention to absolute humidity, to overcome most of the above limitations and proceed towards an informed use of the software's models.

5. Conclusion

Dry mist systems may play a crucial role in combating the phenomenon of urban overheating at local scale. Compared to alternative evaporative technologies, the water consumption is very modest and the risk of wettedness very marginal, especially when the cooling action is smartly controlled. Their beneficial action includes air conditioning energy use minimization, solar radiation attenuation and pollution removal. As mist cooling gains popularity as urban overheating countermeasure and gets more and more used for streetscaping, urban greening plans, comfort enhancement also from private parties, it is extremely important to assess its effectiveness in relation to other typical urban microclimatic phenomena (e.g. canyon effects, evapotranspiration, reduced soil permeability, anthropogenic heat). This can be done using well-established urban microclimatic models, such as ENVI-met. ENVI-met includes a water spray model which, to the best of our knowledge, has never been experimentally validated and still lacks proper documentation.

Against this backdrop, we investigated how misting systems perturb the local urban climate by means of a 3D microclimatic model in ENVI-met, thoroughly validated on the basis of experimental evidence and tested under different design and environmental scenarios. Following a careful setup procedure, our model accurately recreated the trends and impacts of mist cooling at neighbourhood scale considering the competing effects of greenery and urban forcing. Through simulation, we could i) quantify the spatial extension of the cooled area under different environmental conditions and thus complement the experimental results with no need for extensive sensor networks ii) determine the sensitivity of the cooling action to wind speed, water flow rate and nozzle's height above the ground via parametric analysis and iii) derive substantiated design criteria to be applied at both manufacturing and urban planning level. For instance, we demonstrated that mist cooling could be still impactful under windy conditions if the injections are lowered down enough, since the local temperature reduction would still be significant at pedestrian height while the risk of wettedness would be strongly mitigated by the considerable jet deflection.

Further research would target climate dependencies and would include different misting systems to extend the applicability of the above results and further verify the model accuracy.

Acknowledgments

Authors warmly thank the Italian national agency for new technologies, energy and sustainable economic development (ENEA) - under the funding PAR 2017 sub-project D.6 Sviluppo di un modello integrato di smart district urbano - for providing the resources to build the prototype.

References

[1] M. Santamouris, C. Cartalis, A. Synnefa, D. Kolokotsa, On the impact of urban heat island and global warming on the power demand and electricity consumption of buildings—A review, Energy Build. 98 (2015) 119–124. doi:10.1016/j.enbuild.2014.09.052.

[2] M. Santamouris, Recent progress on urban overheating and heat island research. Integrated assessment of the energy, environmental, vulnerability and health impact. Synergies with the global climate change, Energy Build. 207 (2020). doi:10.1016/j.enbuild.2019.109482.

[3] IPCC Special Report, (n.d.).

[4] M. Santamouris, Heat island research in Europe: The state of the art, Adv. Build. Energy Res. 1 (2007) 123–150. doi:10.1080/17512549.2007.9687272.

[5] M. Santamouris, Analyzing the heat island magnitude and characteristics in one hundred Asian and Australian cities and regions, Sci. Total Environ. 512–513 (2015) 582–598. doi:10.1016/j.scitotenv.2015.01.060.

[6] UN-HABITAT, Global Report on Human Settlements 2011: Cities and Climate Change, 2011.

[7] G.Y. Yun, J. Ngarambe, P.N. Duhirwe, G. Ulpiani, R. Paolini, S. Haddad, K. Vasilakopoulou, M. Santamouris, Predicting the magnitude and the characteristics of the urban heat island in coastal cities in the proximity of desert landforms. The case of Sydney, Sci. Total Environ. 709 (2020) 136068. doi:10.1016/j.scitotenv.2019.136068.
[8] O. Aleksandrowicz, M. Vuckovic, K. Kiesel, A. Mahdavi, Current trends in urban heat island mitigation research: Observations based on a comprehensive research repository, Urban Clim. 21 (2017) 1–26. doi:10.1016/j.uclim.2017.04.002.
[9] E.J. Gago, J. Roldan, R. Pacheco-Torres, J. Ordóñez, The city and urban heat islands: A review of strategies to mitigate adverse effects, Renew. Sustain. Energy Rev. 25 (2013) 749–758. doi:10.1016/j.rser.2013.05.057.
[10] G. Ulpiani, E. Di Giuseppe, C. Di Perna, M. D'Orazio, M. Zinzi, Thermal comfort improvement in urban spaces with water spray systems: Field measurements and survey, Build. Environ. 156 (2019) 46–61. doi:https://doi.org/10.1016/j.buildenv.2019.04.007.
[11] G. Ulpiani, Water mist spray for outdoor cooling: A systematic review of technologies, methods and impacts, Appl. Energy. 254 (2019) 113647. doi:10.1016/j.apenergy.2019.113647.
[12] C. Farnham, M. Nakao, M. Nishioka, M. Nabeshima, T. Mizuno, Effect of Water Temperature on Evaporation of Mist Sprayed From a Nozzle, J. Heat Isl. Inst. Int. 10 (2015) 35–44.
[13] T. Ishii, M. Tsujimoto, G. Yoon, M. Okumiya, Cooling System with Water Mist Sprayers for Mitigation of Heat-island Drymist system : Uchimizu, Seventh Int. Conf. Urban Clim. (2009) 2–3.
[14] D. Narumi, K. Shigematsu, Y. Shimoda, Effect of the Evaporative Cooling Techniques by Spraying Mist Water on Reducing Urban Heat Flux and Saving Energy in Apartment House, J. Heat Isl. Inst. Int. 7 (2012) 175–181. http://heatisland2009.lbl.gov/docs/221000-narumi-doc.pdf.
[15] S. Yu, Water spray geoengineering to clean air pollution for mitigating haze in China's cities, Environ. Chem. Lett. 12 (2014) 109–116. doi:10.1007/s10311-013-0444-0.
[16] L.A. Dombrovsky, V.P. Solovjov, B.W. Webb, Attenuation of solar radiation by a water mist from the ultraviolet to the infrared range, J. Quant. Spectrosc. Radiat. Transf. 112 (2011) 1182–1190. doi:10.1016/j.jqsrt.2010.08.018.
[17] K.R. Gunawardena, M.J. Wells, T. Kershaw, Utilising green and bluespace to mitigate urban heat island intensity, Sci. Total Environ. 584–585 (2017) 1040–1055. doi:10.1016/j.scitotenv.2017.01.158.
[18] G. Ulpiani, C. Di Perna, M. Zinzi, Water nebulization to counteract urban overheating : Development and experimental test of a smart logic to maximize energy efficiency and outdoor environmental quality, Appl. Energy. 239 (2019) 1091–1113. doi:10.1016/j.apenergy.2019.01.231.
[19] H.R. Pruppacher, J.D. Klett, Microphysics of Clouds and Precipitation, 1997.
[20] G. Ulpiani, E. Di Giuseppe, C. Di Perna, M.D. Orazio, M. Zinzi, Design optimization of mist cooling for Urban Heat Island mitigation: experimental study on the role of injection density, (2019). doi:10.1088/1755-1315/296/1/012025.
[21] G. Ulpiani, C. Perna, M. Zinzi, Mist cooling in urban spaces: Understanding the key factors behind the mitigation potential, Appl. Therm. Eng. (2020) 115644. doi:10.1016/j.applthermaleng.2020.115644.
[22] H. Yamada, G. Yoon, M. Okumiya, H. Okuyama, Study of cooling system with water mist sprayers: Fundamental examination of particle size distribution and cooling effects, Build. Simul. 1 (2008) 214–222. doi:10.1007/s12273-008-8115-y.
[23] J. Wang, X. Tu, Z. Wang, J. Huang, Application and Numerical Simulation on Water Mist Cooling for Urban Environment Regulation, in: Lect. Notes Comput. Sci., 2010. doi:10.1007/978-3-642-15859-9.
[24] H. Montazeri, B. Blocken, J.L.M. Hensen, CFD analysis of the impact of physical parameters

on evaporative cooling by a mist spray system, Appl. Therm. Eng. 75 (2015) 608–622. doi:10.1016/j.applthermaleng.2014.09.078.
[25] H. Montazeri, Y. Toparlar, B. Blocken, J.L.M. Hensen, Simulating the cooling effects of water spray systems in urban landscapes: A computational fluid dynamics study in Rotterdam, The Netherlands, Landsc. Urban Plan. 159 (2017) 85–100. doi:10.1016/j.landurbplan.2016.10.001.
[26] H. Barrow, C.W. Pope, Droplet evaporation with reference to the effectiveness of water-mist cooling, Appl. Energy. 84 (2007) 404–412. doi:10.1016/j.apenergy.2006.09.007.
[27] C. Farnham, M. Nakao, M. Nishioka, M. Nabeshima, T. Mizuno, Study of mist-cooling for semi-enclosed spaces in Osaka, Japan, Procedia Environ. Sci. 4 (2011) 228–238. doi:10.1016/j.proenv.2011.03.027.
[28] W. Jun-feng, T. Xin-cheng, Experimental Study and Numerical Simulation on Evaporative Cooling of Fine Water Mist in Outdoor Environment, 2009 Int. Conf. Energy Environ. Technol. (2009) 156–159. doi:10.1109/ICEET.2009.44.
[29] M. Kojima, K. Nakashima, S. Management, A Study of Mist Spraying System by Urban Transportation, Des. Innov. Value Towar. a Sustain. Soc. Springer, Dordr. (2012) 720–723.
[30] C. Huang, J. Cai, Z. Lin, Q. Zhang, Y. Cui, Solving model of temperature and humidity profiles in spray cooling zone, Build. Environ. 123 (2017) 189–199. doi:10.1016/j.buildenv.2017.06.043.
[31] M. Santamouris, S. Haddad, M. Saliari, K. Vasilakopoulou, A. Synnefa, R. Paolini, G. Ulpiani, S. Garshasbi, F. Fiorito, On the energy impact of urban heat island in Sydney: Climate and energy potential of mitigation technologies, Energy Build. 166 (2018). doi:10.1016/j.enbuild.2018.02.007.
[32] S. Haddad, G. Ulpiani, R. Paolini, A. Synnefa, M. Santamouris, Experimental and Theoretical analysis of the urban overheating and its mitigation potential in a hot arid city – Alice Springs, Archit. Sci. Rev. (2019) 1–16. doi:10.1080/00038628.2019.1674128.
[33] S. Tsoka, K. Tsikaloudaki, T. Theodosiou, Coupling a building energy simulation tool with a microclimate model to assess the impact of cool pavements on the building's energy performance application in a dense residential area, Sustain. 11 (2019). doi:10.3390/su11092519.
[34] A. Aboelata, S. Sodoudi, Evaluating the effect of trees on UHI mitigation and reduction of energy usage in different built up areas in Cairo, Build. Environ. 168 (2020) 106490. doi:10.1016/j.buildenv.2019.106490.
[35] G. Battista, R. de Lieto Vollaro, M. Zinzi, Assessment of urban overheating mitigation strategies in a square in Rome, Italy, Sol. Energy. 180 (2019) 608–621. doi:10.1016/j.solener.2019.01.074.
[36] M. Bruse, H. Fleer, Simulating surface-plant-air interactions inside urban environments with a three dimensional numerical model, Environ. Model. Softw. 13 (1998) 373–384. doi:10.1016/S1364-8152(98)00042-5.
[37] ISO - International Organization for Standardization, ISO 7726:1998 Ergonomics of the thermal environment - Instruments for measuring physical quantities, 1998.
[38] ENVI-met Model Architecture, (n.d.).
[39] H. Simon, J. Lindén, D. Hoffmann, P. Braun, M. Bruse, J. Esper, Modeling transpiration and leaf temperature of urban trees – A case study evaluating the microclimate model ENVI-met against measurement data, Landsc. Urban Plan. 174 (2018) 33–40. doi:10.1016/j.landurbplan.2018.03.003.
[40] X. Yang, L. Zhao, M. Bruse, Q. Meng, Evaluation of a microclimate model for predicting the thermal behavior of different ground surfaces, Build. Environ. 60 (2013) 93–104. doi:10.1016/j.buildenv.2012.11.008.
[41] ISO - International Organization for Standardization, ISO 10456:2007 Building materials and products: Hygrothermal properties. Tabulated design values and procedures for determining declared and design thermal values, 2007.

[42] UNI Ente Italiano di Normazione, UNI 10351:2015 Materiali e prodotti per edilizia - Proprietà termoigrometriche - Procedura per la scelta dei valori di progetto (in Italian), 1994.
[43] R.B. Clapp, G.M. Hornberger, Empirical equations for some soil hydraulic properties, Water Resour. Res. 14 (1978) 601–604. doi:10.1029/WR014i004p00601.
[44] Dipartimento per il servizio geologico d'Italia - ISPRA Archivio nazionale delle indagini nel sottosuolo (Legge 464/1984), (n.d.).
[45] M.P. Rouault, P.G. Mestayer, R. Schiestel, A model of evaporating spray droplet dispersion, J. Geophys. Res. Ocean. 96 (1991) 7181–7200.
[46] J.B. Edson, Lagrangian model simulation of the turbulent transport of evaporating jet droplets., Thesis. (1990).
[47] L.E. Andreas, Thermal and size evolution of sea spray droplets, CRREL Rep. (1989).
[48] R.B. Bird, W.E. Stewart, E.N. Lightfoot, Diffusivity and the mechanisms of mass transport, Transp. Phenom. (1960) 513–542.
[49] R.Q. Dunham, Rosin-Rammler Distributions in ANSYS Fluent, 2012.
[50] ENVI-met 3.1 Manual, (n.d.).
[51] Eurometeo, (n.d.).
[52] G. Bonafè, Microclima urbano: impatto dell'urbanizzazione sulle condizioni climatiche locali e fattori di mitigazione (in Italian), 2006.
[53] Norme Tecniche per le Costruzioni. DM 17/1/2018 (in Italian), 2018.
[54] F. Bauelos-Ruedas, C. Angeles-Camacho, Sebastin, Methodologies Used in the Extrapolation of Wind Speed Data at Different Heights and Its Impact in the Wind Energy Resource Assessment in a Region, in: Wind Farm - Tech. Regul. Potential Estim. Siting Assess., 2011. doi:10.5772/20669.
[55] A. Murat, A. Sisman, A. Gultekin, B. Dehghan, An Experimental Performance Comparison between Different Shallow Ground Heat Exchangers, World Geotherm. Congr. 2015. (2015).
[56] Turbulence Model in ENVI-met, (n.d.).
[57] H. Montazeri, B. Blocken, J.L.M. Hensen, Evaporative cooling by water spray systems: CFD simulation, experimental validation and sensitivity analysis, Build. Environ. 83 (2015) 129–141. doi:10.1016/j.buildenv.2014.03.022.
[58] G. Swamy, S.M. Shiva Nagendra, U. Schlink, Urban Heat Island (UHI) influence on secondary pollutant formation in a tropical humid environment, J. Air Waste Manag. Assoc. 67 (2017) 1080–1091. doi:10.1080/10962247.2017.1325417.
[59] J. Lindén, H. Simon, P. Fonti, J. Esper, M. Bruse, Observed and modeled transpiration cooling from urban trees in Mainz , Germany, ICUC9 - 9th Int. Conf. Urban Clim. Jointly with 12th Symp. Urban Environ. (2015).
[60] C.J. Willmott, Some comments on the evaluation of model performance, Bull. - Am. Meteorol. Soc. 63 (1982) 1309–1313. doi:10.1175/1520-0477(1982)063<1309:SCOTEO>2.0.CO;2.
[61] C. Ketterer, A. Matzarakis, Comparison of different methods for the assessment of the urban heat island in Stuttgart, Germany, Int. J. Biometeorol. 59 (2015) 1299–1309. doi:10.1007/s00484-014-0940-3.
[62] J.A. Acero, K. Herranz-Pascual, A comparison of thermal comfort conditions in four urban spaces by means of measurements and modelling techniques, Build. Environ. 93 (2015) 245–257. doi:10.1016/j.buildenv.2015.06.028.
[63] S. Tsoka, A. Tsikaloudaki, T. Theodosiou, Analyzing the ENVI-met microclimate model's performance and assessing cool materials and urban vegetation applications–A review, Sustain. Cities Soc. 43 (2018) 55–76. doi:10.1016/j.scs.2018.08.009.
[64] J.A. Villena Del Carpio, D.L. Marinoski, G. Trichês, R. Lamberts, J.V.S. de Melo, Urban pavements used in Brazil: Characterization of solar reflectance and temperature verification in the field, Sol. Energy. (2016). doi:10.1016/j.solener.2016.04.044.

Appendix A

	th (m)	α (-)	τ (-)	ρ (-)	ε (-)	Cs (J/kg·K)	λ (W/m·K)	ρ_{mat} (kg/m³)
Church external wall (from interior to exterior)								
Gypsum plaster	0.02	0.50	0.00	0.50	0.90	960	0.51	1120
Concrete	0.20	0.70	0.00	0.30	0.90	840	1.90	2500
Cement plaster	0.02	0.50	0.00	0.50	0.90	840	0.80	1600
Red brick (only north façade)	0.30	0.60	0.00	0.40	0.90	650	0.44	1500
Church roof (from interior to exterior)								
Concrete slab	0.24	0.40	0.00	0.60	0.90	880	1.09	1100
Waterproofing	0.004	0.77	0.00	0.23	0.87	1000	0.85	2400
Clay roof tiles	0.04	0.50	0.00	0.50	0.90	840	0.81	1700
Windows								
Clear glass	0.02	0.05	0.90	0.05	0.90	750	1.05	2500
Polyclinic wall (from interior to exterior)								
Perforated brick	0.08	0.67	0.00	0.33	0.92	840	0.25	800
Air	0.04	0.00	1.00	0.00	0.96	1006	0.025	1.204
Semi-filled brick	0.25	0.67	0.00	0.33	0.95	840	0.25	800
Polyclinic roof (from interior to exterior)								
Concrete slab	0.24	0.40	0.00	0.60	0.90	880	1.09	1100
Concrete screed	0.05	0.73	0.00	0.27	0.93	1000	0.22	1490
Waterproofing	0.004	0.77	0.00	0.23	0.87	1000	0.85	2400
Box prefabricated annex to the polyclinic (wall and roof, from interior to exterior)								
Plasterboard	0.0125	0.50	0.00	0.50	0.90	840	0.16	800
Glass wool	0.04	0.60	0.00	0.40	0.90	1256	0.04	30
Steel sheet	0.002	0.20	0.00	0.80	0.10	4800	45	800

Table A.1 thermo-opto-physical properties of the materials used for the modelled built elements.

Species	Aspect Ratio	Foliage Shortwave Albedo	Foliage Shortwave Transmittance	Leaf Type
Tilia cordata	1.45	0.18	0.30	Decidous
Tilia cordata	1.56	0.18	0.30	Decidous
Pinus Pinea	1.45	0.60	0.30	Conifer
Platanus Acerifolia	1.33	0.18	0.30	Decidous
Robinia Pseudoacacia	1.71	0.18	0.30	Decidous

Table A.2 Trees specifications.

Type	Albedo	Foliage Shortwave Transmittance	Plant height (m)
Dense grass	0.26	0.30	0.25
Dry grass	0.20	0.30	0.10

Table A.3 Characteristics relating to the grass surface of the model.

Soil type	V	n_s (m^3/m^3)	n_{fc} (m^3/m^3)	n_{wilt} (m^3/m^3)	MatPot (m)	hydr (10^{-6}m/s)	CP ($10^6 J/m^3K$)	b (-)	λ (W/mK)	ε (-)	ρ (-)
Loam	0	0.451	0.240	0.155	-0.478	7	1.212	5.39	0.00	0.98	0.00
Cement	1	0.00	0.00	0.00	0.00	0.00	2.083	0.00	1.63	0.90	0.22
Asphalt:	1	0.00	0.00	0.00	0.00	0.00	2.214	0.00	1.16		
-aged										0.90	0.10
-new	-	-	-	-	-	-	-	-	-	0.98	0.04
-red										0.93	0.07

Table A.4 Physical, hydraulic and optical characteristics of the types of soil considered in the model. The abbreviation V indicates the permeability of the soil: 0 if it is permeable, 1 if it is waterproof. The ε and ρ values are derived from literature [64].

Highlights

- A 3D microclimatic model in ENVI-met is used to simulate a misted urban area
- The model predicts accurately the horizontal and vertical air temperature distribution
- Wind speed plays a major role both in terms of cooling capacity and influence area
- Water flow rate and height of injection can be tuned to regulate the cooling capacity

Numerical modelling and experimental validation of the microclimatic impacts of water mist cooling in urban areas

Elisa Di Giuseppe[a], Giulia Ulpiani[b]*, Claudia Cancellieri[a], Costanzo Di Perna[b], Marco D'Orazio[a], Michele Zinzi[c]

[a] Department of Civil and Building Engineering and Architecture (DICEA), Università Politecnica delle Marche, Via Brecce Bianche 12, 60131 Ancona, Italy
e.digiuseppe@univpm.it (E. Di Giuseppe)
claudia@cancellieri.eu (C. Cancellieri)
m.dorazio@univpm.it (M. D'Orazio)
[b] Department of Industrial Engineering and Mathematical Sciences (DIISM), Università Politecnica delle Marche, Via Brecce Bianche 12, 60131 Ancona, Italy
giuliaulpiani@gmail.com (G. Ulpiani)
c.diperna@univpm.it (C. Di Perna)
[c] ENEA, Via Anguillarese 301, 00123 Rome, Italy
michele.zinzi@enea.it (M. Zinzi)

* Corresponding author.

Abstract

Among water-based mitigation strategies against urban overheating, dry mist systems are especially promising, given their local impact, cost-effectiveness and controllability. Intense cooling capacity has been reported under a variety of climates, however, there is a growing need to define specific design guidelines towards an informed and optimized use of the technology. Parametric analysis on validated models would assist in determining type and degree of correlation between key parameters, as well as magnitude and predictability of the cooling capacity. In this paper, for the first time, a 3D microclimatic model in ENVI-met is used to simulate a misting system installed in Rome, Italy, with high prediction accuracy for the air temperature ($R^2 \simeq 0.87$, RMSE$\simeq$0.84 °C). The calibrated ENVI-met model is used then to perform parameterizations on the water mist system, focused on the role of three key design variables: i) water flow rate, ii) injection height and iii) local wind speed. Results show that the most significant thermal drops tend to occur close but out of the misted perimeter following the wind direction, with cooling effects further stretched for tens of meters. The cooling capacity increases with the total water flow rate (+0.2 °C per 10 l/h increment) and in presence of calm air (+35-40 % per 0.8 m/s deceleration). Lower injections intensify the cooling a pedestrian height, which could be especially beneficial under windy conditions. Further research would target climate dependencies to extend the applicability of the above results and build up cohesive guidelines at the hands of urban planners and practitioners.

Keywords

Water mist spray; Evaporative cooling; Urban climate; Outdoor comfort; Heat mitigation; ENVI-met

Nomenclature and units

A_D	droplet area	m^2
b	Clapp&Hornberger's constant	-
C	Centre	-
CP	volumetric heat capacity	$10^6 J/m^3K$
Cs	specific heat	J/kg·K
d	Wilmott's index of agreement	-
D_v	vapor mass diffusivity	m^2/s
E	East	-
$\bar{e}$	mean air-droplet vapor pressure	Pa
e_a	vapor partial pressure	Pa
e_{sat}	saturation pressure	Pa
f_v	ventilation factor	-
GSR	global solar radiation	W/m^2
hydr	hydraulic conductivity	$10^{-6}m/s$
K	sensible heat transfer coefficient	$W/m^2 \cdot K$
K_q	water vapor diffusion coefficient	m^2/s
L	latent heat of evaporation	W
MatPot	mean Matrix Potential at water saturation	m
MC	misted condition	-
m_D	droplet mass	kg
m_f	mass flow	l/m
N	North	-
N_D	number of droplets	-
n_s	water content at saturation	m^3/m^3
N_v	ventilation number	-
p	total pressure	Pa
Q_{kw}	shortwave radiation	W
Q_{wD}	sources of spray	µg/kg·s
r	Pearson coefficient	-
R^2	Pearson's coefficient of determination	-
r_D	mean droplet radius	µm
RH	relative humidity	%
RMSE	root-mean-square error	°C
R_v	water vapor gas constant	J/kg·K
S	South	-
S_{wD}	sinks of spray	µg/kg·s
$\bar{T}$	mean air-droplet temperature	°C
Ta	ambient temperature	°C
T_D	droplet temperature	°C
T_{env}	radiant temperature of the surroundings	°C
th	thickness	m
T_{wb}	wet-bulb temperature	°C
UC	undisturbed condition	-
u_i	velocity vector	m/s
V	index of permeability of the soil	-
W	West	-
wd	wind direction	°

w_D	amount of liquid droplets within a given air volume	g/m^3 or $\mu g/kg$
ws	wind speed	m/s
x_i	Cartesian coordinates vector	m
α	solar absorptance	-
Δe	vapor pressure difference	Pa
ΔTa	ambient temperature difference between undisturbed and misted conditions	°C
ε	thermal emissivity	-
λ	thermal conductivity	$W/m \cdot K$
ρ	solar reflectance (or albedo)	-
ρ_{mat}	density of materials	kg/m^3
ρ_W	water density	kg/m^3
σ_B	Stefan-Boltzmann constant	$W/m^2 \cdot K^4$
τ	solar transmittance	-
ϕ_D	mean droplet diameter	μm
n_{fc}	water content at field capacity	m^3/m^3
n_{wilt}	water content at wilting point	m^3/m^3

1. Introduction

Urban overheating is a well-known environmental hazard at both global and local scale, as documented by several scientific studies and observations of air temperature trends. Main consequences are the thermal deterioration of both indoor and outdoor thermal environments, serious thermal comfort concerns for human beings, and enhanced cooling energy uses in buildings [1,2]. Measured temperatures' rise and evolution scenarios are the object of many studies. The most significant are those produced under the UN framework by the Intergovernmental Panel on Climate Change [3], dedicated to global strategies and countermeasures to limit the temperature rise to 1.5 °C. Beyond global warming, the "Urban Heat Island" (UHI) phenomenon is a major cause of overheating in the urban built environment, investigated for decades. Its intensity depends on several factors as: climate, size of the city, urban texture, etc. Peak values up to 12 °C are reported in literature, whereas the average maximum orbits around 2 °C [4]. Moreover, UHI intensity is typically higher in cooling dominated climates [5].

Urban overheating has a strong impact on the energy use in buildings especially for cooling, as documented worldwide in [4]. It further enhances the risks related to energy poverty for an impressive share of the global population: 1 billion people living in poorer countries [7] and more than 60 million living in Europe [8]. The risk of skyrocketing energy uses for cooling and the unfeasibility of ensuring decent outdoor thermal conditions for many citizens call for diversified and effective thermal mitigation/adaptation plans and architectural rehabilitation of urban spaces, in the attempt of improving health, comfort and liveability in the outdoor realm [6,7]. Many studies have been carried out to size the impact of different UHI mitigation technologies and strategies: green infrastructures, innovative cool materials, blue technologies, as reviewed in [5,8,9].

Main findings prove that passive solutions offer moderate mitigation potentials (generally below 2 °C) and are effective if applied at large scale in the city. Urban overheating can be combated, at

local scale, through the inclusion of blue features, as evaporative processes largely influence both the natural hydrological balance and the human thermoregulation, thus strongly impacting on comfort and liveability [10]. Especially on hot and dry days or during heat waves, evaporation is a fairly effective way to draw the excessive heat from the air through a thermodynamically spontaneous phase change process, that naturally magnifies as temperature rises (at equal specific humidity) [11] and that is way more intense than a purely sensible heat transfer between air and water [12].

Beyond natural water bodies, a whole spectrum of artificial installations can be considered (ranging from fountains, to sprinklers, to evaporative towers, to ponds). Among them, an especially promising blue mitigator is represented by dry mist systems, namely high-pressure water injectors able to pulverize the water into fine droplets of few tens of microns. The high surface-to-volume ratio promotes flash evaporation, hence i) the water consumption can be minimized compared to alternative technologies and ii) the risk of wettedness, even close to the nozzles, can be neutralized as long as a proper layout is configured [11]. Further, it was experimentally demonstrated that dry misters are beneficial in terms of building energy use minimization: Ishii et al. [13] projected a 10 % air conditioning energy reduction at the expense of 5 % humidity gain per degree of air cooling, whereas Narumi et al. monitored three misting techniques (rooftop spraying, veranda spraying, and outdoor air-conditioning spraying) in an apartment house in Osaka and reported on cooling consumptions decremented by more than 80 % [14]. Other secondary benefits are related to air quality and erythema reduction since finely pulverized droplets help at scavenging dust, removing pollutants [15] and attenuating solar attenuation [16].

These systems could be deployed throughout the cityscape in strategic hot or vulnerable spots to alleviate the risk of heat-related mortality and morbidity with expected higher impact than single massive water bodies [17]. Furthermore, compared to water bodies, these systems can be controlled in capacity and can be triggered by specific events (temperature, humidity, wind speed exceedances or rain occurrences) not to provide evaporative cooling when unneeded or potentially counterproductive [18]. This is especially attractive for heating-dominated countries, where overheating concerns are sporadic yet extreme events.

On the other side, the efficacy of a misting system is largely a function of the environmental conditions. In a recent review by Ulpiani dedicated to mist cooling [11], the author collected data from 12 countries and 7 climatic zones. Air temperature and relative humidity were identified as driving factors, as they dictate the wet bulb depression (difference between dry-bulb and wet-bulb temperature) which represents the theoretical limit for evaporative cooling [19]. Additionally, wind speed (and gusts) proved to be pivotal as directly related to the level of particle dilution [20]. Demonstration of the governing role of local wet bulb depression as both instantaneous and short-term trend is reported in [21], where the cooling capacity of an overhead dry mist system was found to be negatively and positively correlated with solar irradiation and wind speed, respectively. This implies that not just the microclimate of the installation site deeply affects the results, but also the very local urbanscape (e.g. space enclosure, canyon effect, greenery and other competing evaporative sources, wind-breaking features and provisions, etc.). In such a complex scenario, modelling and parameterization, based on adequate experimental validation, are especially useful to determine type and degree of correlation between key parameters, as well as magnitude and predictability of the cooling capacity. This is pre-condition to define substantiated design guidelines towards an informed and optimized use of the technology [11].

Almost all numerical models of mist cooling are platformed in ANSYS Fluent [11]. In 2008, Yamada et al. reproduced a 50 m x 15 m x 4 m semi-enclosed outdoor space in Tokyo (Japan, Cfa climate)

fitted with an overhead misting system, using a mesh grid of 11,200 cells [22]. On a typical summer day (Ta of 33.4 °C, RH of 58 %, ws of 0.1 m/s), the cooling reached -1.5 °C at the spray location and -0.5 °C about 2.5 m away, at the expense of a +0.8 and + 0.3 g/kg gain in absolute humidity, respectively. In 2010, Wang et al. [23] investigated the role of airflow rate and site of installation (open outdoors, semi-enclosed area) when a misting fan was introduced in a 15 m x 10 m x 4 m domain represented by 570,000 hexahedral cells, under initial Ta of 35 °C, RH of 60 % and solar radiation of 600 W/m^2. The change in airflow simply moved the region of higher cooling closer or farther from the injection. On the other hand, the maximum temperature drop more than doubled (from 2 °C to 5 °C) when shifting from the open to the semi-enclosed scenario, bringing out the role of wind. The humidity gain was found to be negligible (1- 6 %) in any case. In 2015, Farnham et al. [12] ran an experimental and numerical study in Osaka (Japan, Cfa climate). They used Fluent to investigate the role of i) water temperature in almost the whole liquid range (8 - 92 °C), ii) the distance from the injection and iii) the initial T, RH conditions (7 cases) by looking at a single injection with mean droplet diameter of 23.4 – 25.5 μm. A 400 cm x 45 cm x 45 cm air volume was discretized into 1-cm tetrahedral mesh near the nozzle, ranging up to 4-cm mesh at the air inlet and outlet, for a total of 1.2 million elements. The cooling ranged between 0.5 and 2.5 °C, with negligible loss due to the different water temperature (0.26 °C when water was heated up from 20 °C to 60 °C). In the same year, Montazeri et al. systematized the CFD analysis of the impact of physical parameters on evaporative cooling by a mist spray system [24]. The authors modelled a 0.585 m x 0.585 m x 1.9 m wind tunnel, meshed into 1,018,725 hexahedral cells, to parameterize i) the inlet air temperature, ii) the inlet air humidity ratio, iii) the inlet airflow rate, iv) the inlet water temperature, v) the inlet droplet mean diameter and vi) the droplet spread. Five different cases were considered for each parameterization. It was found that the maximum temperature drop incremented from 3.3 to 9.3 °C by increasing the air temperature, from 3 to 9 °C by decreasing the humidity ratio, from 0.8 to 7 °C by reducing the relative velocity, from 2 to 9 °C by cooling down the water (in contrast with [12]), from 4 to 10 °C by reducing the mean droplet size and remained fairly unchanged at 5.8 °C when tweaking the spread. The same authors, in [25], extended the simulation to an outdoor location, by modelling a courtyard in the Bergpolder Zuid region of Rotterdam (The Netherlands, Cfb climate), equipped with 15 nozzles featuring mean droplet diameter of 20 μm. A circular inner subdomain of diameter equal to 1,200 m was populated with explicitly modeled buildings, while the surrounding outer hexagonal subdomain (side 1,200 m) was implicitly modeled in terms of roughness, for a total of 6,610,456 hexahedral and prismatic cells. Three different values for i) total mass flow (2 - 9 l/min) and ii) height above the ground (3 - 5 m) were considered. The maximum temperature drop (underneath the injection in the middle of the spray line, at a pedestrian height of 1.75 m) increased from 1 to 7 °C as higher flow rates were processed. Spatially, a 2 °C maximum drop was reported to stretch up to a distance of 8 m from the spray line. By decreasing the height of the injections, the cooling capacity incremented from 5 to 7 °C. Results are to be trusted for relatively low pedestrian ws (0.5 - 1.5 m/s).

Other than Fluent, Q-basic was used at first [26], then also Fire Dynamics Simulator [27] and Simplified Analysis System for Housing Air Conditioning Energy [14]. In some instances [28–30] the software was left unspecified. These models typically apply an Eulerian-Lagrangian approach to follow the discrete phase (water) in its kinetics and thermodynamics inside the continuous medium (air) and thus provide a punctual representation of the two-phase interaction. Yet, as mist cooling gains ground into the world of urban heat island mitigation, there is a need to incorporate and validate its effects in urban-scale simulations, contemplating the complex interplays with other microclimatic

phenomena, distinctive of the urban environment (e.g. canyon effects, evapotranspiration, reduced soil permeability, anthropogenic heat).
ENVI-met is a three-dimensional microclimate modelling system designed to simulate the surface-plant-air interactions in urban environment, based on the fundamental laws of fluid- and thermodynamics. Recently, it has been widely adopted to estimate the thermal benefits of urban heat mitigation strategies [31–36]. This software includes a water droplet dispersion and evaporation model to simulate the cooling effect of water spray. However, to the best of our knowledge, no study reports on experimentally-validated water mist models corroborated by multi-point in-situ measurements using ENVI-met. This study contributes to the current body of knowledge on urban overheating countermeasures based on evaporative cooling in two ways: i) by assessing the effectiveness of the software ENVI-met in predicting the microclimate perturbation in the misted area and ii) by determining substantiated design criteria to be applied at both manufacturing and urban planning level. The calibration of the ENVI-met model for water misting poses some challenges, essentially due to the non-trivial interlacement between droplets' behaviour and the other climate-impinging urban elements: a suite of solutions is proposed and discussed, leading to accurate simulations that capture real trends and evolutions. Recommended settings are presented to be used in future scenario analysis for UHI mitigation.

2. Materials and method

In this paper, ENVI-met version 4.4.3 is used to model a grid of overhead dry misters installed in a green playground in Rome (Italy, Csa climate). The simulation results for both the "misted condition" (MC) and the "undisturbed condition" (UC) of the site are validated on the basis of the thermal and hygrometric mapping obtained through a bespoke sensor network. The calibrated ENVI-met model is then used to perform parameterizations on the water mist system, focused on the role of three key design variables: i) wind speed, ii) water flow rate and iii) height of nozzles above the ground. Next section 2.1 provides information on the experimental rig, while the model is described in section 2.2. Results from the model validation and subsequent parameterizations are reported in section 3 and conclusively discussed in section 4.

2.1 Experimental rig

The dry mist system was erected in a green area of about 50 m x 16 m, stretched along the north-south axis, in the East of Rome city (Italy, 41°52'34.7"N 12°33'59.6"E, 44.5 m a.s.l.) during summer 2018. Low-rise residential blocks, originally for military officials, dominate the local landscape. The perimeter is framed with ornamental bush specimens, about 1 m high and dense in foliage. A line of five linden trees runs approximately 11 m away from the eastern boundary. The trees are 9.6 m inter-spaced, with a mean girth of 0.25 m. At 3 m above the ground, the crown expands within a 3.5 m radius from the trunk, on average. Consequently, solar shading is provided from 4:30 pm on.
The green area is enclosed by a church, the elders' bowls club and the local polyclinic along the east-west axis, a small playground due north and a lower-floor street running along the southern border. Strewn with toys, it is destined to families, notably those with children under 4 years old. The quite concealed position and designated use make it the perfect test rig for the misting system: low dominant wind speeds, proximity to vulnerable population (children, youngsters, mothers and elders) and proximity to gathering points (church and its square, playground, sports clubs, healthcare facilities) (Figure 1).

The injections, consisting of 24 hollow-cone nozzles, were suspended through a system of pulleys and tensioned cables at an average height of 2.8 m, in line with customary setups [11] and distributed in 4 parallel strings of 6 nozzles each. The interspace was 1 m along the string and 1.25 m in-between the strings. A self-compensating 70 bar water pump, absorbing about 990 W_e, was utilized to pressurize the water supplied from a local fountain, with a flow rate of 1.5 l/min. In order to quantify the droplet diameter distribution, the nozzles were previously tested under a pressure of 1000 psi (68.9 bar) using water at 21.1 °C in a test room whose humidity was maintained at 40-50 %. Patternation measurements were conducted using the SETscan OP600. The cloud of dispersed droplets featured mean Sauter diameter around 10 µm, with the smallest droplets under 7 µm in diameter and the biggest over 27 µm.

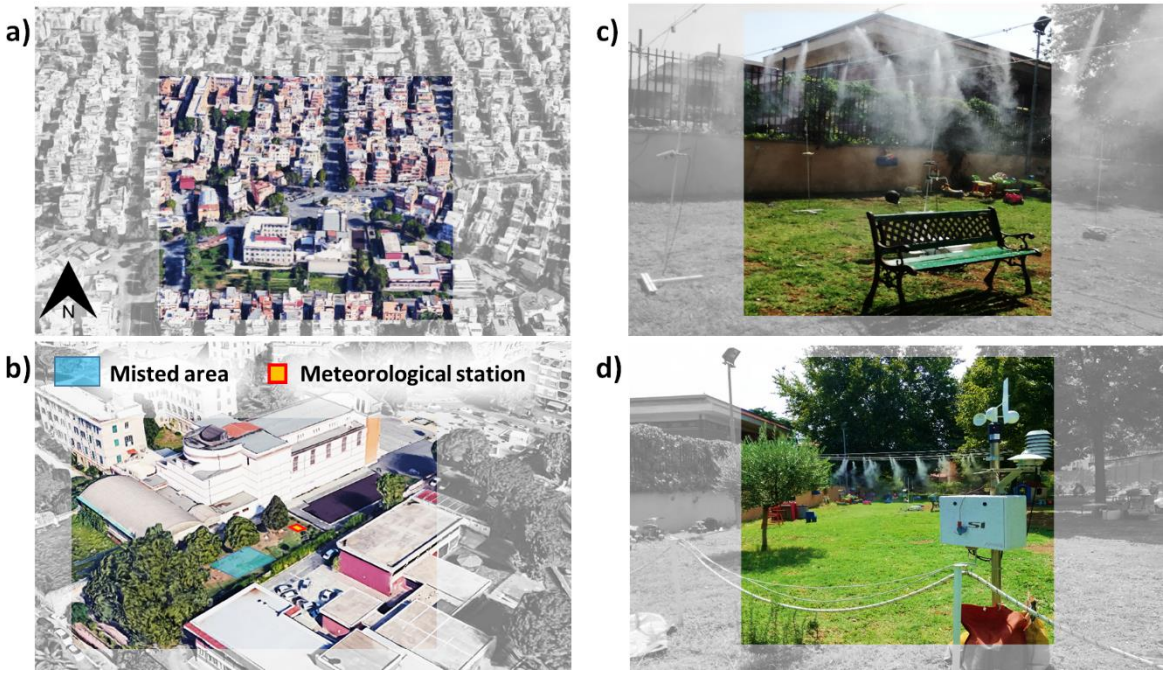

Figure 1 Aerial view of the urban district of Centocelle, Rome (a), close-up on the installation site (b), detail of the misting system (c), detail of the meteorological station and relative position to the misted area (d)

The microclimatic conditions in July-August in Rome reflect typical hot-summer Mediterranean characteristics (Csa Köppen-Geiger class) with temperatures about 8.7 °C above the annual mean and protracted dry conditions (around 17 mm of rain compared to a monthly average of 114 mm) [18].
The dry mist system was tested under diverse weather conditions on different days [10]. However, ENVI-met was calibrated on one day (see section 2.2.3), when the misting operated continuously from 11 am to 7 pm (CET/UTC+2). A suite of sensors recorded the perturbation induced by the mist. Notably:

- a weather station was installed about 16 m away from the ground-projected perimeter of the misting matrix, to characterize the undisturbed condition for comparative analysis. The station measured Ta (accuracy 0.2 °C), RH (accuracy 1.5 %), GSR (accuracy 5 %), ws and wd (accuracy 1.5 % and 1 °) with a time step of 1 minute.
- A grid of 5 thermohygrometers (accuracy ± 0.2 °C and ±2 %) was placed at 1.1 m above the ground, in compliance with ISO 7726 in case of standing subjects [37]. One sensor was placed in the middle of the misted area, while the remaining four were distributed underneath the outermost lines of nozzles along the cardinal directions. This sensing network mapped the spatial heterogeneity and the temporal variability of cooling and humidification. Accordingly,

it featured high responsiveness (10 s response time), low risk of saturation (by means of anti-wetting HDPE covers) and sun-protection (white screens).

The meteorological station was aligned with the central, northern and southern thermohygrometers to be exposed to equal solar radiation in view of the local shading elements. Water temperature was also monitored by performing time-discretized measurements with a PT100 during the day: it ranged within 19±1 °C.

The schematics of the sensor distribution in the misted area is showed in Figure 2, in overlap with the nodes of ENVI-met's grid and receptors, that will be described in section 2.2.1.

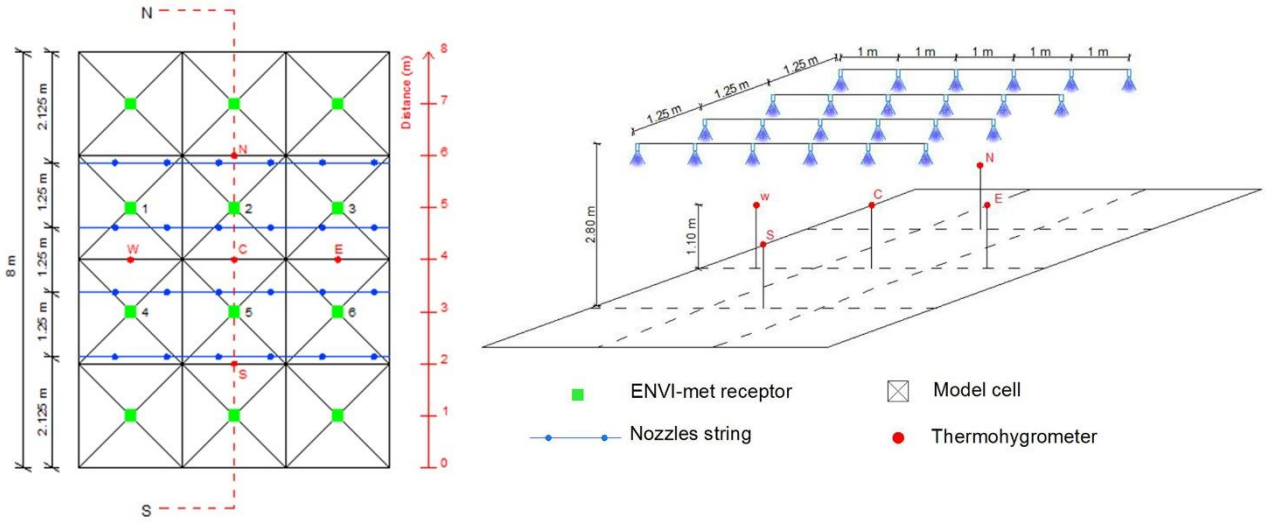

Figure 2 Schematics of the misted area with the nozzles' distribution overlapped to the ENVI-met model cells. Thermohygrometers and ENVI-met receptors are also indicated. Thermohygrometers are identified with letters according to their position: N (north), C (centre), S (south), W (west), E (east). The North (N) - South (S) section of the area is identified for subsequent analyses.

2.2. Numerical model

ENVI-met is a software based on a three-dimensional model for the simulation of surface-plant-air interactions, often used to simulate urban environments [36]. It includes a full 3D Computational Fluid Dynamics model which solves the Reynolds-averaged non-hydrostatic Navier-Stokes equations for each grid in space and for each time step [38]. The software also includes models for: shortwave and longwave radiation fluxes with respect to shading, reflection and re-radiation from buildings, soils and vegetation; evapo-transpiration and sensible heat flux from the vegetation [39]; water balance and water uptake of vegetation; dynamic heat balance in the buildings envelope; water- and heat exchange inside the soil; dispersion of gases and particles and their deposition on pervious and impervious surfaces [38]. ENVI-met also includes the possibility to model water sprayed into the local atmosphere as a specific "particle dispersing source". The main input parameters required to perform ENVI-met simulations include meteorological data, features and properties of ground surfaces, vegetation and buildings, initial soil wetness and temperature profiles [40]. The following sub-sections provides details on the ENVI-met model developed within this study.

2.2.1. Model Area and characteristics of buildings and surfaces

Stretched over 800 m², the park was discretized with 50x50x30 grid cells (XxYxZ) in the ENVI-met area input file. The horizontal resolution was 2 m, whereas the vertical resolution was 0.5 m from ground-level to 3 m height, then followed a 20 % telescoping increment to the top of the domain (about 180 m). Six "nesting grids" surrounding the core of the 3D model were included at the borders,

to take into account the local roughness and thermal contribution given by the surrounding buildings and the asphaltic/green surfaces around (Figure 3).

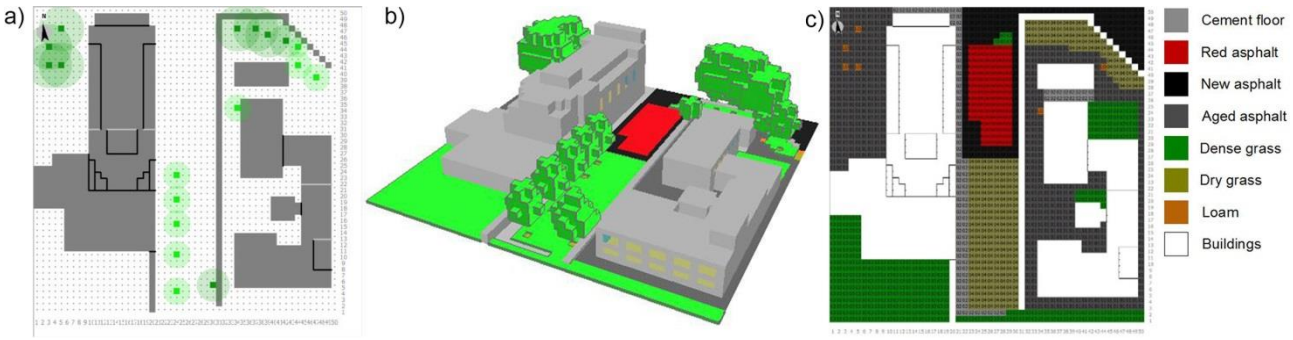

Figure 3 Plan view (a), 3D view (b), plan view with soil features (c) of the geometric model

The two buildings included in the core domain were characterized in terms of envelope's thermo-physical properties, based on standard values tabulated in ISO 10456 [41] and UNI 10351 [42]. Erected in the early 30s, the church is built in reinforced concrete, with brick roofing tiles, plastered on all facades, but the northern one, which is covered with red bricks. The polyclinic dates back to the 60s, hence the structure is in reinforced concrete, plastered infill wall and flat waterproofed roof. Given the specific dating, we assumed no thermal insulation.

The local arboreal species (linden, pine, sycamore and robinia) were included in the dedicated ENVI-met module to rely on appropriate proportion, while the grassy mantle was specified through the "Plants" database, within the sub-categories dense and dry grass.

The other types of soil surfaces present in the study area were therefore defined in the software database "soil" (Figure 3(c)). The soil parameters were obtained through the Clapp & Hornberger hydraulic scheme which allows to describe the thermal conductivity of the soil according to its water content [43]. The stratigraphic profile of the soil for a thickness of 4.5 m was defined on the basis of documentation available on the site of the Department for the Geological Service of Italy [44]. Appendix A reports the summary tables on: the thermo-opto-physical properties of the materials used for the modelled built elements and the main characteristics of trees and soils.

Finally, within the study area, the "receptors" have been defined, i.e. the projections of the vectors in the vertical direction used to probe the simulation results (atmospheric data, exchanged radiative flows and soil characteristics). As displayed in Figure 2, 12 receptors were located in the misted area, while another receptor was placed at the weather station location.

2.2.2. Water mist cooling properties

The water nozzles can be inserted in ENVI-met as punctual "water sources" at the center of the grid cells. Having cells of 2 m x 2 m, 6 water sources (each corresponding to 4 nozzles) were placed in the misted area in correspondence with the receptors, but at the specific height of 2.8 m, providing a total water flow of 90 l/h (15 l/h per water source), which is equivalent to the experimental supply (Figure 2). Their features were managed in the section "pollutant conditions" of the project advanced settings in ENVI-met.

According to the technical documentation provided by M. Bruse (personal communication, September 29, 2020), ENVI-met computes the energy required to evaporate the water and the corresponding local decrease in air temperature. Unevaporated droplets are entrained in the wind flow and are subject to sedimentation processes with a downward settling velocity depending on their size.

The main simplification relies on the particle tracing. Two main approaches are commonly used in CFD analysis, both considering that the droplet diameter would decrease along with evaporation until the droplet has vanished. The first one is the discrete approach, according to which different droplets sizes in the air volume are grouped into n bins and evaporation at their surface is numerically translated into a shift of the number of droplets towards smaller bins [45]. The second is the Lagrangian approach, in which the state and size of each droplet is monitored and calculated individually. Both ways are not realistic for a relativity small sub model of ENVI-met, in terms of required computing resources and calculation time. To simplify the process of droplet evaporation, the droplets do not change their size (nor their mass) in ENVI-met, but their quantity. The prognostic variable is the amount of liquid droplets within a given air volume, w_D (g/m^3) which is related to the number of droplets N_D and the mean droplet radius r_D (μm) as follows:

$$N_D = \frac{w_D}{0.001 \cdot \rho_w \cdot \frac{4}{3}\pi \cdot r_D^3} \quad (1)$$

Beyond evaporation, ENVI-met considers a number of drivers for the spatial and temporal distribution of water spray, namely advection, diffusion, transport, local production (sources of spray) and sedimentation (sinks of spray). Transport is assumed to be instantaneous as very small droplets tend to behave like gases. As such, the droplets follow the air flow stream lines without inertial delays and the only extra velocity component is the settlement velocity due to gravitational forces. All other parameters (e.g. turbulent diffusion) are assumed to be equal to each other inert mass component. Overall, the partial differential equation that describes the atmospheric balance over time is of the same form of the advection-diffusion equation, used for the dispersion of gases and particulate matter:

$$\frac{\partial w_D}{\partial t} + u_i \frac{\partial w_D}{\partial x_i} = \frac{\partial}{\partial x_i}\left(K_q \frac{\partial w_D}{\partial x_i}\right) + Q_{w_D}(x,y,z) + S_{w_D}(x,y,z) \quad (2)$$

where u_i={u,v,w} is the wind velocity vector corresponding to the Cartesian coordinates x_i={x,y,z}, K_q is the water vapor diffusion coefficient while Q_{w_D} and S_{w_D} are the source and sink terms, respectively. In Eq. 2, w_D is expressed in μg/kg. The rate of evaporation is strongly dependent on the droplet's temperature, which is estimated through the energy conservation equation:

$$L(T_D)\frac{\partial m_D}{\partial t} = A_D \cdot K \cdot (T_D - T_a) + Q_{kw} + A_D \cdot \sigma_B \varepsilon (T_D^4 - T_{env}^4) \quad (3)$$

where L is the latent heat, A_D is the droplet surface area ($4\pi r_D^2$), K is the sensible heat transfer coefficient between droplet and air (inclusive of molecular and turbulent processes), Q_{kw} is the shortwave radiation, σ_B is the Stefan-Boltzmann constant, ε the emissivity and T_{env} is the radiant temperature of the surroundings (representative of the longwave radiative fluxes from the environment). Based on the transient resolution of Pruppacher and Klett's heat transfer equation, Edson [46] and Andreas [47] observed that sprayed droplets tend to quickly approach the wet bulb temperature T_{wb}, regardless of the initial conditions. As such, the estimation of T_D can be directly replaced by the estimation of T_{wb}. This simplified procedure is adopted in ENVI-met.

The change of mass of a single droplet depends on the vapor pressure difference Δe between air and droplet according to the following equation:

$$\frac{\partial m_D}{\partial t} = -4\pi r_D \cdot f_v \cdot D_v \cdot \frac{\Delta e}{\left(1 - \frac{\bar{e}}{p}\right) R_v \bar{T}} \quad (4)$$

where $\bar{T}$ and $\bar{e}$ are the arithmetic means of the droplet and air temperatures and of the saturation (e_{sat}) and vapour partial (e_a) pressures, respectively, Δe is the difference between $e_{sat}(T_D)$ and e_a, p is the

total pressure, R_v is the water vapor gas constant (taken at 461.5 J/kgK), whereas D_v and f_v are the vapor mass diffusivity and the ventilation factor, calculated according to Bird et al. [48] and Rouault et al. [45] respectively:

$$D_v = 2.4995 \cdot 10^{-5} \left(\frac{T_a}{292.88}\right)^{2.334} \quad (5)$$

$$f_v = \begin{cases} 0.78 + 0.308\, N_v, & for\ N_v \leq 1.4 \\ 1.0 + 0.108\, N_v^2 & elsewhere \end{cases} \quad (6)$$

The ventilation factor takes into account the motion of air around the droplet due to wind flow and settling of the droplet, based on N_v, which is a function of the Schmidt and Reynolds numbers.
In the simulations, the water density was set to 1 g/cm^3 to suit the measured temperature range (19±1 °C), while the droplet's mean diameter was set to reflect that measured by patternation (see Section 2.1). As stated above, ENVI-met represents the whole cloud of droplets by a single mean diameter, rather than a statistical distribution (e.g. Rosin Rammler, commonly adopted in other CFD software [49]). This simplification may underestimate both the cooling potential (since smaller droplets are not concerned) and the humidification (since larger droplets are not concerned). To verify which mean diameter best captured the experimental temperatures, we carried out a sensitivity analysis. Fig. 4 shows that smaller diameters performed better than that experimentally measured (10 µm). This was likely ascribable to the differences between the test room and the actual urban setting where solar radiation, wind and other factors enhanced the evaporation rate and the break-up into child particles. Diameters as low as 3 µm were statistically compared by quantifying the difference from the hourly averaged experimental temperature. By setting a particle diameter of 5 µm, the best RMSE, Pearson coefficient (r) and R^2 were attained (see Fig. 4). This setting was maintained in all subsequent simulations. The water sources were activated in the model from 11 a.m. to 7.00 p.m. as in the experimental conditions.

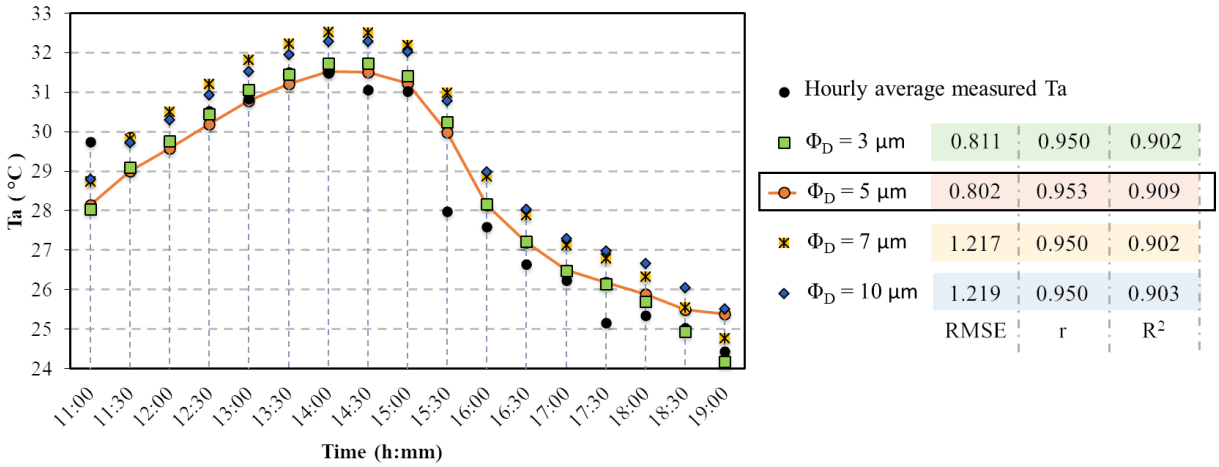

Figure 4 Sensitivity analysis to tune the mean droplet diameter. Tabulated results refer to the difference between the hourly average of the measured air temperature and the corresponding simulated value for different diameters at the central receptor.

2.2.3. Boundary and operational conditions

In the time window of the monitoring campaign, the 25th of August provided an optimal frame to simulate the mist cooling: high air temperature (average above 33 °C during the central hours of the day), cloudlessness and uninterrupted activation of the pump.

The start time was set at 5:00 a.m. of the 24th of August and the total simulation time at 48 hours [50]. Hence, a spin-up time of 19 hours was adopted. Using the metereological measurements and ENVI-met's "simple forcing" option, we set Ta and RH boundary conditions in the 11 a.m.-7 p.m. time slot. Data from a nearby weather station were used to cover the remaining hours of the day [51]. The temperature and relative humidity profiles are shown in Figure 5. The solar irradiation adjustment was set at 0.87 to fit the measurements.

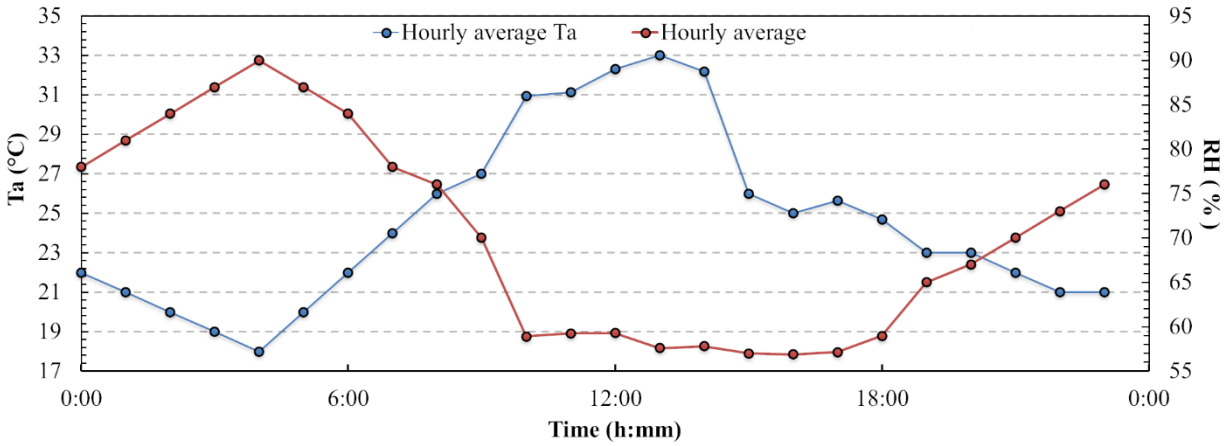

Figure 5 Ta and RH profiles on the simulated day.

The initial meteorogical conditions and the main advanced project settings are reported in Table 1. The roughness length at the measurement site was set at 0.3 m considering data reported in [52,53] for a suburban area. Wind speed at 10 m height was imposed at 2.4 m/s, considering the average speed value recorded on the ground by the climatic station (1.2 m/s) and the formula by Camacho et al. [54]. To estimate the wind direction, a frequency distribution analysis was performed, revealing a dominant south-westerly component (225 °). The imposed wind speed and direction values were confirmed by the data available online collected from a nearby climatic station [51]. The initial soil temperature conditions were set according to [55], while for the RH the default values were retained. The standard K-epsilon model was used to account for turbulence and gusts by describing the distribution and evolution of the kinetic energy in the air based on production, advection, diffusion and destruction, as well as its dissipation rate [56]. However, it was found in the literature that changing the turbulent model has negligible impact on water spray simulation [57].

The simulation time step was dynamically adjusted by ENVI-met considering the different solar angles during the days, which were mantained at the default values of 40 deg and 50 deg. The timestep was set at 2 s under the threshold of 50 deg and at 1 second over this value. The update timing was left at the default value. The output timing was set at 30 minutes for buildings and receptors and 60 minutes for the other files.

Parameters		***Value***
Wind	ws measured at 10 m height (m/s)	2.4
	wd (°)	225
	roughness length at measurement site	0.3
Ta	min. (°C)	18.0
	max. (°C)	33.0
RH	min. at 2 m height (%)	56.9
	max. at 2 m height (%)	90.0

T_i	initial building indoor temperature (°C)	26.0
Cloud cover	low clouds	0.0
	medium clouds	0.0
	high clouds	0.0
Initial soil conditions		
Soil layer	*Soil humidity (%)*	*Initial temperature (°C)*
Upper layer (0-20 cm)	70.0	25.8
Middle layer (20-50 cm)	75.0	24.8
Deep layer (50-200 cm)	75.0	19.8
Bedrock layer (below 200 cm)	75.0	17.8

Table 1 Initial meteorogical conditions and main advanced project settings

2.2.4.Simulations and sensitivity analysis on wind speed, nozzle height and density

The simulations were conducted for both the UC and for the MC scenarios. The simulated Ta and RH at receptors' level were compared to the experimental trends. Once validated (results in section 3.1), the model was used to assess the impact of the water mist cooling system on the microclimatic conditions (section 3.2). Further, to unveil the mitigation potential of the misting system and identify the room for design optimization, a sensitivity analysis was carried out in terms of: i) water flow rate, ii) injection height and iii) local wind speed (section 3.3). The following design variants were modelled and compared:

- three water flows, by doubling and halving the base-case number of injections per equal perimeter area (i.e.180 l/h, 90 l/h and 45 l/h);
- three injection heights, by moving 0.5 m above and below the base-case (i.e. 2.3 m and 3.3 m).

For each design option, the influence of wind speed was estimated by varying the 2 m value from 1 m/s to 3 m/s with a 1 m/s step, to be compared with the base-case value of 1.2 m/s. The combination of design and environmental parameterizations resulted in a total of 36 model variants.

3. Results

3.1. ENVI-met model validation

The accuracy of ENVI-met simulations at different heights and locations, under the misted and undisturbed conditions was examined with reference to the observed data. Concerning the UC, Figure 6 shows the comparison between the values measured by the climatic station and those simulated (Ta, RH, GSR). Owing to the vertical grid resolution, values are averaged between the cells centres at 0.5 m and 1.5 m, to be closest to the weather station. It can be observed how the simulated values of Ta and GSR represent a good estimate of the real trends, especially in the central and hottest hours of the day. On the other hand, the average relative humidity was systematically underestimated by the model. This has been widely reported in previous research, mostly due to the fact that the ENVI-Met model for relative humidity calculations has a limitation in the estimation of emissions and other anthropogenic sources as well as of the nocturnal plant transpiration [58,59].

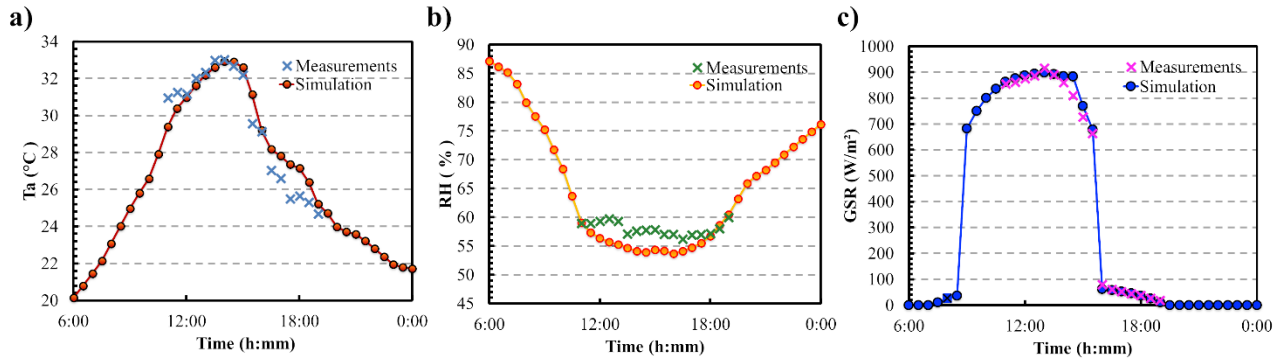

Figure 6 Comparison between the average hourly quantities measured and simulated every half an hour in the period 11 a.m-7 p.m.: Ta (a), RH (b) and GSR (c)

Table 2 shows the main statistics on the model accuracy: Pearson's coefficient of determination (R^2), Root Mean Square Error (RMSE) and Wilmott's index of agreement (d) [40,60]. The reliability increases for $R^2 \rightarrow 1$, RMSE$\rightarrow$0 and d$\rightarrow$1. Air temperature is well estimated (R^2=0.93, d=0.97) in line with the studies by Yang e al. [40] (R^2=0.94, RMSE=1.01 K), Ketterer e al. [61] (R^2=0.88, RMSE=0.28 K), Acero e al. [62] (R^2=0.92). The RMSE for RH lies within the range commonly reported in literature (2.04 %-10.20 %) [63]. Based on these results, we concluded that the ENVI-met model could provide reasonable predictions of Ta under UC.

	R^2	**RMSE**	**d**
Mean hourly Ta	0.93	0.98	0.97
Mean Hourly RH	0.29	2.7	0.38

Table 2 Performance indicators for the ENVI-met model under UC, based on measured and simulated Ta and RH (sample size for each receptor:17)

Concerning the MC, the simulated and measured values of Ta were examined between 11 a.m. and 19 p.m at each thermohygrometers' location. The validation was thus based on 85 pairs of values (17 for each point) (Figure 7, Table 3). The R^2 and d values indicate a strong agreement between simulated and measured Ta. The R^2 ranges from 0.81 to 0.93 depending on the site, with an average of 0.87, whereas d ranges from 0.93 to 0.98, being 0.96 on average. The RMSE never exceeds 0.99 °C and is 0.84 °C on average.

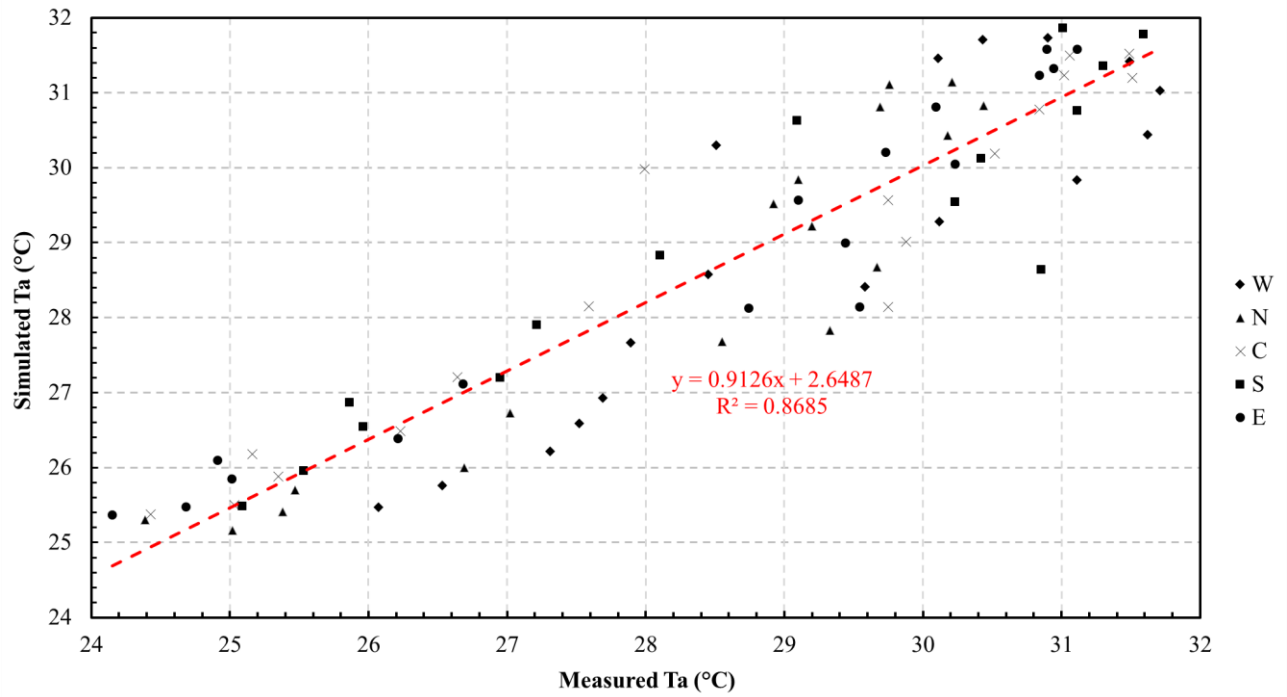

Figure 7 Comparison between simulated and measured values of Ta every half an hour in the period 11 a.m-7 p.m. at the thermohygrometers' locations

	R^2	RMSE (°C)	d
Ta (N)	0.87	0.79	0.96
Ta (S)	0.88	0.87	0.96
Ta (W)	0.81	0.99	0.93
Ta (C)	0.91	0.80	0.97
Ta (E)	0.93	0.73	0.98
Ta (all points)	0.87	0.84	0.96

Table 3 Performance indicators for the ENVI-met model under MC, based on measured and simulated Ta at the thermohygrometers' locations

By way of example, Figure 8 reports the trend of Ta at the centre of the misted area by comparing the output of the thermohygrometer C with the average between the two surrounding central receptors. Over peak hours (12 p.m to 3 p.m.) the absolute difference in average temperature is always less than 0.5 ° C. At 3.30 p.m. the measured Ta suddenly drops, due to the partial shading of the tree canopy. The simulation fails at capturing this transient phenomenon. Alignment is re-established within one hour.

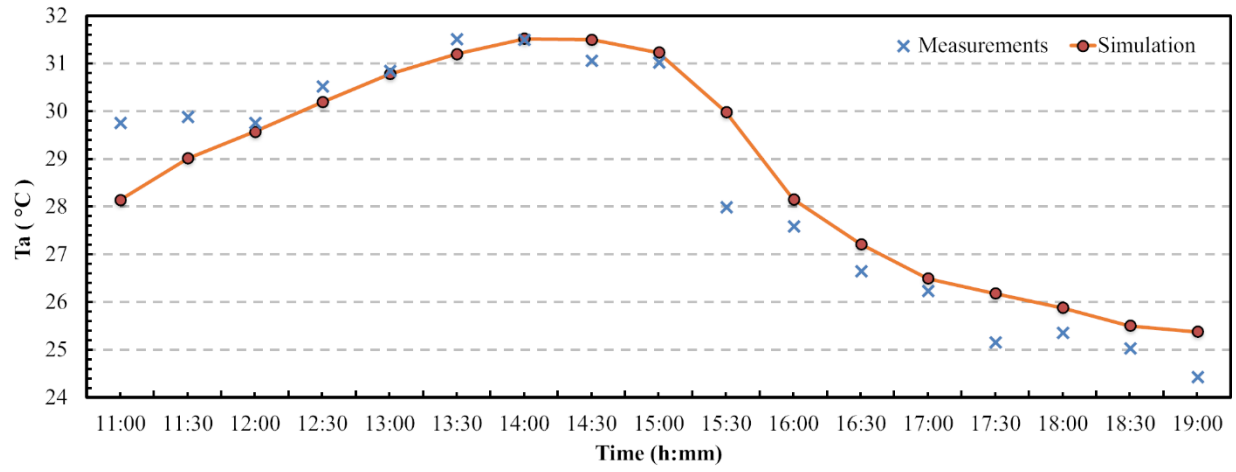

Figure 8 Comparison between average hourly measured and simulated Ta every half an hour in the period 11 a.m-7 p.m., collected at the centre of the misted area.

Figure 9 displays the box-plots of the measured and simulated Ta along the North-South section of the misted area (section line indicated in Figure 2), so as to compare trends in space. From the analysis of the experimental values (blue box-plots) recorded by the thermohygrometers at points S (south), C (centre), N (north), it can be observed that Ta decreases following the wind direction from south to north, owing to the transport of the misted droplets. The phenomenon is also correctly captured in the simulation (red box-plots). The offset between the medians at locations S and N (4 m apart) is approximately 0.8 °C, while that between the southernmost and northernmost receptors (6 m apart) reaches 1.35 °C.

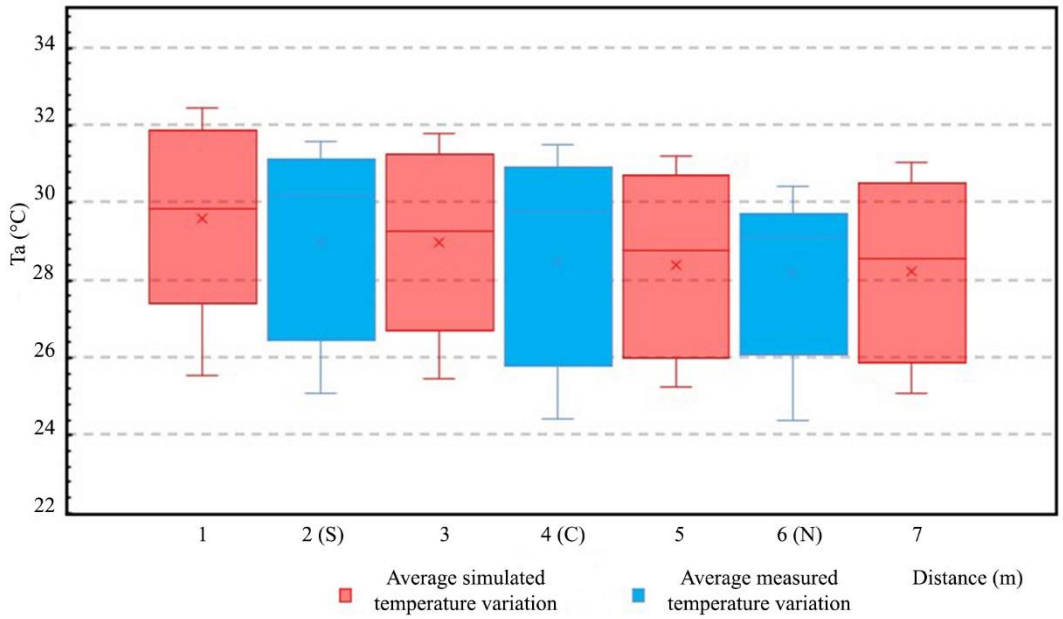

Figure 9 Box-plots of the measured (blue) and simulated (red) Ta along the N-S section of the misted area, collected every half an hour in the period 11 a.m-7 p.m.

3.2. Assessment of the impact of water mist cooling on the microclimatic conditions

With the ENVI-met model validated under both UC and MC conditions, we proceeded with the quantification of the thermal distribution induced by the mist system in the test area, to then verify the effect on the microclimate of the wider neighbourhood context.

Figure 10 shows the spatial distribution of ΔTa (difference between MC and UC) in the whole simulation domain, at 1.25 m (cell centre closest to the thermohygrometers' height) and 1.75 m (reference height of a standing person). The thermal maps refer to the peak hour (2 p.m.). The temperature ranges from about 31°C to about 34°C, consistent with the recordings of the weather station. The highest values are found over the asphalted area south-east of the domain, while the lowest ones correspond to the green area to the north-east. Significant thermal differences occur in the area right beneath the nozzles, whose effects spread further downwind, towards the north-east quadrant. At a height of 1.25 m, ΔTa peaks at 1.98 °C at 2 m distance from receptor #3 (refer to Figure 2) due north, while the minimum temperature difference (< 0.3°C) is recorded at the same distance, but due south. The evaporative cooling propagates in the north-east direction, following the wind, with reductions in the order of 0.3-0.5°C up to about 24 m away from the misted perimeter. At

a height of 1.75 m, the average thermal deviations are greater as they are detected closer to the nozzles, yet the maximum is only slightly higher (2 °C) and is recorded at the same location.

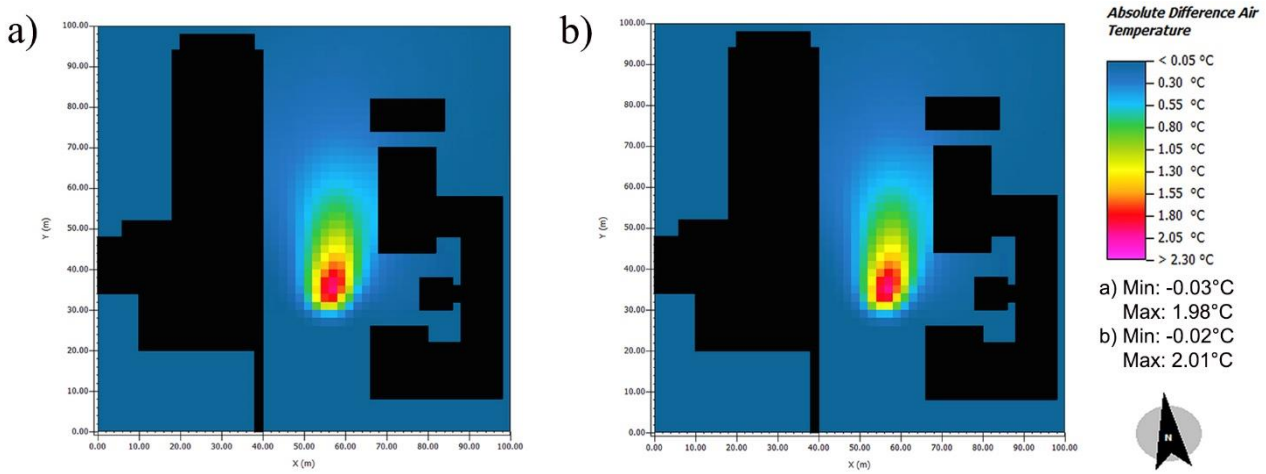

Figure 10 Simulated temperature drop in the test area at a height of 1.25 m (a) and of 1.75 m (b) at 2 p.m.

Figure 11 shows the daily ΔTa trend in the test area at 1.25 m and at 1.75m above the ground, computed as the average at the nearest receptors to N, S, W, C and E locations (see Figure 2 for reference).

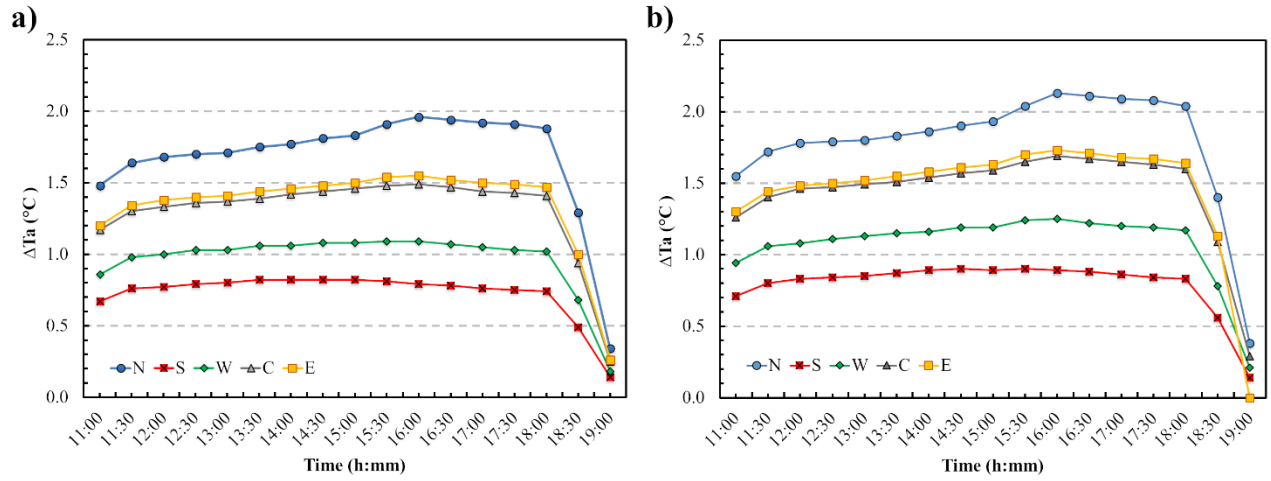

Figure 11 Simulated ΔTa in the test area (points N, S, W, C, E) at a height of 1.25 m (a) and 1.75 m (b).

The ΔTa distribution follows a similar trend at all points: generally, the most significant mean difference occurs during the hottest hours of the day, notably between 3.30 p.m. and 4 p.m. In fact, when the air temperature rises, evaporation accentuates [11,18]. The difference decreases considerably from 6 p.m. and completely vanishes half an hour after injection cessation (7.30 p.m.). At 1.25 m (Figure 11a), the maximum ΔTa is observed at point N, where it peaks just below 2 °C. Second in line are points E and C, where the thermal differences exceed 1.50 °C during the central hours of the day with a rather overlapped trend, followed by point W, whose ΔTa touches 1 °C. At point S, the smallest deviations are observed (less than 1 °C) and are maintained throughout the time of injection. At 1.75 m the thermal differences induced by the misting system are slightly higher, but with a similar spatial heterogeneity (Figure 11b).

These results confirm what has already been noted on the influence of the wind direction (Figure 9): as the microparticles of liquid water are entrained in the airflow towards the north-east, a greater local cooling effect is observed downwind. The box-plots of ΔTa along the N-S section of the site (Figure 12) highlight both the greater cooling effect and the greater dispersion of data, proceeding from south to north in the misted area.

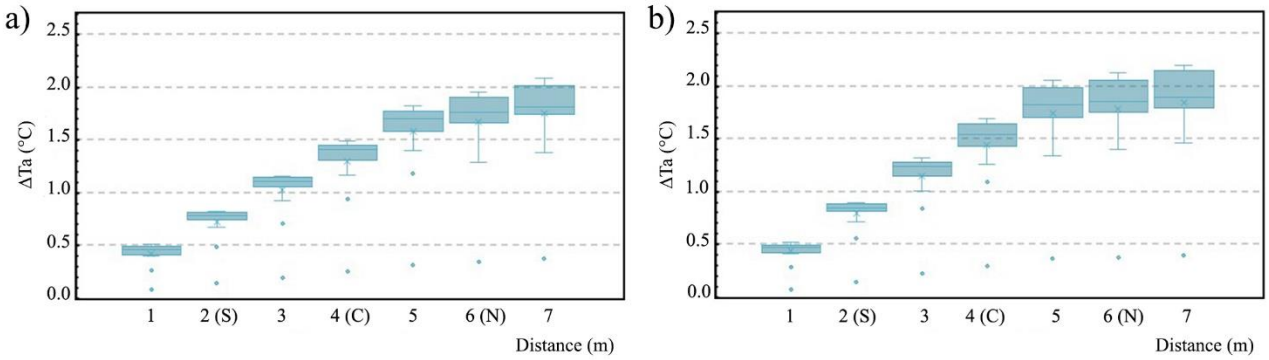

Figure 12 Box-plots of ΔTa in the test area along the N-S section at a height of 1.25 m (a) and 1.75 m (b).

3.3. Sensitivity Analysis

In this section, the mitigation potential of the mist system is analysed for the design variants described in 2.2.4, related to water flow rate, injection height and local wind speed. The graphs in Figure 13 summarize the results in terms of maximum ΔTa (recorded at 2 p.m.) at the point of maximum temperature variation (north-east of the misted area) and at a height of 1.25 m, depending on the water flow rate and for the different wind speeds considered. The three figures refer to the different injection heights, namely 2.3 m, 2.8 m (base case) and 3.3 m, in the order.

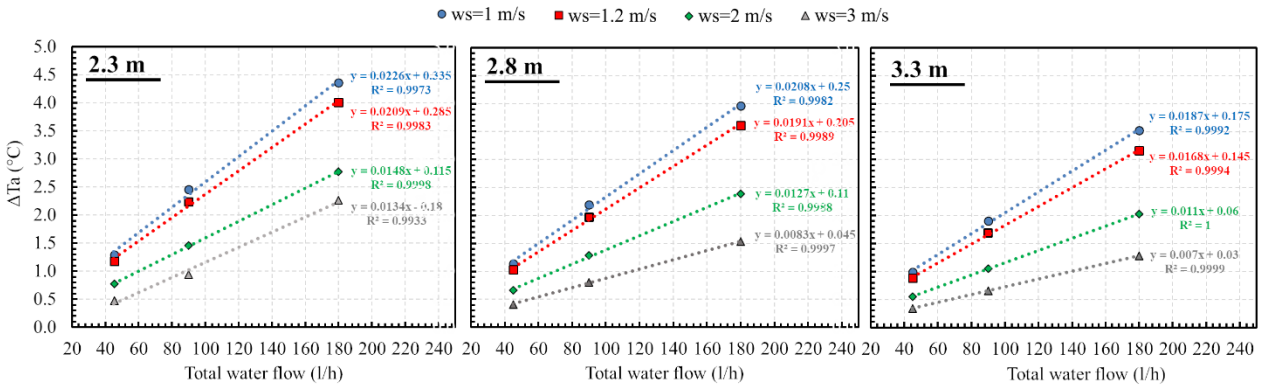

Figure 13 Maximum ΔTa recorded at 2 pm in the north-east side of the misted area and at a height of 1.25 m, as a function of water flow rate and wind speed, for injection heights of 2.3 m, 2.8 m and 3.3 m.

As expected, ΔTa increases with the water flow rate, i.e. the number of nozzles in the misted area, and decreases with higher nozzles heights. Looking at the figures, it is also clear that the mitigation potential of the water mist coolers is decreasing with an increasing wind speed. In particular, when wind speed is increasing to 2 m/s, the average decrease of the cooling potential is about 35-40 % regardless of the water flow rate. When the injection is set at 2.8 m and for ambient temperatures around 33°C, an increase in water flow rate of 10 l/h determines a magnification of the maximum

temperature delta of nearly 0.2 °C for low wind speeds (around 1-1.2 m/s), 0.1 °C at 2 m/s and <0.1 °C for higher speeds. This is also visible in the thermal maps in Figure 14 compared to those of Figure 10: here we plot the temperature drop of the model with a doubled water flow rate compared to the base case, and wind speed of 1 m/s (Figure 14 a and b) and 3 m/s (Figure 14 c and d). In presence of higher flow rate and lower wind speed, the cooling effect is significantly enhanced. On another note, higher wind speeds extend the area of influence of the system, thus providing cooling to a potentially wider number of users, although in a milder fashion. The vertical profile of the temperature drop appears fairly constant when we compare the maps at 1.25 m and 1.75 m.

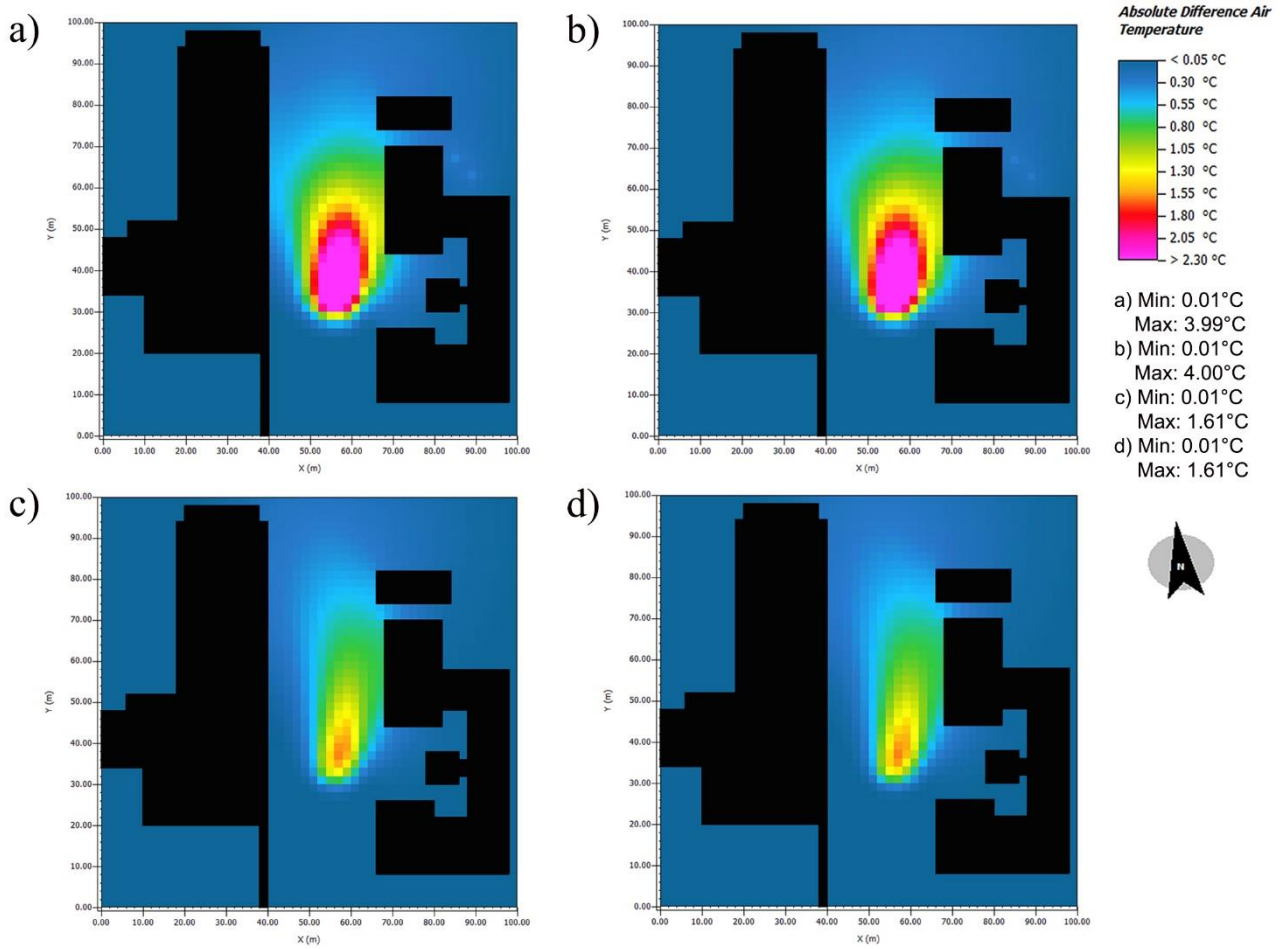

Figure 14 Simulated temperature drop in the misted area at 2 p.m with the following settings: nozzles height of 2.80 m, doubled water flow rate (180 l/h), wind speed 1 m/s at a height of 1.25 m (a) and of 1.75 m (b), wind speed 3 m/s at a height of 1.25 m (c) and of 1.75 m (d)

Looking at the leftmost and rightmost charts in Figure 13, the mitigation potential decreases by 0.1-0.5 °C when the nozzle height reaches 3.3 m and increases by 0.1-0.7 °C when the height is reduced to 2.3 m. The thermal maps in Figure 15 show that at 2.3 m and in presence of higher water flow rates, a significant cooling effect can be achieved even at relatively high wind speeds of 3 m/s (Figure 15 c and d) with the benefit of a wider cooled area.

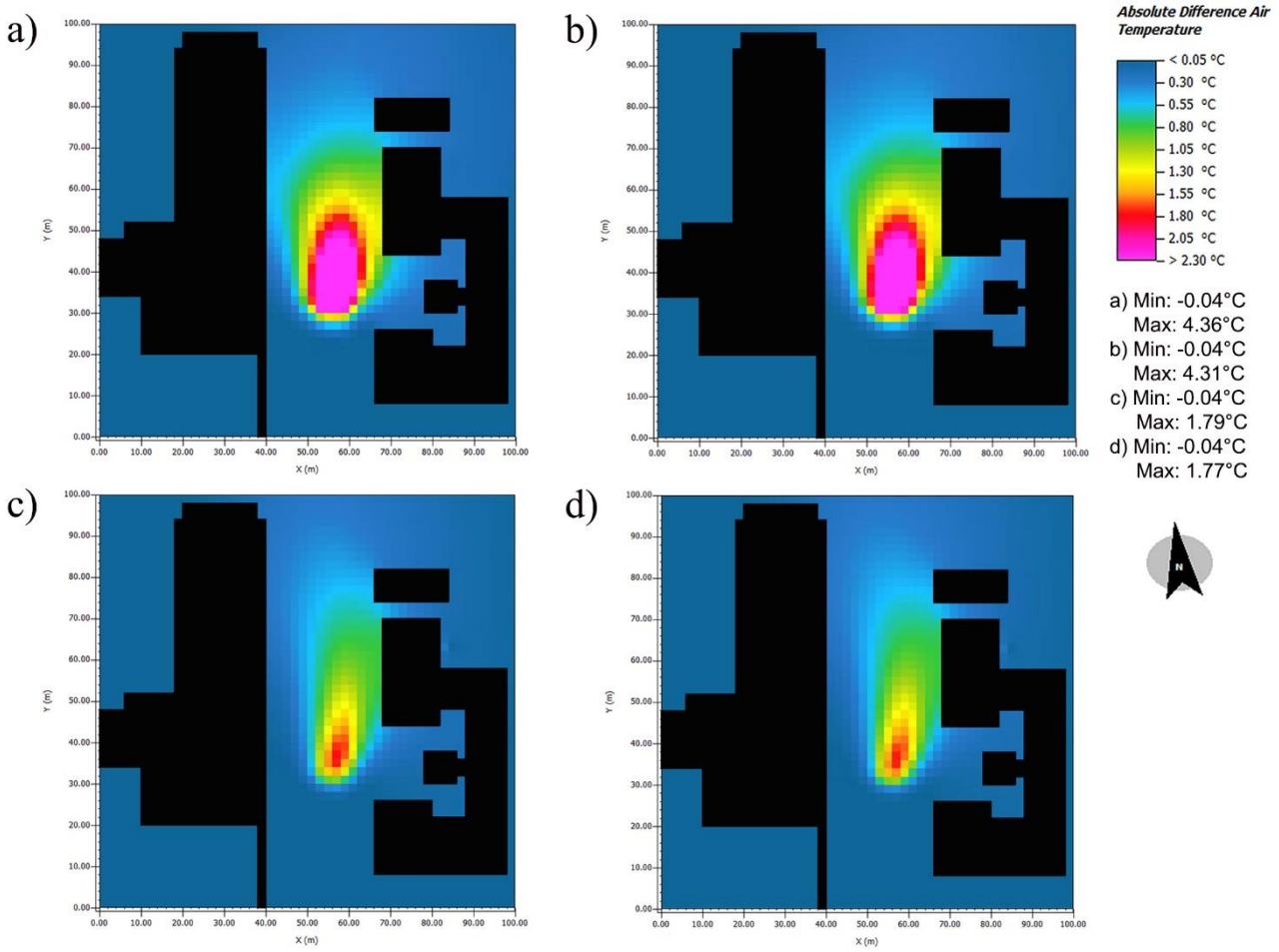

Figure 15 Simulated temperature drop in the misted area at 2 p.m with the following settings: nozzles height of 2.30 m, doubled water flow rate (180 l/h), wind speed 1 m/s at a height of 1.25 m (a) and of 1.75 m (b), wind speed 3 m/s at a height of 1.25 m (c) and of 1.75 m (d)

Finally, Figure 16 represents the vertical profiles of Ta and ΔTa recorded at 2 p.m. at the point of maximum temperature variation in the base case model compared to that of the models with different injection height. Once again, the greatest cooling effect is confirmed for a height of 2.3 m. In all cases, the maximum cooling effect is recorded in the model cell where the injectors are located, or immediately below, then it decays moving towards the soil. Interestingly, the cooling effect is also maintained at higher heights.

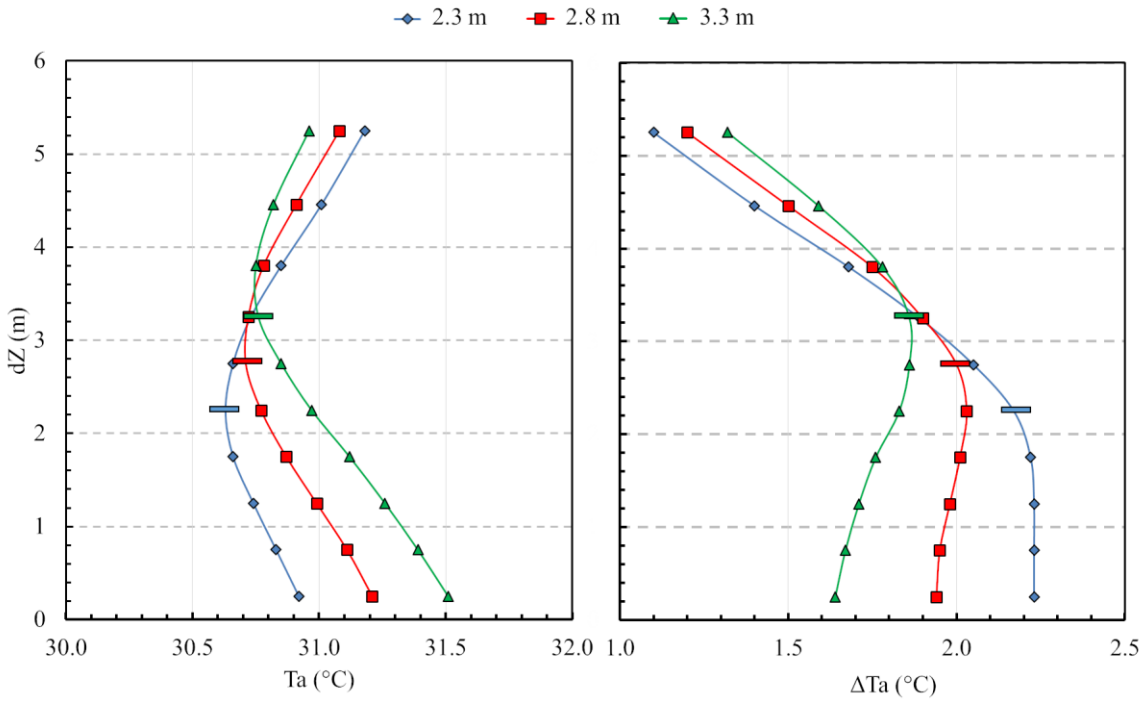

Figure 16 Vertical profiles of Ta (left side) and ΔTa (right side) recorded at 2 p.m. in the north-east side of the misted area in the base case model (red line) compared to that of the models with increased (green line) and decreased (blue line) nozzles height. The rectangular indicators represent the height of the nozzles along the vertical profile.

4. Discussion

In this study, a water spray model was developed in ENVI-met. Compared to other CFD platforms, ENVI-met's approach to water spray tracking relies on two simplifying assumptions: i) all droplets have the same diameter (no statistical distribution) and ii) the amount of droplets in a given air volume changes due to evaporation, but not their size. By not considering any statistical distribution, ENVI-met's water spray model might be prone to inaccuracies both in terms of cooling and humidification, since the droplet size governs the heat and mass transfer rates between the continuous (air) and discrete (water) phase. To overcome this issue, a preliminary tuning procedure on the mean droplet diameter was proposed. The results reasonably matched the experimental data from a real case in urban settings in terms of temperature evolution both under undisturbed and misted conditions as quantified by Pearson's coefficient of determination, Root Mean Square Error and Wilmott's index of agreement. With a horizontal discretization of 2 m x 2 m and a vertical discretization of 0.5 m, the temperature distribution was replicated with good accuracy both horizontally and vertically. Notably, the vertical profile of the temperature difference beneath the injections responded to a Lorentzian-like distribution, matching the experimental results by Ulpiani et al. [10]. Conversely, the model failed at predicting the relative humidity, as also reported elsewhere.

The simulations tracked the cooling action in and out of the misted perimeter, allowing to quantify the spatial extension of the influence area. Indeed, it was proved that the most significant thermal drops (1.95 °C at 1.25 m height) occurred close but out of the misted perimeter, following the wind direction. Temperature reductions (in the order of 0.3-0.5 °C) persisted downwind, up to about 24 m away from the misted perimeter. The mist cooling was most impactful, on average, during the hottest hours of the day, which is in line with well-established results in literature [11] and is a direct consequence of psychrometric conditions more conducive to evaporative cooling.

As displayed in Figures 6-9, there was a systematic offset between measured and simulated air temperature (amounting at 1 °C, on average), which was positive during morning hours (before midday) and negative during afternoon and evening hours (after 3.30 p.m.). Conversely, over peak hours, the absolute values were captured almost perfectly. It is straightforward to assume that the effect of solar shading from the tree leaves and the buildings all around was not fully reflected in the simulation and, as such, represented a major source of error. Also, the morning time mismatch suggests that the model may have not captured the decline in evaporative cooling potential that occurred due to the concurrent evaporation of condensed moisture and water stored in the green soil overnight. From Figure 7, it is also evident that the dispersion of values incremented at higher air temperatures (over 28-29 °C). The reason might be found in the increased local turbulence that is engendered close to ground level as a result of mightier upward moving thermals, which may have had an impact on the dilution and dispersion of droplet particles.

The sensitivity analysis further delved into the role played by water flow rate, injection height and wind speed. As expected, at 1.25 m above the ground, the temperature difference in the misted scenario compared to the undisturbed case increased with the density of nozzles and decreased with higher injection height. This is in contrast with the simulation results by Yamada et al., in which nor the number of nozzles (varied from 1 to 3, at 2.5 m intervals) nor the size (average diameter change in the order of 10 μm) significantly affected the cooling potential [22]. The cooling decreased by 0.1-0.5 °C when the nozzle height was lifted to 3.3 m and increased by 0.1-0.7 °C when the height was reduced to 2.3 m, compared to the baseline at 2.8 m. It was also clearly demonstrated that the cooling capacity of mist coolers diminished with increasing wind speed (average decrease of 35-40 % in response to 0.8 m/s acceleration). Notably, when the injection was set at 2.8 m above the ground, and for ambient temperatures around 33°C, an increase in water flow rate of 10 l/h determined a magnification of the maximum temperature drop of nearly 0.2 °C for low wind speeds (around 1-1.2 m/s), 0.1 °C for winds of 2 m/s and <0.1 °C for higher speeds. Hence, doubling the number of nozzles caused the maximum ΔTa to rise from 1.97 °C to 3.62 °C, with extra +0.3 °C under light breeze (1 m/s). Conversely, the drop decreased down to 1.53 °C when the wind blew at the maximum considered speed of 3 m/s.

This study offers itself as a guideline for other users in the setup of water spray modelling scenarios in ENVI-met, to be gradually refined as more data and documentation will be available. Indeed, the evaporative cooling provided by the present water spray system is not high in absolute values and thus non-optimal for the software validation. Further verification may be needed to substantiate our findings. On the other hand, the model captured with good accuracy the experimental magnitude and the trends both in space and in time. This entails that the underlying equations well reflected the effects of diffusion, dilution, directionality, dynamic variability and the interlacement with other phenomena pertaining to the local surroundings. Moreover, experimental and modelled results are in good agreement only for a droplet diameter distribution that is very close with that obtained by direct measurement and deviate for smaller or larger diameters. This demonstrates that the model responds with sufficient accuracy, despite the assumptions. Further research will be conducted to test different experimental setups and thus different evaporative cooling intensities under diverse climatic contexts and possibly with due attention to absolute humidity, to overcome most of the above limitations and proceed towards an informed use of the software's models.

5. Conclusion

Dry mist systems may play a crucial role in combating the phenomenon of urban overheating at local scale. Compared to alternative evaporative technologies, the water consumption is very modest and the risk of wettedness very marginal, especially when the cooling action is smartly controlled. Their beneficial action includes air conditioning energy use minimization, solar radiation attenuation and pollution removal. As mist cooling gains popularity as urban overheating countermeasure and gets more and more used for streetscaping, urban greening plans, comfort enhancement also from private parties, it is extremely important to assess its effectiveness in relation to other typical urban microclimatic phenomena (e.g. canyon effects, evapotranspiration, reduced soil permeability, anthropogenic heat). This can be done using well-established urban microclimatic models, such as ENVI-met. ENVI-met includes a water spray model which, to the best of our knowledge, has never been experimentally validated and still lacks proper documentation.

Against this backdrop, we investigated how misting systems perturb the local urban climate by means of a 3D microclimatic model in ENVI-met, thoroughly validated on the basis of experimental evidence and tested under different design and environmental scenarios. Following a careful setup procedure, our model accurately recreated the trends and impacts of mist cooling at neighbourhood scale considering the competing effects of greenery and urban forcing. Through simulation, we could i) quantify the spatial extension of the cooled area under different environmental conditions and thus complement the experimental results with no need for extensive sensor networks ii) determine the sensitivity of the cooling action to wind speed, water flow rate and nozzle's height above the ground via parametric analysis and iii) derive substantiated design criteria to be applied at both manufacturing and urban planning level. For instance, we demonstrated that mist cooling could be still impactful under windy conditions if the injections are lowered down enough, since the local temperature reduction would still be significant at pedestrian height while the risk of wettedness would be strongly mitigated by the considerable jet deflection.

Further research would target climate dependencies and would include different misting systems to extend the applicability of the above results and further verify the model accuracy.

Acknowledgments

Authors warmly thank the Italian national agency for new technologies, energy and sustainable economic development (ENEA) - under the funding PAR 2017 sub-project D.6 Sviluppo di un modello integrato di smart district urbano - for providing the resources to build the prototype.

References

[1] M. Santamouris, C. Cartalis, A. Synnefa, D. Kolokotsa, On the impact of urban heat island and global warming on the power demand and electricity consumption of buildings—A review, Energy Build. 98 (2015) 119–124. doi:10.1016/j.enbuild.2014.09.052.

[2] M. Santamouris, Recent progress on urban overheating and heat island research. Integrated assessment of the energy, environmental, vulnerability and health impact. Synergies with the global climate change, Energy Build. 207 (2020). doi:10.1016/j.enbuild.2019.109482.

[3] IPCC Special Report, (n.d.).

[4] M. Santamouris, Heat island research in Europe: The state of the art, Adv. Build. Energy Res. 1 (2007) 123–150. doi:10.1080/17512549.2007.9687272.

[5] M. Santamouris, Analyzing the heat island magnitude and characteristics in one hundred Asian and Australian cities and regions, Sci. Total Environ. 512–513 (2015) 582–598. doi:10.1016/j.scitotenv.2015.01.060.

[6] UN-HABITAT, Global Report on Human Settlements 2011: Cities and Climate Change, 2011.

[7] G.Y. Yun, J. Ngarambe, P.N. Duhirwe, G. Ulpiani, R. Paolini, S. Haddad, K. Vasilakopoulou, M. Santamouris, Predicting the magnitude and the characteristics of the urban heat island in coastal cities in the proximity of desert landforms. The case of Sydney, Sci. Total Environ. 709 (2020) 136068. doi:10.1016/j.scitotenv.2019.136068.
[8] O. Aleksandrowicz, M. Vuckovic, K. Kiesel, A. Mahdavi, Current trends in urban heat island mitigation research: Observations based on a comprehensive research repository, Urban Clim. 21 (2017) 1–26. doi:10.1016/j.uclim.2017.04.002.
[9] E.J. Gago, J. Roldan, R. Pacheco-Torres, J. Ordóñez, The city and urban heat islands: A review of strategies to mitigate adverse effects, Renew. Sustain. Energy Rev. 25 (2013) 749–758. doi:10.1016/j.rser.2013.05.057.
[10] G. Ulpiani, E. Di Giuseppe, C. Di Perna, M. D'Orazio, M. Zinzi, Thermal comfort improvement in urban spaces with water spray systems: Field measurements and survey, Build. Environ. 156 (2019) 46–61. doi:https://doi.org/10.1016/j.buildenv.2019.04.007.
[11] G. Ulpiani, Water mist spray for outdoor cooling: A systematic review of technologies, methods and impacts, Appl. Energy. 254 (2019) 113647. doi:10.1016/j.apenergy.2019.113647.
[12] C. Farnham, M. Nakao, M. Nishioka, M. Nabeshima, T. Mizuno, Effect of Water Temperature on Evaporation of Mist Sprayed From a Nozzle, J. Heat Isl. Inst. Int. 10 (2015) 35–44.
[13] T. Ishii, M. Tsujimoto, G. Yoon, M. Okumiya, Cooling System with Water Mist Sprayers for Mitigation of Heat-island Drymist system : Uchimizu, Seventh Int. Conf. Urban Clim. (2009) 2–3.
[14] D. Narumi, K. Shigematsu, Y. Shimoda, Effect of the Evaporative Cooling Techniques by Spraying Mist Water on Reducing Urban Heat Flux and Saving Energy in Apartment House, J. Heat Isl. Inst. Int. 7 (2012) 175–181. http://heatisland2009.lbl.gov/docs/221000-narumi-doc.pdf.
[15] S. Yu, Water spray geoengineering to clean air pollution for mitigating haze in China's cities, Environ. Chem. Lett. 12 (2014) 109–116. doi:10.1007/s10311-013-0444-0.
[16] L.A. Dombrovsky, V.P. Solovjov, B.W. Webb, Attenuation of solar radiation by a water mist from the ultraviolet to the infrared range, J. Quant. Spectrosc. Radiat. Transf. 112 (2011) 1182–1190. doi:10.1016/j.jqsrt.2010.08.018.
[17] K.R. Gunawardena, M.J. Wells, T. Kershaw, Utilising green and bluespace to mitigate urban heat island intensity, Sci. Total Environ. 584–585 (2017) 1040–1055. doi:10.1016/j.scitotenv.2017.01.158.
[18] G. Ulpiani, C. Di Perna, M. Zinzi, Water nebulization to counteract urban overheating : Development and experimental test of a smart logic to maximize energy efficiency and outdoor environmental quality, Appl. Energy. 239 (2019) 1091–1113. doi:10.1016/j.apenergy.2019.01.231.
[19] H.R. Pruppacher, J.D. Klett, Microphysics of Clouds and Precipitation, 1997.
[20] G. Ulpiani, E. Di Giuseppe, C. Di Perna, M.D. Orazio, M. Zinzi, Design optimization of mist cooling for Urban Heat Island mitigation: experimental study on the role of injection density, (2019). doi:10.1088/1755-1315/296/1/012025.
[21] G. Ulpiani, C. Perna, M. Zinzi, Mist cooling in urban spaces: Understanding the key factors behind the mitigation potential, Appl. Therm. Eng. (2020) 115644. doi:10.1016/j.applthermaleng.2020.115644.
[22] H. Yamada, G. Yoon, M. Okumiya, H. Okuyama, Study of cooling system with water mist sprayers: Fundamental examination of particle size distribution and cooling effects, Build. Simul. 1 (2008) 214–222. doi:10.1007/s12273-008-8115-y.
[23] J. Wang, X. Tu, Z. Wang, J. Huang, Application and Numerical Simulation on Water Mist Cooling for Urban Environment Regulation, in: Lect. Notes Comput. Sci., 2010. doi:10.1007/978-3-642-15859-9.
[24] H. Montazeri, B. Blocken, J.L.M. Hensen, CFD analysis of the impact of physical parameters

on evaporative cooling by a mist spray system, Appl. Therm. Eng. 75 (2015) 608–622. doi:10.1016/j.applthermaleng.2014.09.078.
[25] H. Montazeri, Y. Toparlar, B. Blocken, J.L.M. Hensen, Simulating the cooling effects of water spray systems in urban landscapes: A computational fluid dynamics study in Rotterdam, The Netherlands, Landsc. Urban Plan. 159 (2017) 85–100. doi:10.1016/j.landurbplan.2016.10.001.
[26] H. Barrow, C.W. Pope, Droplet evaporation with reference to the effectiveness of water-mist cooling, Appl. Energy. 84 (2007) 404–412. doi:10.1016/j.apenergy.2006.09.007.
[27] C. Farnham, M. Nakao, M. Nishioka, M. Nabeshima, T. Mizuno, Study of mist-cooling for semi-enclosed spaces in Osaka, Japan, Procedia Environ. Sci. 4 (2011) 228–238. doi:10.1016/j.proenv.2011.03.027.
[28] W. Jun-feng, T. Xin-cheng, Experimental Study and Numerical Simulation on Evaporative Cooling of Fine Water Mist in Outdoor Environment, 2009 Int. Conf. Energy Environ. Technol. (2009) 156–159. doi:10.1109/ICEET.2009.44.
[29] M. Kojima, K. Nakashima, S. Management, A Study of Mist Spraying System by Urban Transportation, Des. Innov. Value Towar. a Sustain. Soc. Springer, Dordr. (2012) 720–723.
[30] C. Huang, J. Cai, Z. Lin, Q. Zhang, Y. Cui, Solving model of temperature and humidity profiles in spray cooling zone, Build. Environ. 123 (2017) 189–199. doi:10.1016/j.buildenv.2017.06.043.
[31] M. Santamouris, S. Haddad, M. Saliari, K. Vasilakopoulou, A. Synnefa, R. Paolini, G. Ulpiani, S. Garshasbi, F. Fiorito, On the energy impact of urban heat island in Sydney: Climate and energy potential of mitigation technologies, Energy Build. 166 (2018). doi:10.1016/j.enbuild.2018.02.007.
[32] S. Haddad, G. Ulpiani, R. Paolini, A. Synnefa, M. Santamouris, Experimental and Theoretical analysis of the urban overheating and its mitigation potential in a hot arid city – Alice Springs, Archit. Sci. Rev. (2019) 1–16. doi:10.1080/00038628.2019.1674128.
[33] S. Tsoka, K. Tsikaloudaki, T. Theodosiou, Coupling a building energy simulation tool with a microclimate model to assess the impact of cool pavements on the building's energy performance application in a dense residential area, Sustain. 11 (2019). doi:10.3390/su11092519.
[34] A. Aboelata, S. Sodoudi, Evaluating the effect of trees on UHI mitigation and reduction of energy usage in different built up areas in Cairo, Build. Environ. 168 (2020) 106490. doi:10.1016/j.buildenv.2019.106490.
[35] G. Battista, R. de Lieto Vollaro, M. Zinzi, Assessment of urban overheating mitigation strategies in a square in Rome, Italy, Sol. Energy. 180 (2019) 608–621. doi:10.1016/j.solener.2019.01.074.
[36] M. Bruse, H. Fleer, Simulating surface-plant-air interactions inside urban environments with a three dimensional numerical model, Environ. Model. Softw. 13 (1998) 373–384. doi:10.1016/S1364-8152(98)00042-5.
[37] ISO - International Organization for Standardization, ISO 7726:1998 Ergonomics of the thermal environment - Instruments for measuring physical quantities, 1998.
[38] ENVI-met Model Architecture, (n.d.).
[39] H. Simon, J. Lindén, D. Hoffmann, P. Braun, M. Bruse, J. Esper, Modeling transpiration and leaf temperature of urban trees – A case study evaluating the microclimate model ENVI-met against measurement data, Landsc. Urban Plan. 174 (2018) 33–40. doi:10.1016/j.landurbplan.2018.03.003.
[40] X. Yang, L. Zhao, M. Bruse, Q. Meng, Evaluation of a microclimate model for predicting the thermal behavior of different ground surfaces, Build. Environ. 60 (2013) 93–104. doi:10.1016/j.buildenv.2012.11.008.
[41] ISO - International Organization for Standardization, ISO 10456:2007 Building materials and products: Hygrothermal properties. Tabulated design values and procedures for determining declared and design thermal values, 2007.

[42] UNI Ente Italiano di Normazione, UNI 10351:2015 Materiali e prodotti per edilizia - Proprietà termoigrometriche - Procedura per la scelta dei valori di progetto (in Italian), 1994.
[43] R.B. Clapp, G.M. Hornberger, Empirical equations for some soil hydraulic properties, Water Resour. Res. 14 (1978) 601–604. doi:10.1029/WR014i004p00601.
[44] Dipartimento per il servizio geologico d'Italia - ISPRA Archivio nazionale delle indagini nel sottosuolo (Legge 464/1984), (n.d.).
[45] M.P. Rouault, P.G. Mestayer, R. Schiestel, A model of evaporating spray droplet dispersion, J. Geophys. Res. Ocean. 96 (1991) 7181–7200.
[46] J.B. Edson, Lagrangian model simulation of the turbulent transport of evaporating jet droplets., Thesis. (1990).
[47] L.E. Andreas, Thermal and size evolution of sea spray droplets, CRREL Rep. (1989).
[48] R.B. Bird, W.E. Stewart, E.N. Lightfoot, Diffusivity and the mechanisms of mass transport, Transp. Phenom. (1960) 513–542.
[49] R.Q. Dunham, Rosin-Rammler Distributions in ANSYS Fluent, 2012.
[50] ENVI-met 3.1 Manual, (n.d.).
[51] Eurometeo, (n.d.).
[52] G. Bonafè, Microclima urbano: impatto dell'urbanizzazione sulle condizioni climatiche locali e fattori di mitigazione (in Italian), 2006.
[53] Norme Tecniche per le Costruzioni. DM 17/1/2018 (in Italian), 2018.
[54] F. Bauelos-Ruedas, C. Angeles-Camacho, Sebastin, Methodologies Used in the Extrapolation of Wind Speed Data at Different Heights and Its Impact in the Wind Energy Resource Assessment in a Region, in: Wind Farm - Tech. Regul. Potential Estim. Siting Assess., 2011. doi:10.5772/20669.
[55] A. Murat, A. Sisman, A. Gultekin, B. Dehghan, An Experimental Performance Comparison between Different Shallow Ground Heat Exchangers, World Geotherm. Congr. 2015. (2015).
[56] Turbulence Model in ENVI-met, (n.d.).
[57] H. Montazeri, B. Blocken, J.L.M. Hensen, Evaporative cooling by water spray systems: CFD simulation, experimental validation and sensitivity analysis, Build. Environ. 83 (2015) 129–141. doi:10.1016/j.buildenv.2014.03.022.
[58] G. Swamy, S.M. Shiva Nagendra, U. Schlink, Urban Heat Island (UHI) influence on secondary pollutant formation in a tropical humid environment, J. Air Waste Manag. Assoc. 67 (2017) 1080–1091. doi:10.1080/10962247.2017.1325417.
[59] J. Lindén, H. Simon, P. Fonti, J. Esper, M. Bruse, Observed and modeled transpiration cooling from urban trees in Mainz , Germany, ICUC9 - 9th Int. Conf. Urban Clim. Jointly with 12th Symp. Urban Environ. (2015).
[60] C.J. Willmott, Some comments on the evaluation of model performance, Bull. - Am. Meteorol. Soc. 63 (1982) 1309–1313. doi:10.1175/1520-0477(1982)063<1309:SCOTEO>2.0.CO;2.
[61] C. Ketterer, A. Matzarakis, Comparison of different methods for the assessment of the urban heat island in Stuttgart, Germany, Int. J. Biometeorol. 59 (2015) 1299–1309. doi:10.1007/s00484-014-0940-3.
[62] J.A. Acero, K. Herranz-Pascual, A comparison of thermal comfort conditions in four urban spaces by means of measurements and modelling techniques, Build. Environ. 93 (2015) 245–257. doi:10.1016/j.buildenv.2015.06.028.
[63] S. Tsoka, A. Tsikaloudaki, T. Theodosiou, Analyzing the ENVI-met microclimate model's performance and assessing cool materials and urban vegetation applications–A review, Sustain. Cities Soc. 43 (2018) 55–76. doi:10.1016/j.scs.2018.08.009.
[64] J.A. Villena Del Carpio, D.L. Marinoski, G. Trichês, R. Lamberts, J.V.S. de Melo, Urban pavements used in Brazil: Characterization of solar reflectance and temperature verification in the field, Sol. Energy. (2016). doi:10.1016/j.solener.2016.04.044.

Appendix A

	th (m)	α (-)	τ (-)	ρ (-)	ε (-)	Cs (J/kg·K)	λ (W/m·K)	ρ_{mat} (kg/m³)
Church external wall (from interior to exterior)								
Gypsum plaster	0.02	0.50	0.00	0.50	0.90	960	0.51	1120
Concrete	0.20	0.70	0.00	0.30	0.90	840	1.90	2500
Cement plaster	0.02	0.50	0.00	0.50	0.90	840	0.80	1600
Red brick (only north façade)	0.30	0.60	0.00	0.40	0.90	650	0.44	1500
Church roof (from interior to exterior)								
Concrete slab	0.24	0.40	0.00	0.60	0.90	880	1.09	1100
Waterproofing	0.004	0.77	0.00	0.23	0.87	1000	0.85	2400
Clay roof tiles	0.04	0.50	0.00	0.50	0.90	840	0.81	1700
Windows								
Clear glass	0.02	0.05	0.90	0.05	0.90	750	1.05	2500
Polyclinic wall (from interior to exterior)								
Perforated brick	0.08	0.67	0.00	0.33	0.92	840	0.25	800
Air	0.04	0.00	1.00	0.00	0.96	1006	0.025	1.204
Semi-filled brick	0.25	0.67	0.00	0.33	0.95	840	0.25	800
Polyclinic roof (from interior to exterior)								
Concrete slab	0.24	0.40	0.00	0.60	0.90	880	1.09	1100
Concrete screed	0.05	0.73	0.00	0.27	0.93	1000	0.22	1490
Waterproofing	0.004	0.77	0.00	0.23	0.87	1000	0.85	2400
Box prefabricated annex to the polyclinic (wall and roof, from interior to exterior)								
Plasterboard	0.0125	0.50	0.00	0.50	0.90	840	0.16	800
Glass wool	0.04	0.60	0.00	0.40	0.90	1256	0.04	30
Steel sheet	0.002	0.20	0.00	0.80	0.10	4800	45	800

Table A.1 thermo-opto-physical properties of the materials used for the modelled built elements.

Species	Aspect Ratio	Foliage Shortwave Albedo	Foliage Shortwave Transmittance	Leaf Type
Tilia cordata	1.45	0.18	0.30	Decidous
Tilia cordata	1.56	0.18	0.30	Decidous
Pinus Pinea	1.45	0.60	0.30	Conifer
Platanus Acerifolia	1.33	0.18	0.30	Decidous
Robinia Pseudoacacia	1.71	0.18	0.30	Decidous

Table A.2 Trees specifications.

Type	Albedo	Foliage Shortwave Transmittance	Plant height (m)
Dense grass	0.26	0.30	0.25
Dry grass	0.20	0.30	0.10

Table A.3 Characteristics relating to the grass surface of the model.

Soil type	V	n_s (m^3/m^3)	n_{fc} (m^3/m^3)	n_{wilt} (m^3/m^3)	MatPot (m)	hydr (10^{-6}m/s)	CP ($10^6 J/m^3K$)	b (-)	λ (W/mK)	ε (-)	ρ (-)
Loam	0	0.451	0.240	0.155	-0.478	7	1.212	5.39	0.00	0.98	0.00
Cement	1	0.00	0.00	0.00	0.00	0.00	2.083	0.00	1.63	0.90	0.22
Asphalt:	1	0.00	0.00	0.00	0.00	0.00	2.214	0.00	1.16		
-aged										0.90	0.10
-new	-	-	-	-	-	-	-	-	-	0.98	0.04
-red										0.93	0.07

Table A.4 Physical, hydraulic and optical characteristics of the types of soil considered in the model. The abbreviation V indicates the permeability of the soil: 0 if it is permeable, 1 if it is waterproof. The ε and ρ values are derived from literature [64].

Fig 1

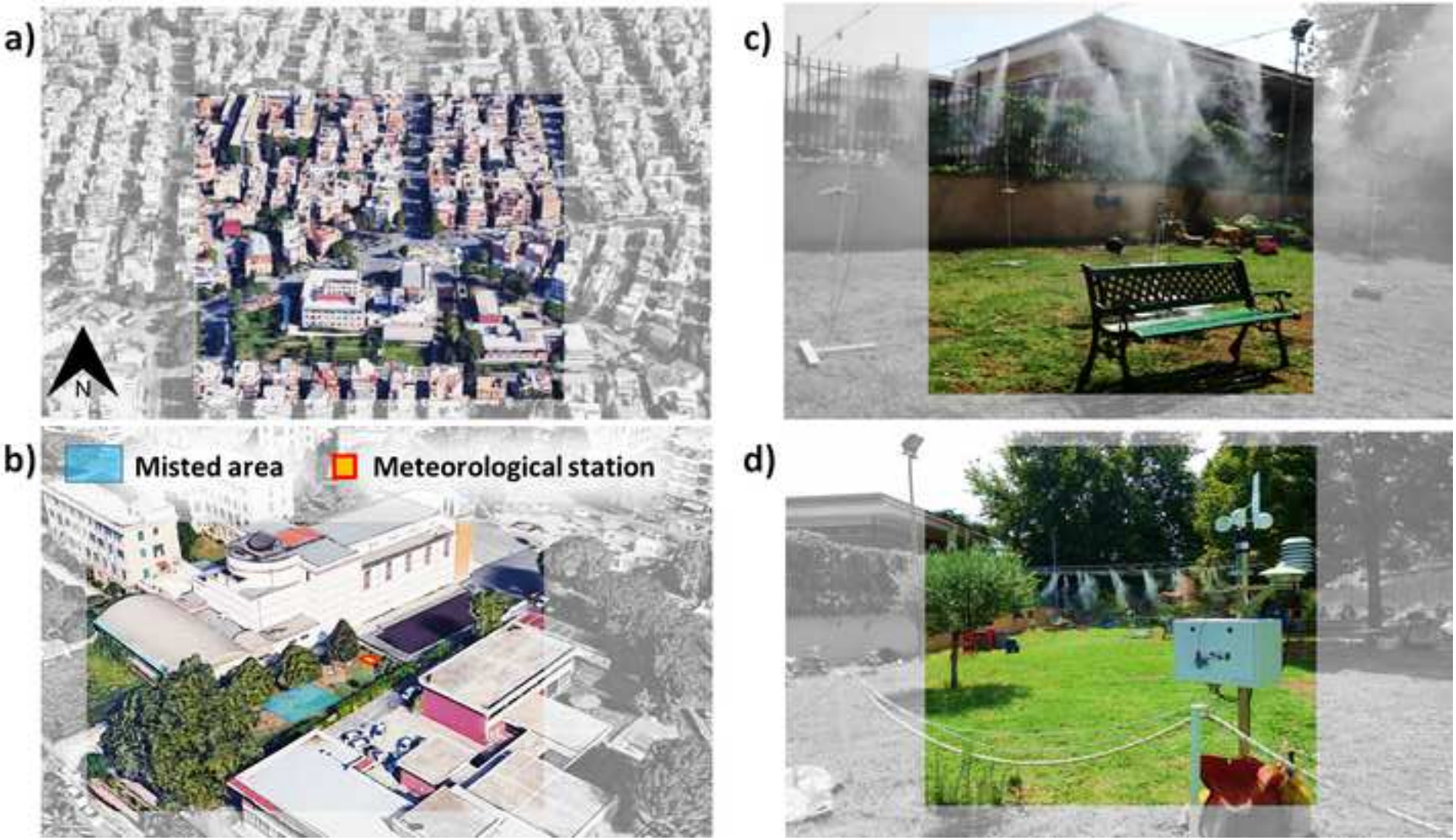

Fig 2

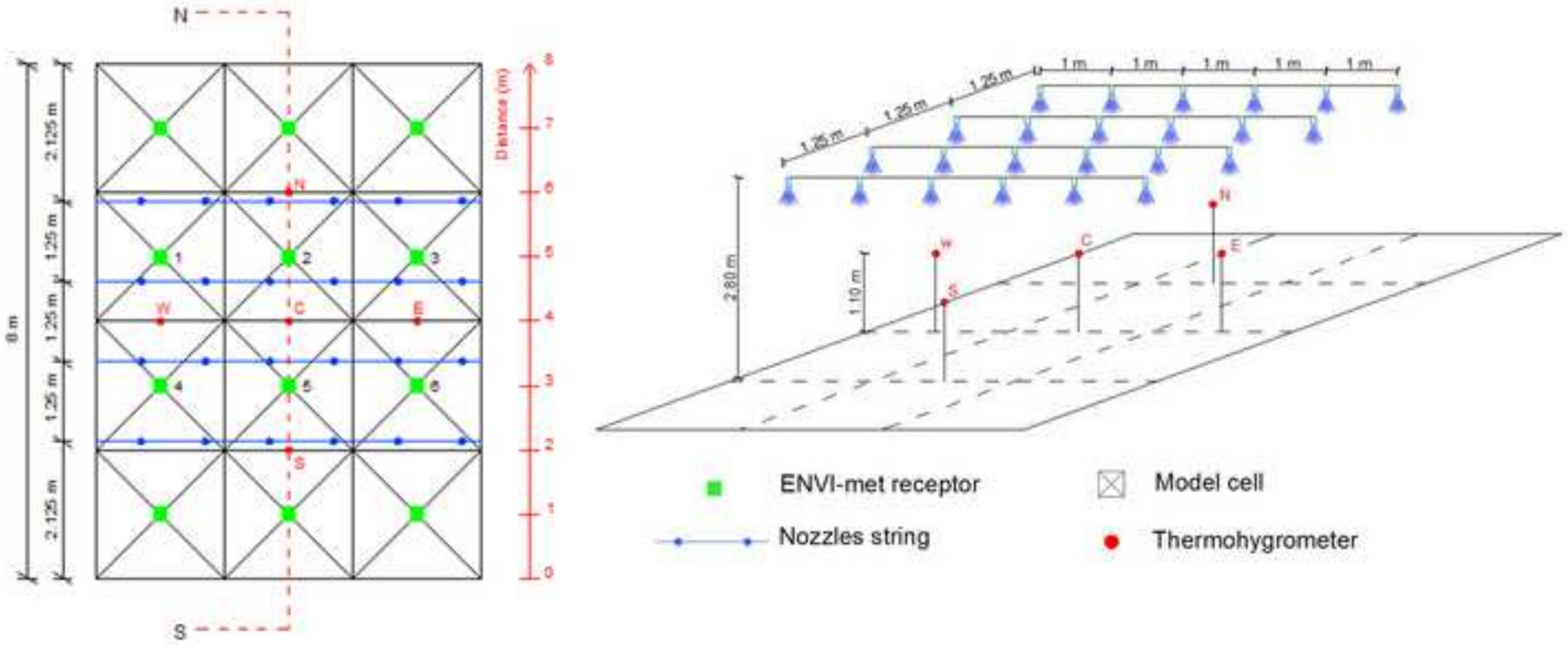

Fig 3

Click here to access/download;Figure;Fig 3 300dpi.jpg

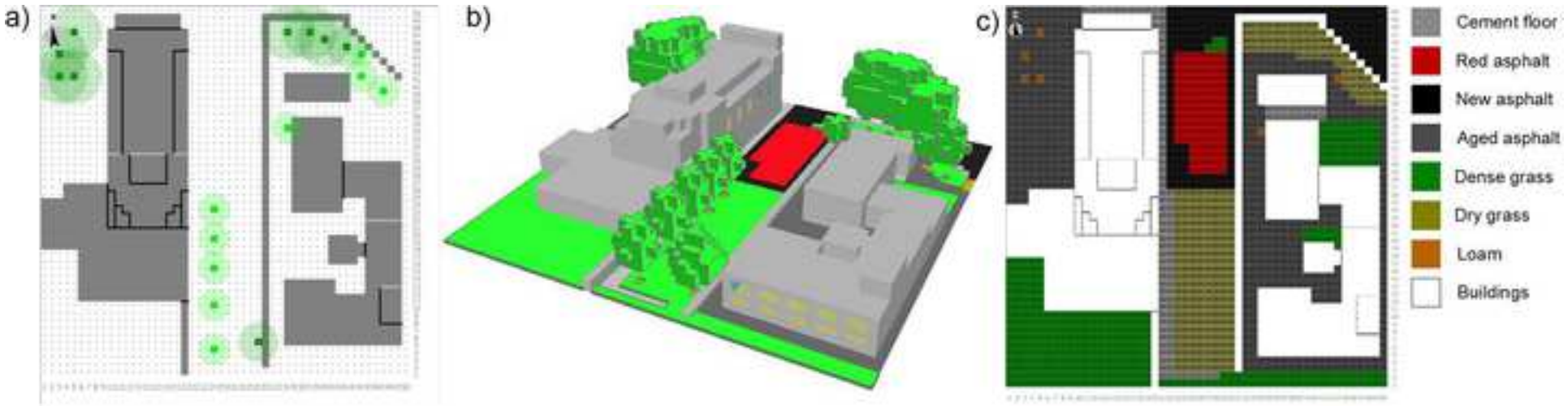

Fig 4

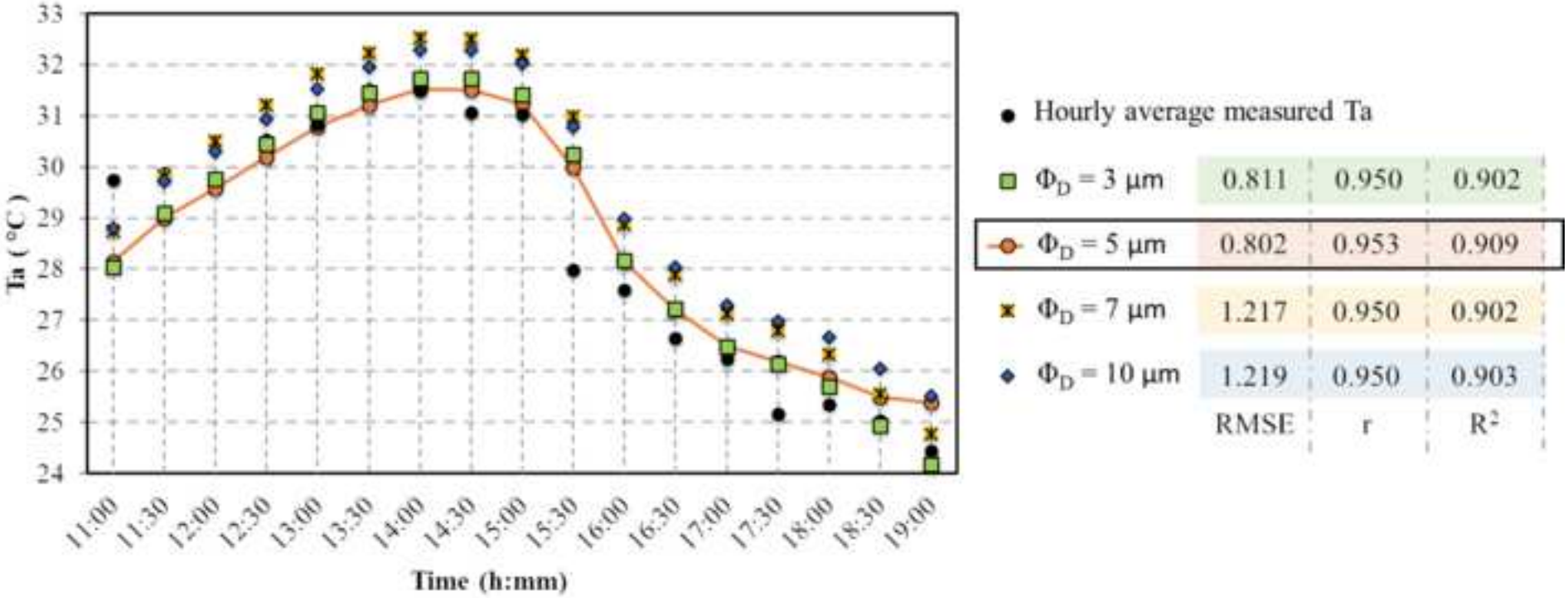

Fig 5

Click here to access/download;Figure;Fig 5 300dpi.jpg

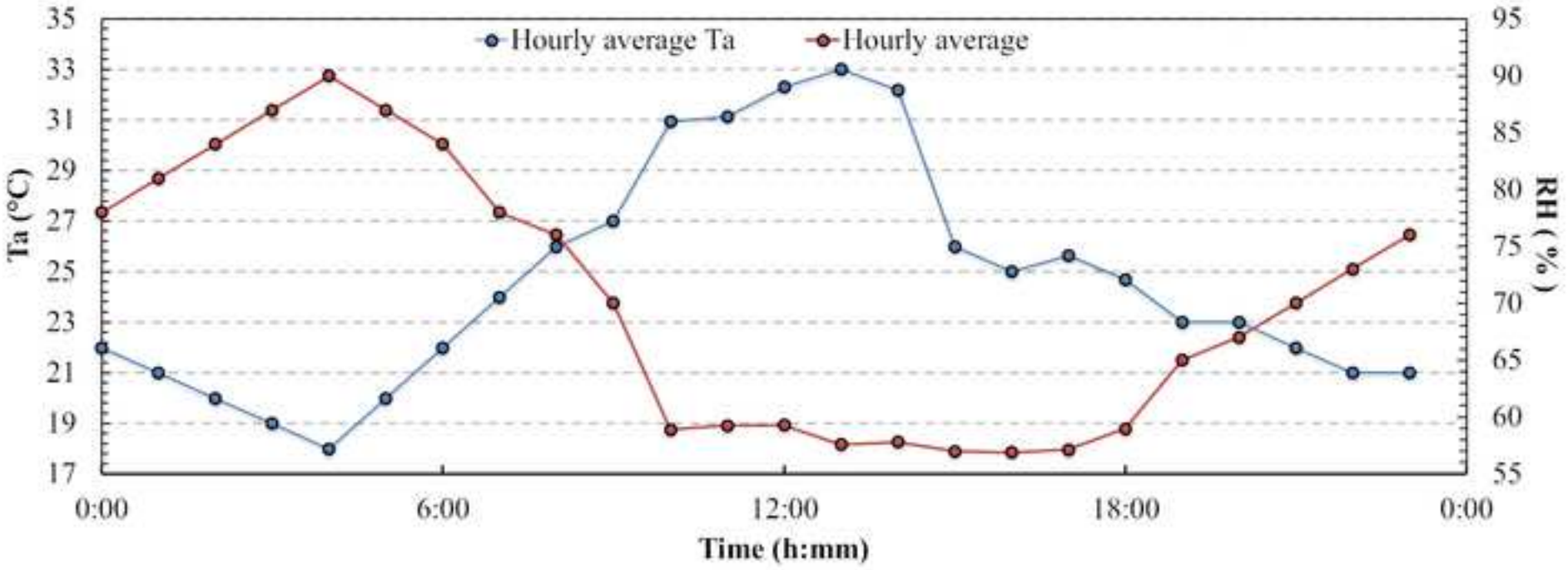

Fig 6

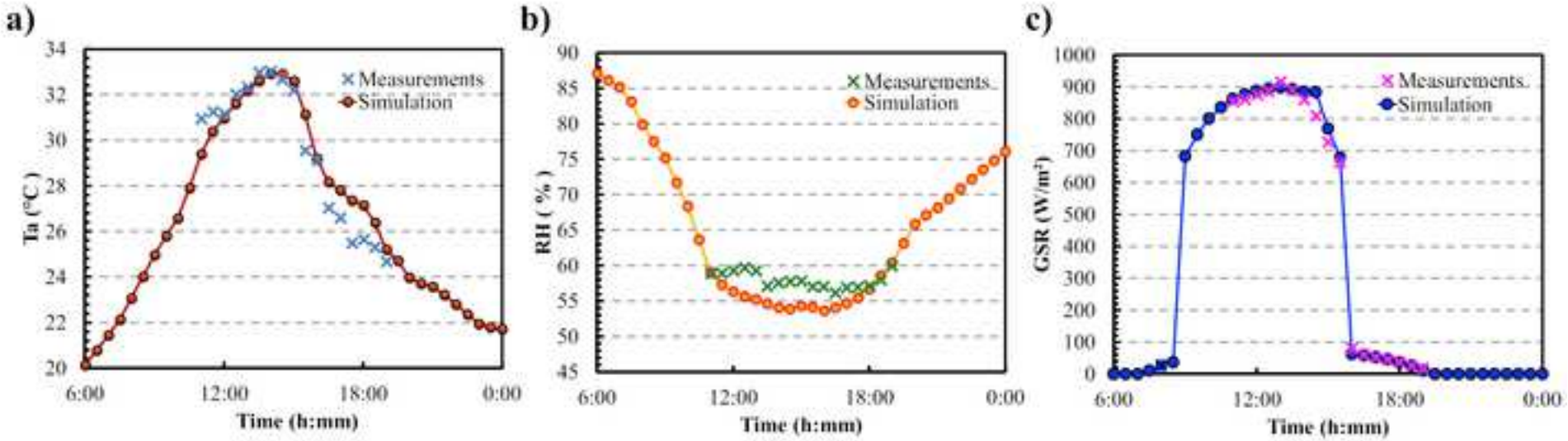

Fig 7

Click here to access/download;Figure;Fig 7 300dpi.jpg

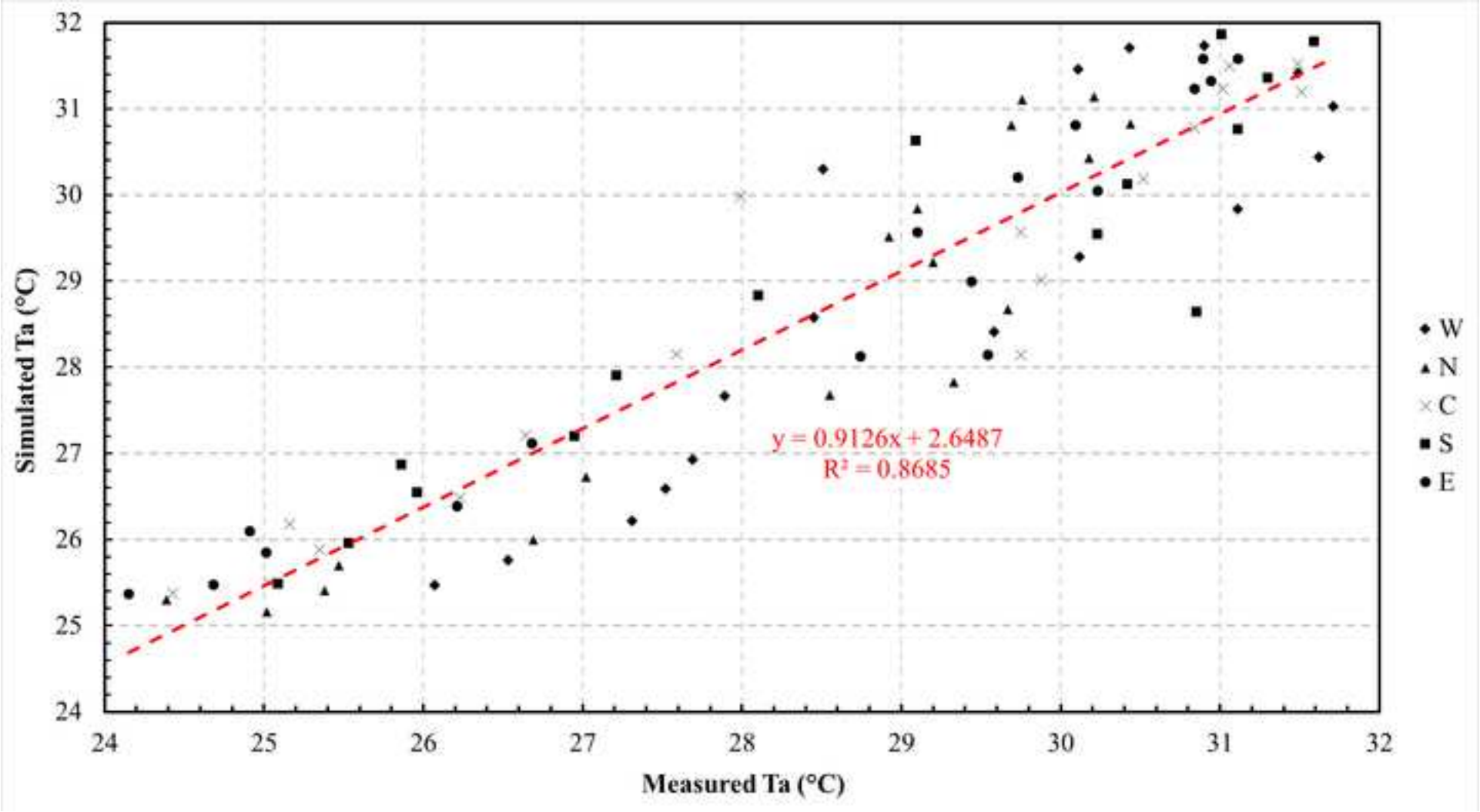

Fig 8

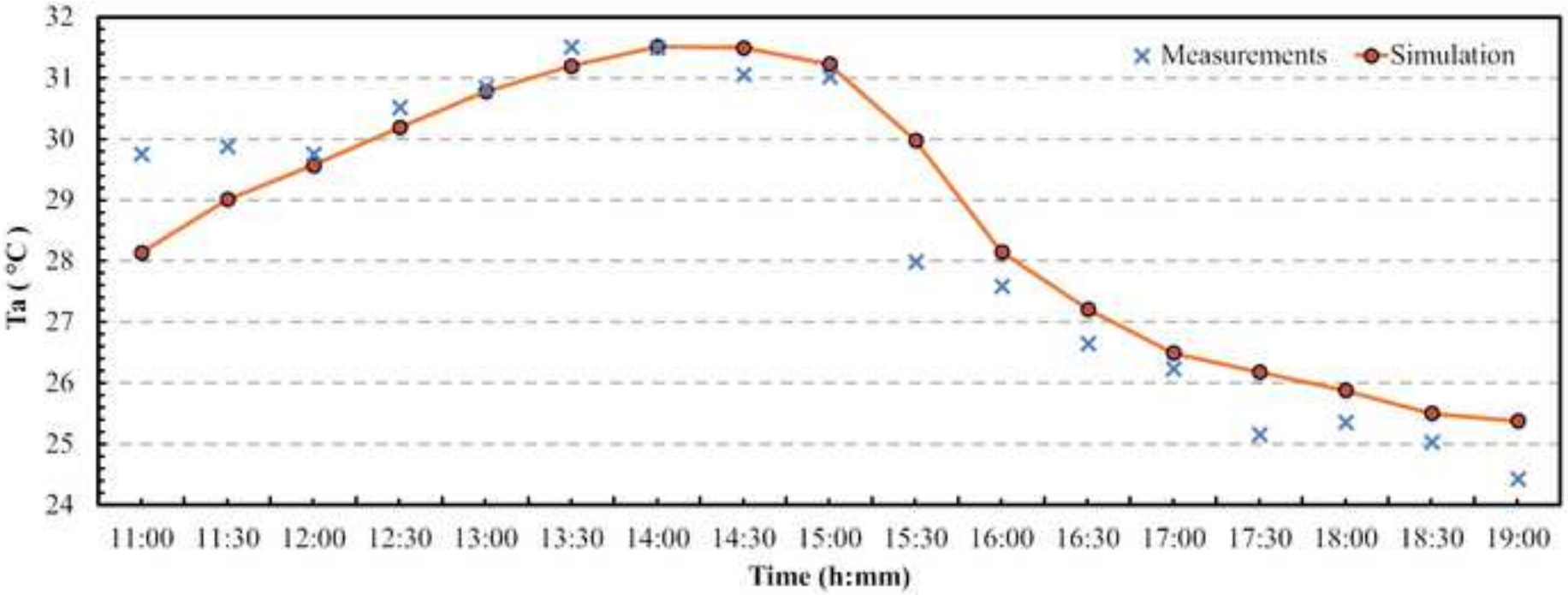

Fig 9

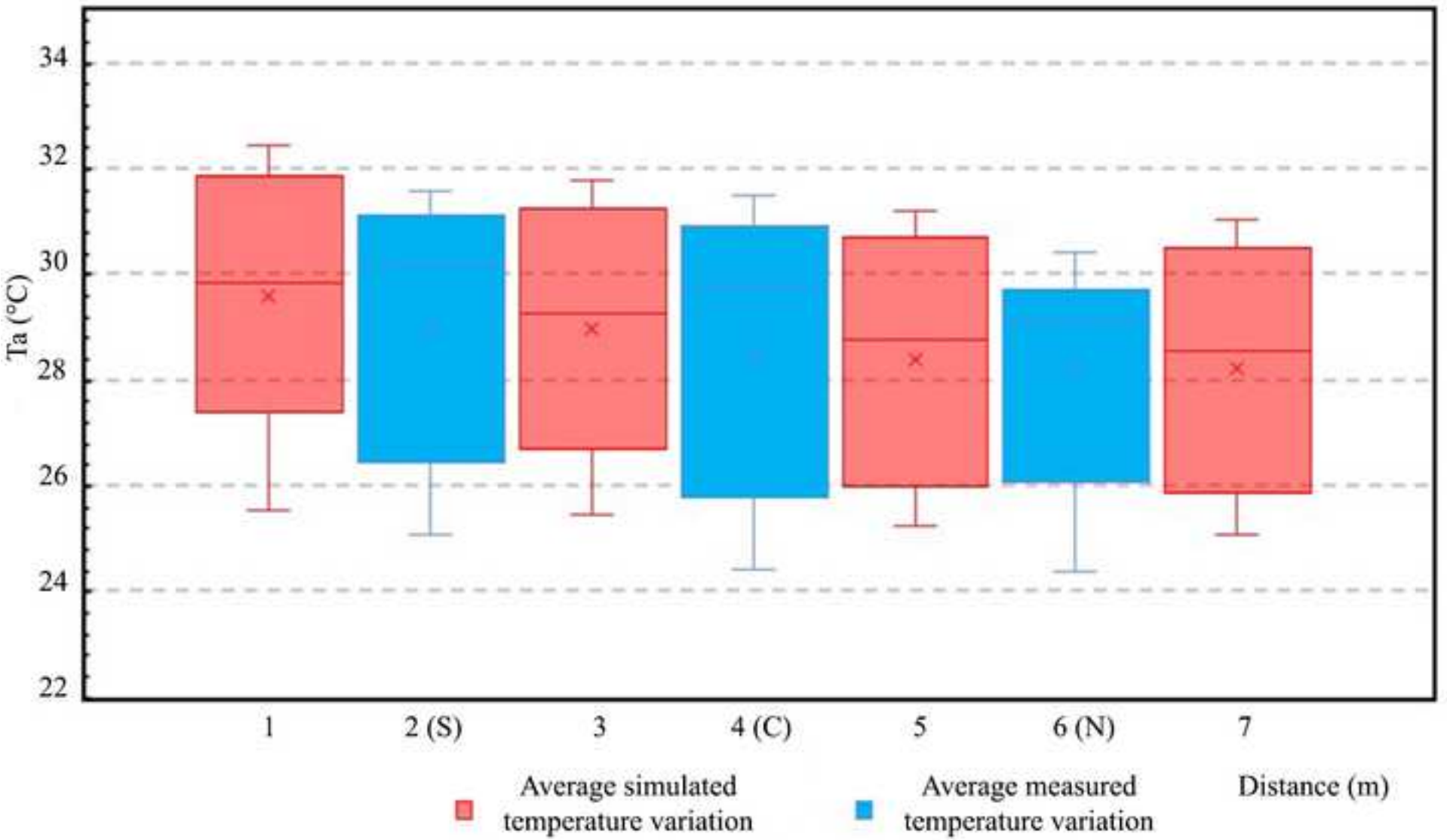

Fig 10

Click here to access/download;Figure;Fig 10 300dpi.jpg

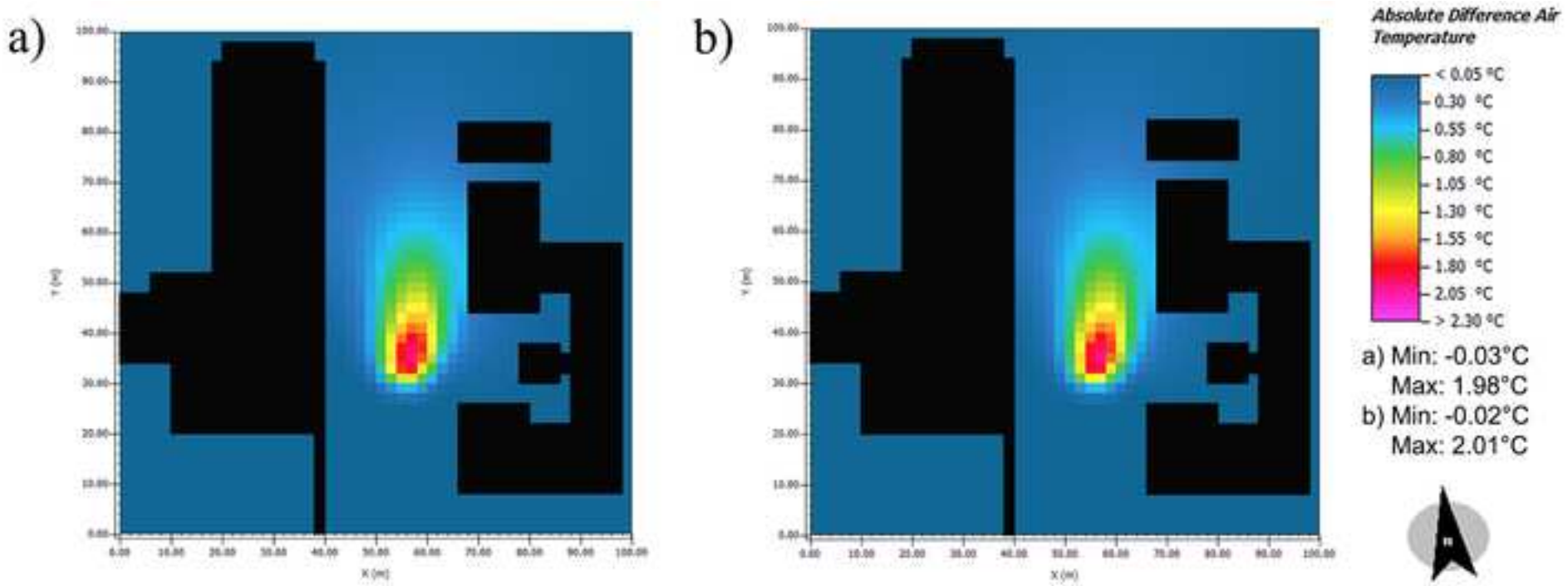

Fig 11

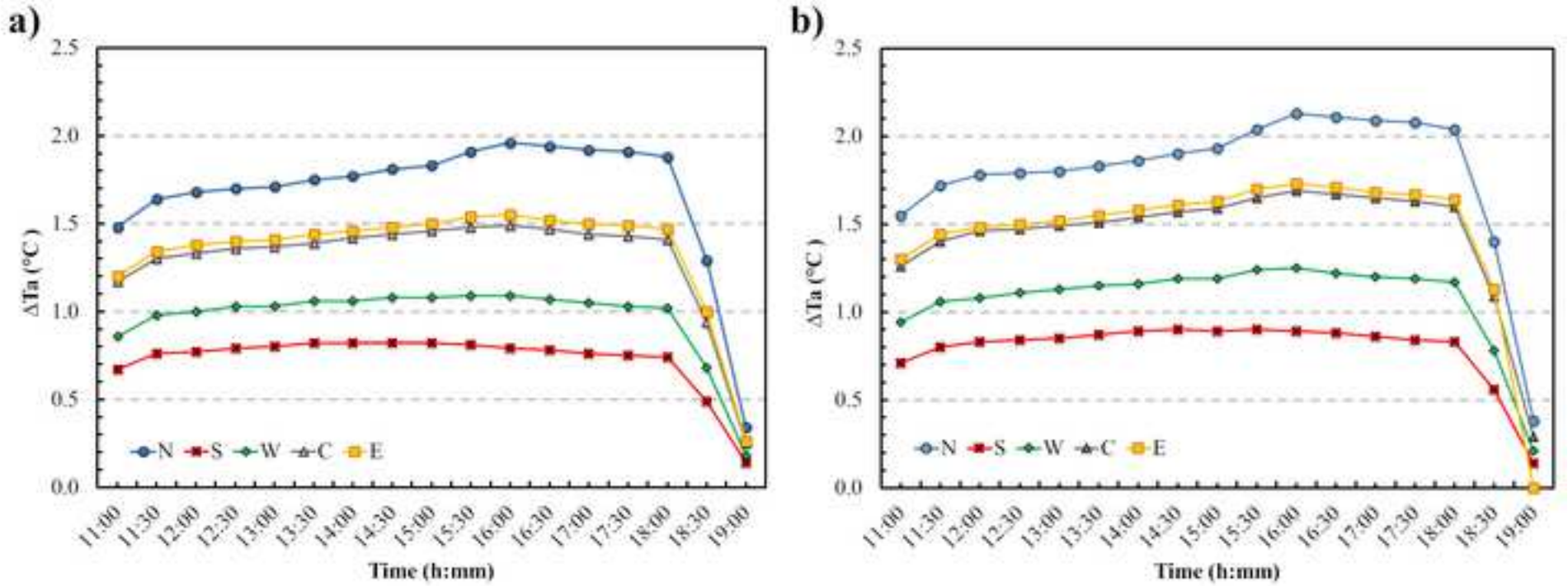

Fig 12

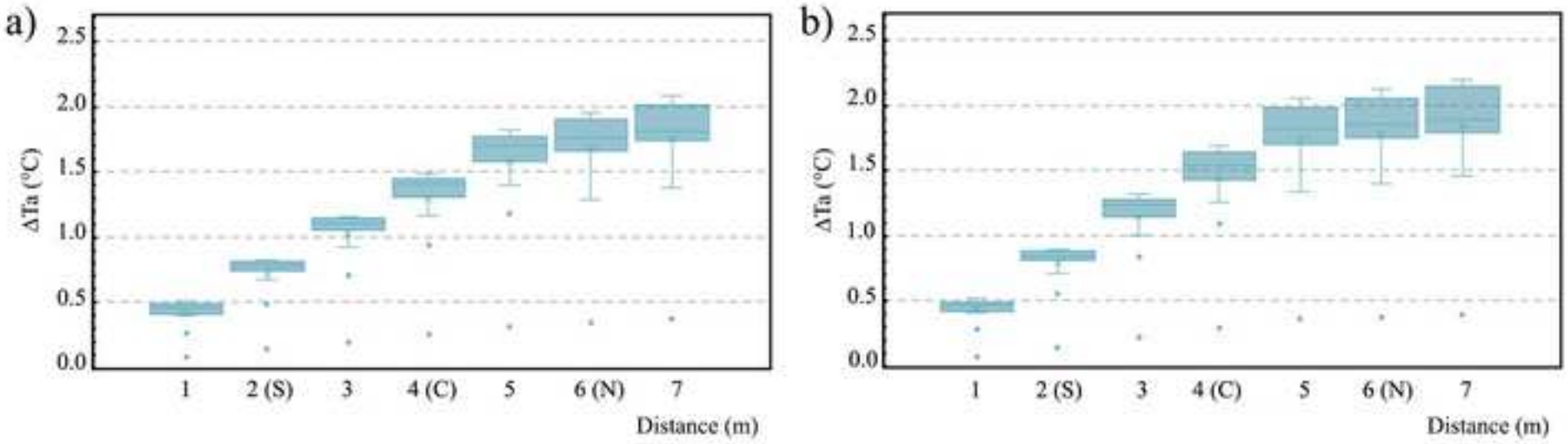

Fig 13

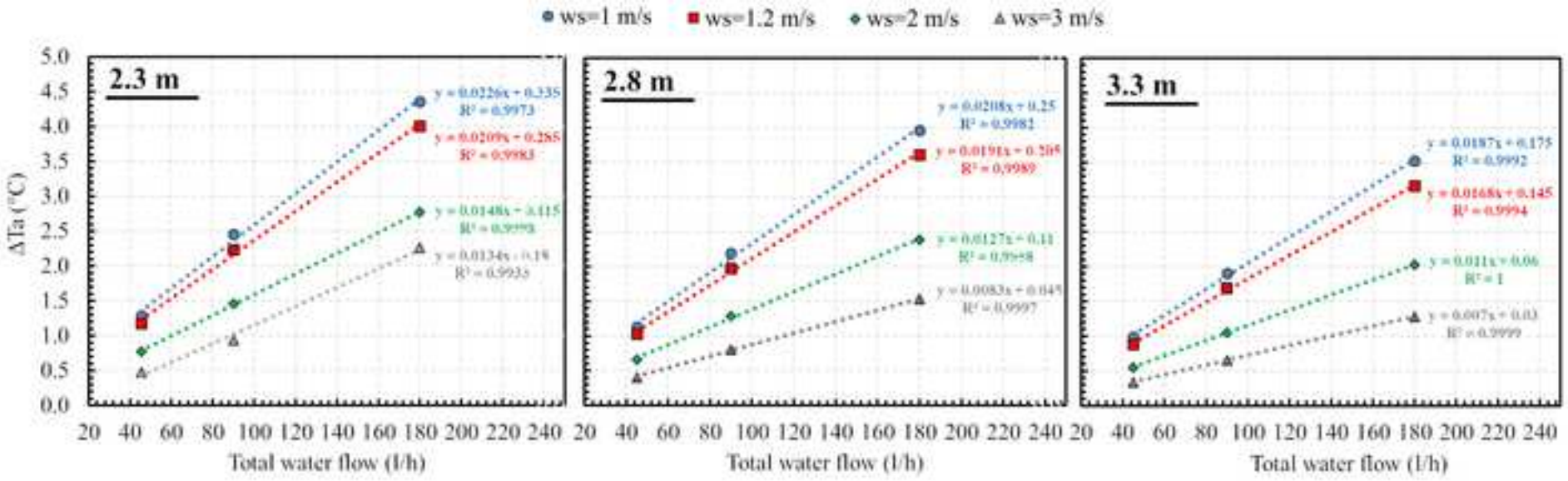

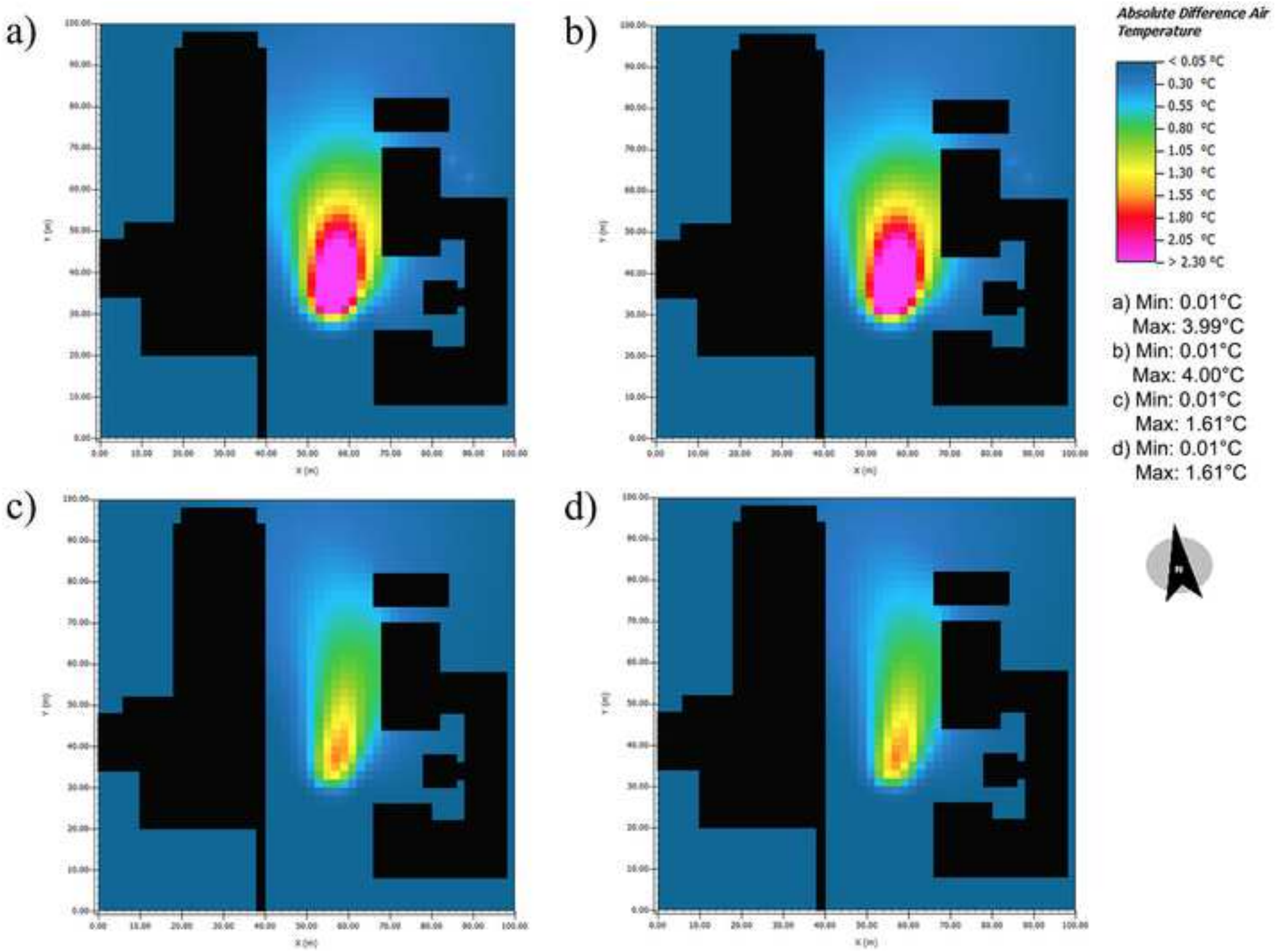

Fig 15

Click here to access/download;Figure;Fig 15 300dpi.jpg

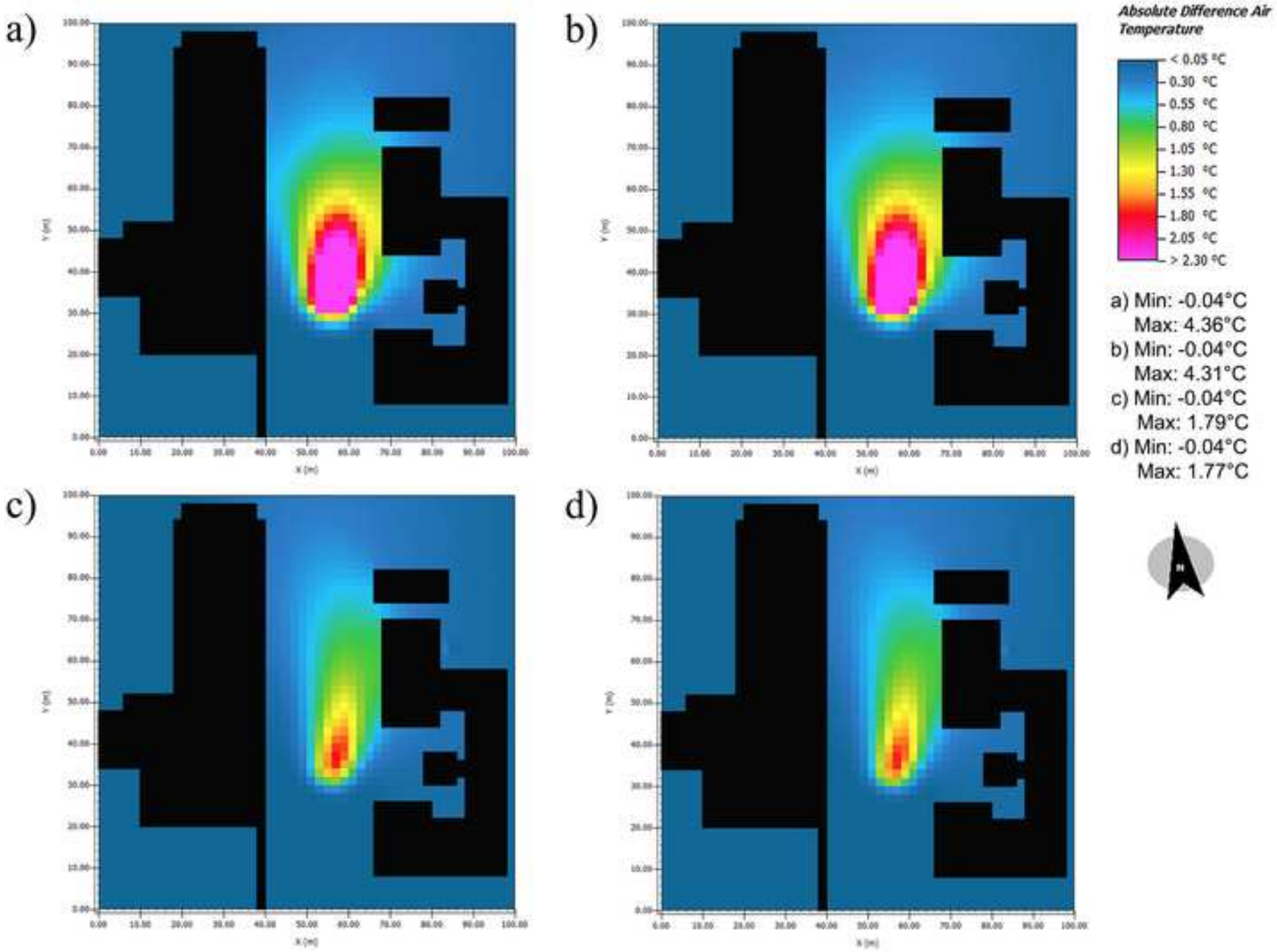

Fig 16

Click here to access/download;Figure;Fig 16 300dpi.jpg

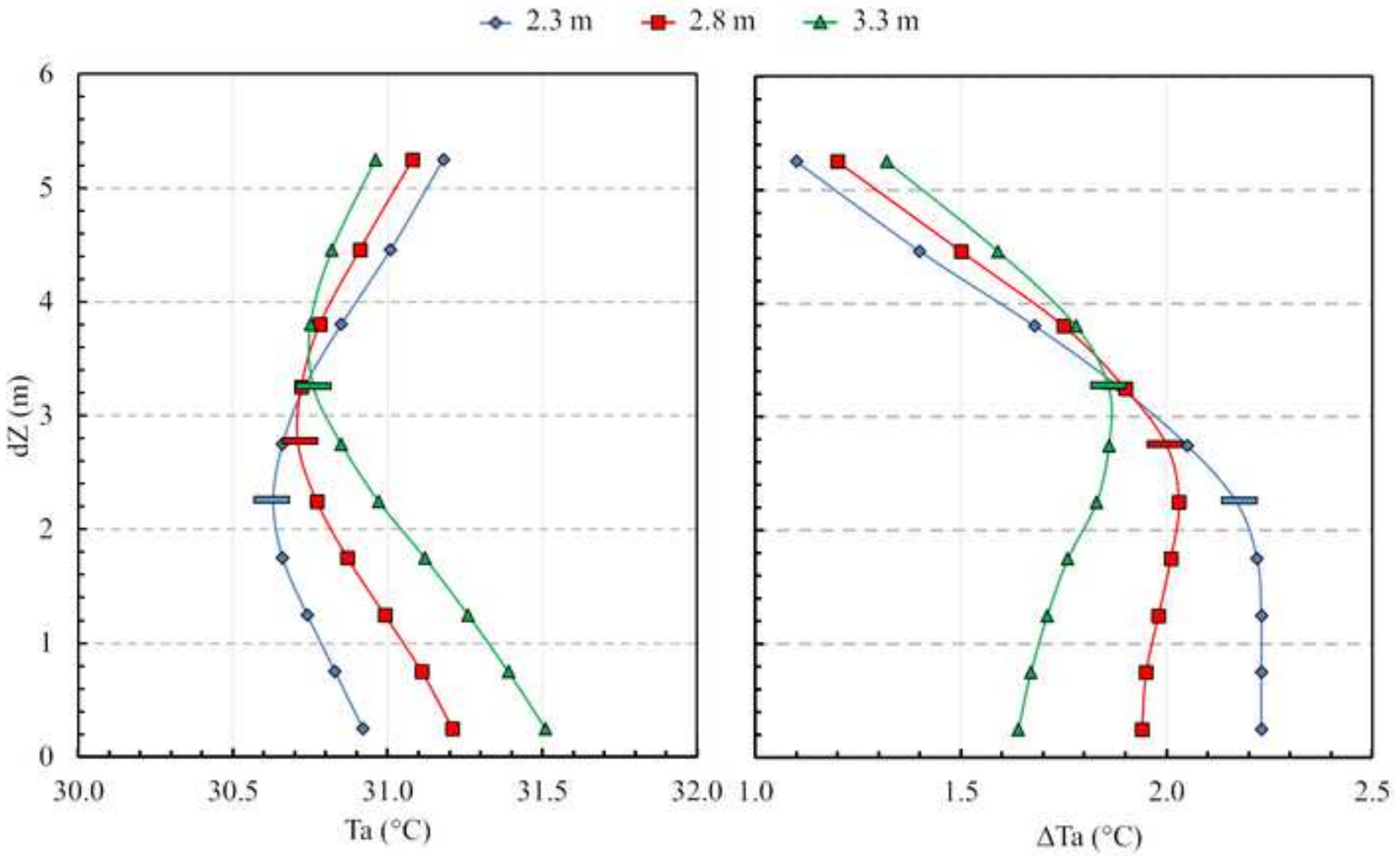

Declaration of interests

☒ The authors declare that they have no known competing financial interests or personal relationships that could have appeared to influence the work reported in this paper.

☐The authors declare the following financial interests/personal relationships which may be considered as potential competing interests:

CRediT author statement

E. Di Giuseppe: Conceptualization, Methodology, Investigation, Writing-Original Draft, Writing-Reviewing and Editing. **G. Ulpiani:** Conceptualization, Methodology, Investigation, Visualization, Writing-Original Draft preparation, Writing-Reviewing and Editing. **C. Cancellieri**: Software, Validation, Visualization. **C. Di Perna**: Resources, Supervision, Writing-Reviewing and Editing. **M. D'Orazio***:* Resources, Supervision, Writing- Reviewing and Editing. **M. Zinzi**: Resources, Writing- Reviewing and Editing.